View metadata, citation and similar papers at core.ac.uk

brought to you by CORE

provided by OTHES

universität wien

DISSERTATION

Titel der Dissertation

„Probing for local synaptic connectivity in the adult mouse auditory cortex“

Verfasser

Bruno Miguel Da Palma Pedrosa Fontinha

angestrebter akademischer Grad

Doktor der Naturwissenschaften (Dr.rer.nat.)

Wien, 2012

Studienkennzahl lt. Studienblatt:	A 091490
Dissertationsgebiet lt. Studienblatt:	Molekulare Biologie
Betreuer:	Dr. Simon Rumpel

Table of Contents

1. Abstract iv

2. Zusammenfassung vi

3. Introduction 1

3.1. Neuronal circuits of the neocortex 3

3.1.1. Excitatory circuits: pyramidal cells and their fundamental intrinsic communication 4

3.1.1.1. Excitatory neurons in layer 5 5

3.1.1.2. Excitatory neurons in layer 4 8

3.1.1.3. Excitatory neurons in layer 2/3 8

3.2. Recurrent connectivity: local circuitry is the heart of cortical computation 10

3.3. Overall anatomical model of cortical function 15

3.4. Connectivity features of the mammalian auditory cortex 17

3.5. Optogenetics and neural circuits 20

3.6. Channelrhodopsin as a tool to assess neural circuitry 21

4. Aim 24

5. Experimental Procedures 25

5.1. Experimental subjects 25

5.2. Slice preparation 25

5.3. Electrophysiology 26

5.4. Measurement of synaptic connection strengths 27

5.5. Spontaneous EPSPs analysis 30

5.6. Test for overrepresentation of reciprocally connected neurons 31

5.7. Extracellular stimulation 31

5.8. Decomposition of the synaptic conductance 33

5.9. Drugs 34

5.10. Plasmid constructs 34

5.11. Preparation and delivery of adeno-associated virus 35

5.12. Stereotaxic viral injections 36

5.13. In vitro characterization of ChR2-expressing neurons 37

5.14. Chronic cranial window implantation 38

5.15. Behaviour procedures 39

5.15.1. Habituation 41

5.15.2. Perceptual task 42
5.15.3. In vivo photostimulation 42
6. Results 44
6.1. Features of local cortical connectivity in the adult naïve mice 45
6.1.1. Intrinsic electrophysiological properties of pyramidal neurons in the adult mouse auditory cortex 47
6.1.2. Features of EPSP amplitudes, kinetics and reliability 50
6.1.3. Variability in postsynaptic transmission 53
6.1.4. Explanation of the variability in mean connection strengths with a binominal model of transmitter release 56
6.2. Relative contribution of excitation/inhibition drive onto layer 2/3 pyramidal neurons with temporal resolution 65
6.3. Features of local cortical connectivity upon the acquisition of an artificial-driven behaviour 71
6.3.1. Characterization of light-induced responses in channelrhodopsin-expressing pyramidal neurons 72
6.3.2. Optical photostimulation in auditory cortex can drive behaviour in freely moving mice 78
6.3.3. Impact of artificial-guided behaviour in local synaptic connectivity 79
6.3.4. Comparable spontaneous neuronal activity in trained and non-trained mice ……...84
7. Discussion 86
7.1. Sparse connectivity and long-tailed distribution of synaptic weights 86
7.2. Network of few “strong” and many “weak” excitatory connections 87
7.3. The variability in mean connection strengths can be largely captured by differences in neurotransmitter release probability and number of release sites 89
7.4. Large fraction of presynaptic inputs required to reach spiking threshold 91
7.5. Excitatory / inhibitory balance in the adult auditory cortex 92
7.6. Optical stimulation of the auditory cortex can drive behaviour in the adult mouse ……..96
7.7. Intrinsic properties of optogenetically stimulated neurons in vivo 98
7.8. Local synaptic connectivity features upon photostimulation-driven behaviour ……100
8. References 103

9. Acknowledgements 113
10. Curriculum Vitae 114

1. Abstract

The current mechanistic view on how the brain is able to store memories over long periods of time is based on two key concepts. The first is that memories are stored in the configuration of the connectivity of neurons in an assembly and in the set of synaptic weights of those connections; the second being that experience can mold and rewire the network connectivity and its synaptic weights. It becomes clear that the understanding of cortical function will always require the unraveling of synaptic connectivity in cortical circuits, that is, establishing the wiring diagrams between individual neurons.

In the present work, a first effort was made in order to investigate the excitatory synaptic local circuitry in the adult mouse auditory cortex, a brain area critically involved in sound encoding required for proper associative motivational leaning.

For this purpose, coronal whole-brain slices from adult (8-14 weeks old) C57Bl6/6J mice were used. Several simultaneous quadruple whole-cell recordings from layer 2/3 and layer 5 pyramidal neurons were made, a method that allows for quantitative functional measures of synaptic connectivity at the level of individually indentified neurons. It was observed that local circuitry is characterized by low connection probabilities between pairs of neurons, and that bidirectional connections are more common than expected in a random network. The distribution of synaptic connections strengths (defined as the peak of excitatory postsynaptic potential (EPSP) amplitude), has a heavier tail and implies that synaptic weight is concentrated among few synaptic connections. In both layers it was found the existence of rare but reliable large-amplitude synaptic connections, which are likely to contribute strongly to reliable information processing. Moreover, another central finding is that the EPSP amplitude variability can be ascribed to changes in the number of release presynaptic sites, or due to the probability of neurotransmission release, implying that modulations in synaptic transmission can be described by changes in both parameters independently.

In the second part, the relative contribution, with precise temporal resolution, of excitatory and inhibitory drives that impinge onto layer 2/3 pyramidal neurons was investigated. The strict balance of these two synaptic conductances plays a critical role in cortical function and in the shaping of the tuning properties of cortical neurons. It is

of utmost importance to describe how this balance is achieved and maintain. By means of intracortical extracellular stimulation of two independent but convergent input pathways into layer 2/3 neurons, synaptic conductances could be recorded and decomposed into their excitatory and inhibitory components. It was observed that excitatory/inhibitory balance is of equal magnitude in both stimulated pathways, and that on average a time difference less than 2 ms between the arrival of inhibition compared with the excitation favors for a monosynaptic nature of the stimulated intracortical projections that synapses onto the recorded layer 2/3 pyramidal neurons. On the other hand, it was observed that on almost half of the recorded neurons, the excitation conductance was flanked by two inhibitory barrages, a phenomenon never described so far. A possible feedback or feedforward inhibitory circuitry made by local interneurons could explain this observation.

In the third part, one final question was posed: are the features that describe local synaptic circuitry changed upon optogenetic manipulation in a behavioural task? By means of combining expression of channelrhodopsin in auditory cortex pyramidal neurons, with their direct photostimulation in the context of a behaviour task, it was possible to assess the role of a subset of neurons in driving behaviour. Possible changes in their intrinsic interconnectivity were also studied upon learning. Though extremely labour intense, it was concluded that ChR2-based optical microstimulation can be used to dissect the impact of precisely timed action potentials in a subset of neurons in driving behaviour. Whole-cell recordings from layer 2/3 neurons from the subset of mice that reached correct performance levels were performed as before. It was observed that ChR2-expressing neurons in trained mice had similar intrinsic excitability features when compared with non-trained mice. The recorded EPSP amplitudes from pairs of connected neurons had similar rages among both groups of mice, indicating that periodic depolarizations of ChR2-positive neurons does not induce any synaptic scaling effect in these neurons.

2. Zusammenfassung

Die grundlegenden Funktionsweisen wie unser Gehirn neue Informationen speichert beruht auf zwei Theorien. Erstens, Neuronen verbinden sich zu einem Netzwerk mit unterschiedlichen starken Verbindungen zueinander. Zweitens, äußere Einflüsse können diese Verbindungen verändern. Dadurch können sich neue Neuronen dem Netzwerk anschließen oder sich auch die Stärke der Verbindungen von bereits im Netzwerk vorhandenen Neuronen ändern. Um mehr über die Funktionsweise unseres Gehirns zu erfahren ist es absolut notwendig ein Schaltdiagramm corticaler Netzwerke zu haben der alle Verbindungen der Neuronen zueinander enthält.

In dieser Arbeit untersuchten wir die synaptischen Verbindungen im auditorischen Cortex, eine Hirnregion wichtig für die Prozessierung von Tönen in verschiedenen assoziativen Lernparadigmen.

Wir verwendete coronale Hirnschnitte von erwachsenen (8-14 Wochen alten) C57Bl6/6J Mäusen. Wir machten gleichzeitig ganz-Zell Ableitungen von vier Pyramidenzellen der Schicht 2/3 und der Schicht 5. Diese Methode erlaubt es die synaptische Verbindungsstärke zwischen diesen vier Neuronen zu messen. Wir fanden eine niedrige Verbindungswahrscheinlichkeit zwischen gleichzeitig gemessen Neuronen und weiters dass die Wahrscheinlichkeit einer bidirektionalen Verbindung zwischen zwei zufällig ausgewählte Neuronen höher war als erwartet. Die Verteilung der Stärken der synaptischen Verbindungen (der höchste Punkt der Amplitude des postsynaptischen Potentials (EPSP)) zeigte wenige starke Verbindungen. Dies deutet darauf hin, dass synaptische Verbindungen in lokalen Netzwerken von seltenen aber dafür starken Verbindungen dominiert werden. Wir fanden diese Verbindungen in beiden untersuchten Hirnschichten was darauf hindeutet, dass diese seltenen aber starken Verbindungen die Grundlage der Informationsverarbeitung in corticalen Netzwerken sein könnte. Wir fanden auch, dass die Variabilität der EPSP Amplitude entweder durch die veränderte Wahrscheinlichkeit der Neurotransmitterfreisetzung oder durch eine veränderte Anzahl der freigesetzten Neurotransmittervesikel auf der praesynaptischen Seite entstehen kann. Dies deutet darauf hin, dass beide Parameter Wahrscheinlichkeit und Anzahl unabhängig voneinander sind.

Im zweiten Teil untersuchten wir den relativen Anteil des erregenden und inhibierenden Stroms zu Schicht 2/3 Neuronen mit präziser zeitlicher Auflösung. Die strikte Balance zwischen diesen Strömen ist kritisch für die Funktion corticaler Netzwerke und für die Anpassung der Eigenschaften corticaler Neuronen. Daher ist es notwendig herauszufinden, wie diese Balance aufrechterhalten wird. Wir stimulierten extrazellulär zwei unabhängige von einander zu Schicht 2/3 führende Nervenbahnen und maßen die synaptisch erregende und inhibierende Leitfähigkeit von Schicht 2/3 Neuronen. Wir fanden das die Balance zwischen erregenden und inhibierenden Strömen gleich groß für beide Nervenbahnen war und weiters, dass das Eintreffen der inhibierenden Ströme 2ms schneller war als das der erregenden Ströme. Dies deutet darauf hin, dass diese intercorticalen Nervenbahnen monosynaptisch mit Schicht 2/3 Neuronen verbunden sind. Interessanterweise fanden wir, dass fast 50 Prozent aller erregenden Ströme gleichzeitig mit zwei inhibitorischen Strömen eintrafen. Dies wurde vorher nicht beschrieben und könnte auf ein feedback oder feedforward Netzwerk lokaler Interneuronen zurückzuführen sein.

In dritten Teil untersuchten wir ob optogenetische Manipulation während eines Verhaltensexperiments die Eigenschaften lokaler corticaler Netzwerke verändert. Wir expremierten Channelrhodopsin in Pyramidenzellen des auditorischen Cortex und photostimulierten diese Zellen während eines Verhaltensexperiments. Dadurch ist es uns Möglich festzustellen ob diese Neuronen ein bestimmtes Verhalten auslösen können. Wir untersuchten auch, ob sich die spezifischen Verbindungen dieser Nervenzellen während des Lernens einer Verhaltensaufgabe ändern. Wir fanden, dass die Stimulation durch Channelrhodopsin dazu verwendet werden kann, den Einfluss präzise getimter Aktionspotentiale auf das erlernen einer Verhaltensaufgabe zu untersuchen. Weiters führten wir ganz-Zell Ableitungen an Schicht 2/3 Neuronen von Mäusen die die Verhaltensaufgabe gelernt hatten durch. Wir fanden heraus, dass sich die Erregbarkeit von Neuronen in diesen Mäusen nicht von der Erregbarkeit von Neuronen in wildtyp Mäusen unterscheidet. Wir konnten keine Unterschiede in den EPSP Amplituden verbundenen Neuronen feststellen. Dies deutet darauf hin, dass die durch Channelrhodopsin ausgelöste Depolarisation nicht zu einer stärkeren Verbindung zwischen diesen Neuronen führt.

3. Introduction

When David Hubel acknowledged Vernon Mountcastle, "…whose discovery of columns in the somatosensory cortex was surely the single most important contribution to the understanding of cerebral cortex since Cajal...", during his Nobel lecture (1981), maybe he was not aware of the attractive fatalness of such concept. Nowadays, the cortical column has emerged as an imperative concept to explain the functional organization and the communication architecture of the neocortex. In fact, to Western eyes reared on classical and neoclassical forms, the columns seem an existential necessity to build the world. So convincing they are, and so central to our present day concepts, that vast resources in human and machine time are being devoted to defining every element and every connection in the cortical column so that a facsimile can be recreated *in silico* (Markram, 2006; Helmstaedter et al., 2007).

However, how do cortical neurons organize themselves into the networks that express not only individual properties like orientation selectivity or ocular dominance, but arrange these circuits to express a precise *mappa mundi* of these properties? Nowadays, it is generally accepted that, in addition to its layered structure, the neocortex also organizes its functionality in the vertical dimension, but, as with the layers, the size and the shape of these vertical organizations vary greatly (e.g. Mountcastle et al., 1957; Hubel and Wiesel, 1974). Since recent times, a concept of a "canonical circuit" for the neocortex has been developed, which embodies the idea of a repeated local circuit that performs some fundamental computations that are common to all areas of the neocortex (Douglas et al., 1989; Douglas and Martin, 1991). The canonical circuit (Figure 3.1) is firmly based on statistical analysis of the connections between the different types of cortical neurons and their physiology. The vast majority of these connections are intracortical, interlaminar or within the same lamina. It captures some of the essential attributes of the rules that govern the connections between different cell types that allow the multiple functions of cortical circuits to be made. Phenomena such as recurrent excitation and inhibition, or amplification of weak inputs from thalamus, or even the balance between excitation and inhibition, are embedded in the cortical circuitry (e.g. Binzegger et al., 2004). How these attributes are employed and deployed depends, of course, on the demands of a specific cortical area. But to which extent can neocortical neurons and the circuits they form be considered canonical by themselves? One can

suggest that in the concept of a "canonical circuit" one can find the means to reconcile the structure of neocortex with its functional architecture. The canonical microcircuit respects the known connectivity of the neocortex, and it is flexible enough to change transiently the architecture of its network in order to perform the required computations. In a very simplifying view, the neocortex might consist of repeated copies of the same fundamental circuit.

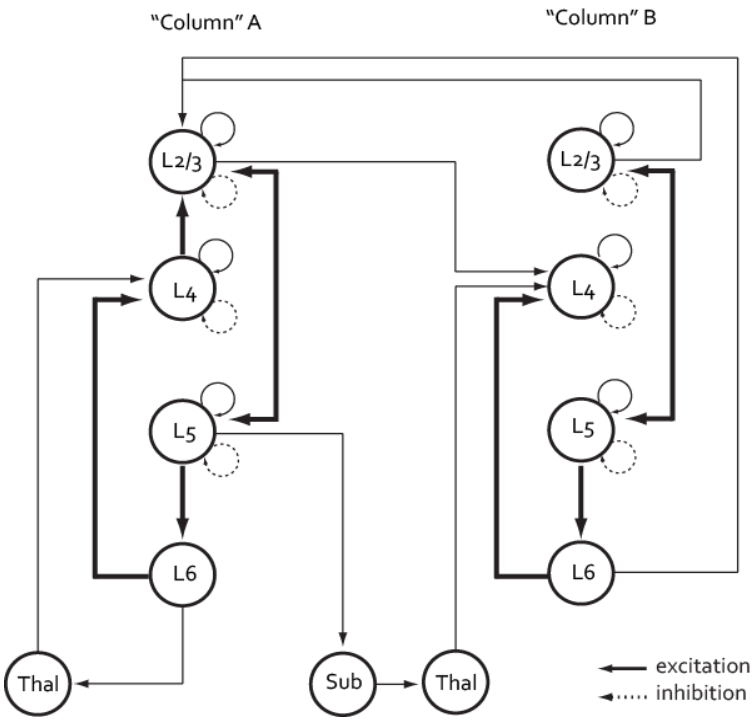

Figure 3.1. ***Diagram representing the dominant interactions between excitatory cell types in the canonical microcircuit****. Ascending, thalamocortical input is perceived as entering layer 4 (and layer 6), being then relayed from layer 4 to layer 3 (and thence to layer 2), from layer 3 to layer 5 and from layer 5 to 6. Modified or integrated versions of that information are sent to other cortical regions from pyramidal cells in all layers, particularly layer 2/3, and to other cortical and subcortical regions from the deeper layers. Neurons from different cortical layers are represented as circles, being "Lx" the layer in which its soma is located. Thal: thalamus; Sub: other subcortical structures, such as basal ganglia (adapted from Douglas and Martin, 1991, 2004; for review see Thomson and Bannister, 2003)*

At the end, perhaps the most important feature of Mountcastle's concept of functional columns was its ease of generalization. In spite of some opinions that the concept of column failed miserably as a unifying principle for the cerebral cortex (e.g. Horton and Adams, 2005) – mainly due to the fact that dendrites originating from the cells bodies

spread well beyond a given elementary column, so as their axonal arbors (Gilbert and Wiesel, 1979) - the idea of elementary modules that could, by repetition, generate an "entire" cortex is nowadays universal, and one has at his disposal a paradigm for probing the functional architecture and connectivity of any sensory area of the neocortex.

3.1. Neuronal circuits of the neocortex

The neocortex can be defined as a thin, extended, convoluted sheet of tissue with a surface area of approximately 2600 cm^2, and thickness of 3 to 4 mm, that varies over five orders of magnitude in volume from shrew to whale, that supports the processing of input from an unlikely range of sensory modalities allowing detection of vibration, temperature, sound and chemicals, and that then provides output to an equally unlikely range of motor structures, allowing an animal to fly, swim, walk, jump, and run. It contains up to 28×10^9 neurons and roughly the same number of glial cells. The neurons can be grouped into three major classes: pyramidal cells (present in all cortical layers except layer 1), spiny nonpyramidal cells (spiny interneurons, located in the middle layers, especially layer 4), and aspiny nonpyramidal cells (smooth interneurons, present in all layers). About 80% of neurons are spiny and excitatory and form 85% of the synapses, while about 20% of the neurons are smooth and inhibitory, forming only 15% of the overall synapses, because of their smaller ramifications (Jones, 1984; Lund, 1984; Mountcastle, 1997; Douglas and Martin, 2004; Markram et al., 2004).

In the last decade, several new techniques have been developed to reveal synaptically connected neurons, including whole-cell paired recordings (Song et al., 2005; Thomson and Lamy, 2007), serial electron microscopy reconstructions (Bock et al., 2011), viral tracing (Wickersham et al., 2007), calcium imaging probing (Peterlin et al., 2000), reverse correlation imaging (Aaron and Yuste, 2006), and photostimulation with caged glutamate (Callaway and Katz, 1993; Yoshimura et al., 2005; Paker and Yuste, 2011). By using such a variety of methods, it is nowadays assumed that cortical neurons are connected with each other and with neurons in other parts of the brain by a vast number of synapses, of the order of 10^{12}, in a nonrandom way. The cortex is organized vertically into six laminae, and horizontally into groups of cells linked synaptically across the

vertical laminae (but see Huntley and Jones, 1991 and DeFelipe et al., 2002 for exceptions in primates and nonprimates). The basic unit of the mature neocortex is the "minicolumn", a narrow chain of neurons extending vertically across the cellular layers 2/3 perpendicular to the pial surface (Mountcastle, 1978), and each "minicolumn" in primates contains ~80-100 neurons, except for the striate cortex where the number is ~2.5 times larger. A cortical column is a complex processing and distributing unit that links a number of inputs to a number of outputs via overlapping internal processing chains.

The enormous strides made in understanding the formation and operation of the neocortical circuits have been matched by the detailed analyses of the cellular and synaptic physiology of the elements that make up the neocortical circuits. Rapid advances in theory have also begun to clarify the nature of the computations carried out by the neocortical microcircuits. There are now many different models of cortical circuits, based on experimental data or theoretical considerations. For historical reasons, most models of biologically defensible circuits rely heavily on data from cat and primate visual cortex, but cell types and patterns of connections have also been described in many other cortical areas, with the contribution from rodent somatosensory and auditory cortex being perhaps the most prominent in recent years (Shen et al., 1999; Sato et al., 2007; Ohki et al., 2005; Anderson et al., 2006; Anderson et al., 2010; Atencio and Schreiner, 2010; for review Thomson and Bannister, 2003; Douglas and Martin, 2004; Petersen, 2007).

3.1.1. Excitatory circuits: pyramidal cells and their fundamental intrinsic communication

The projection patterns of pyramidal axons and multiple-field potential recordings *in vitro* (for review see Thomson and Lamy, 2007) have provided the basis for an almost unidirectional flow of excitation within a cortical microcircuit. In its simplest form, specific thalamocortical input arriving in layer 4 (and 6) is perceived as being relayed from layer 4 to 3 (and hence to layer 2), from layer 3 to layer 5 and from 5 to 6, the processed information then leaving layer 3 for other cortical regions and from deeper layers to other cortical and subcortical areas. Excitatory connections to glutamatergic

cells in the opposite direction, from layer 3 to layer 4 and from 5 to 3 are infrequent and weak. In contrast, these “back projections” involve inhibitory interneurons, either via the axons of the inhibitory cells themselves, or via excitatory inputs to interneurons in the recipient layers.

The principal neurons in the neocortex are excitatory pyramidal neurons receiving several thousand synaptic inputs and are found in layers 2 to 6 (Figure 3.2). Although pyramidal cells share many distinctive anatomical features, they are far from a homogeneous group. Even within a layer there are several morphological subtypes, often projecting to different cortical and subcortical regions. For instance, layer 5 pyramidal neurons have longer apical dendrites and fewer oblique apical dendrites than layer 2/3 pyramidal neurons. Moreover, the apical tuft of pyramidal neurons receives excitatory synaptic inputs that have different presynaptic origins to those that form synapses onto more proximal apical dendrites or basal dendrites (Spruston, 2008; Douglas and Martin, 2004).

3.1.1.1. Excitatory neurons in layer 5

The predominant inputs to layer 5 (and to layer 5 pyramidal dendrites in layer 3) appear to be short and long range cortical projections. Layer 5 pyramidal neurons project to a wide range of subcortical targets including (depending on cortical region) ‘‘non-specific’’ thalamic nuclei, superior colliculus, pons and spinal cord, as well as to other cortical regions and to the contralateral cortex. In cat visual cortex, corticotectal neurons (projecting to regions such as the superior colliculus) are large, with a well-formed basal dendritic arbor and a long apical dendrite that forms a well-developed tuft in layers 2 and 1. In contrast, the apical dendrites of small to medium-sized CT layer 5 cells rarely extend beyond layers 2/3 (Hubener et al., 1990). Layer 5 pyramidal neurons display two distinct firing patterns first described in rat cortex (Connors and Gutnick, 1990) as “intrinsically burst firing” and “regular spiking” cells. The first ones are large pyramids with long apical dendrites whose axons project to the superior colliculus and /or pons, while the smaller, shorter layer 5 pyramids that project to the opposite hemisphere are “non-bursters” that appear to project inter-hemispherically. Layer 5 contains two main morphological types of pyramidal neurons on the one hand the thin untufted pyramids

that project to the opposite hemisphere, and on the other hand the thick tufted pyramids that project subcortically, such as the superior colliculus and the pons (Wang and McCormick, 1993), and are characterized by being large, burst-firing, and with long apical dendrites extending up to layers 2 and 1 (Connors et al., 1982; Chagnac-Amitai et al., 1990). It is only these larger pyramidal cells in layer 5 that could access directly the afferent inputs to the superficial layers, including the back projections from high cortical areas and inputs from calbidin-containing thalamic matrix cells. Moreover, layer 5 pyramidal axons arborize most densely within layer 5, but can also send projections to all other layers, as seen in rats and primates (for review see Markram, 1997). It is also the large layer 5 pyramids that are the major recipient of a highly focused and extremely dense descending excitation from layer 3 pyramidal cells. The smaller, adapting cells appear to receive little or none of this input (Thomson and Bannister, 1998). For example, by simultaneously recording from (and stimulating) three or more neighbouring layer 5 pyramidal neurons, it was found that when two neurons are connected to each other, the probability that they will share input from a third neuron is higher than expected in a randomly connected network (Song et al., 2005).

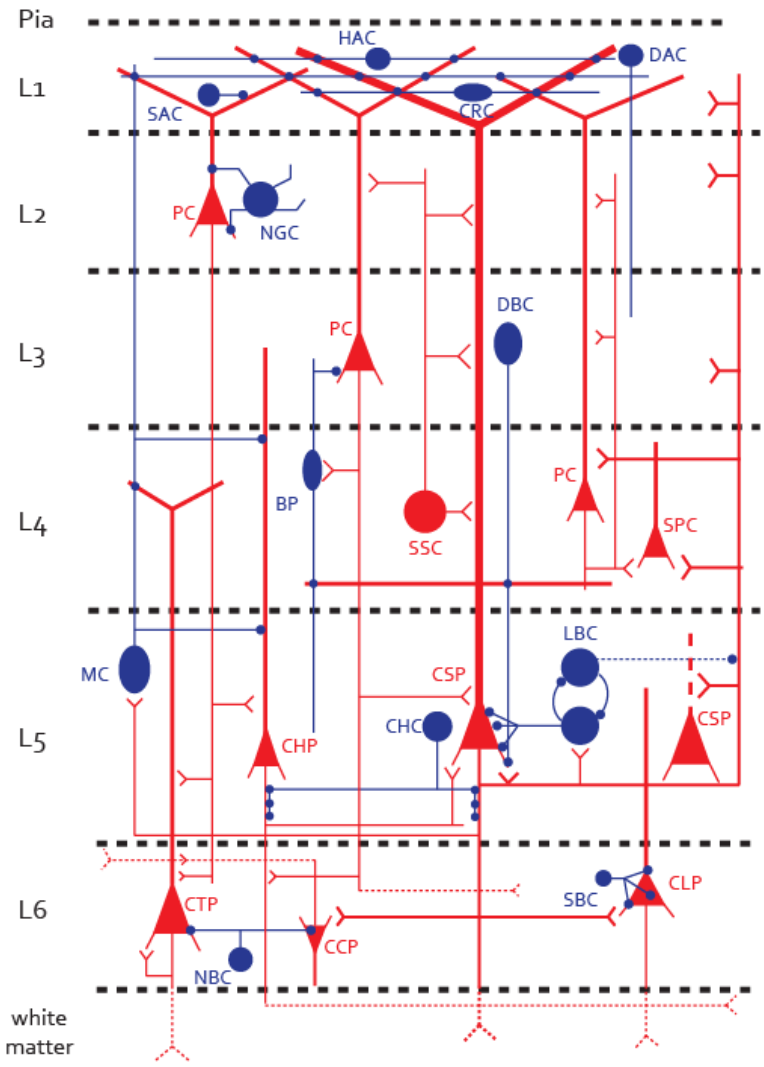

Figure 3.2. ***Simplified schematic representation of the neocortical main neurons.*** *Pictures illustrates a six-layer cortical column, where Lx on the left indicate the cortical layer where a give neuronal somata is embedded in. Red indicates excitatory neurons, their dendrites and axons; blue indicates inhibitory neurons, their dendrites and axons. Inhibitory synapses are marked as blue dots and red forks are indicative for excitatory synapses. Axons projecting beyond the cortical dimensions are indicated by dotted lines. For the pyramidal cells, axons are thin lines relative to the dendrites; for the inhibitory neurons only axons are schematized. Legend: BP, bipolar cell; CCP, corticocortical pyramid; CHC, chandelier cell; CHP, cortico-hemispheric cell; CLP, cortico-claustral pyramid; CRC, Cajal-Retzius cell; CSP, cortico-spinal pyramidal; CTP, cortico-thalamic pyramid; DBC, double bouquet cell; HAC, horizontal axon cell; LBC, large basket cell; MC, Martinotti cell; NBC, nest basket cell; HGC, neurogliaform cell; PC, pyramidal cell; SBC, small basket cell; SPC, star pyramidal cell; SSC, spiny stellate cell; DAC, descending axon cell; SAC, shot axon cell (adapted and based on Markram, 2010; Markram et al., 2004; Thomson and Larry, 2007).*

3.1.1.2. Excitatory neurons in layer 4

Layer 4 contains two broad classes of spiny excitatory cells: pyramidal cells with apical dendrites that extend into layer 1 and glutamatergic spiny stellate cells which lack prominent apical dendrites and are largely confined to layer 4, which receive most of their inputs within this layer (Lund, 1984), and are an important target population for direct thalamic innervations. The axons of layer 4 spiny neurons make a dense, topographically precise projection to layer 3 (and to upper layer 5) in rat and cat (e.g. Burkhalter, 1989) where they innervate pyramidal cells and (rather less commonly) interneurons (Thomson et al., 2002). Both pyramidal cells and spiny stellate cells contribute to these projections and both provide local and horizontal projections within layer 4. In layer 4 of cat visual cortex, some spiny cell axons make the majority of their synapses within layer 4, others form a larger proportion in layer 3 (Binzegger et al., 2004), where it has been stated that each layer 4 spiny neuron converge to 300-400 layer 3 pyramidal target cells.

3.1.1.3. Excitatory neurons in layer 2/3

Superficial layer 2/3 pyramidal neurons constitute the majority of cells in the neocortex (Zilles, 1990), though they are not easily divisible into separate morphological classes, as in the case of neurons in layer 4. Their morphology is similar to layer 5 pyramidal neurons – namely, possessing a triangular-shape soma – but the apical dendrite is thinner and shorter (Larkman et al., 1992). These differences in dendritic length and diameter have implications for their electrical compactness and integrative properties (Larkman et al., 1992; Zador et al., 1995). They are thought to be fundamental for cortical tasks such as feature selection and perceptual grouping (Grossberg and Raizada, 2000; Binzegger et al., 2004). Layer 2/3 neurons receive their inputs predominantly from other L2/3 pyramidal neurons and L4 spiny stellate neurons (Lubke et al., 2003; Binzegger et al., 2004). These inputs project almost exclusively to the basal and apical oblique dendrites. Inputs to the apical tuft are thought to be feedback connections from higher cortical areas and nonspecific thalamic nuclei (Felleman and Van Essen, 1991). These connections show synaptic depression, can elicit action potentials, and can be potentiated by theta-burst stimulation (Walcott and Langdon, 2002).

Pyramidal neurons in layer 2/3 collectively form a horizontal lattice of long-range, periodic axonal projections, known as the superficial patch system (Douglas and Martin, 2004). Layer 2/3 pyramidal axons, in all species studied, arborize primarily in layers 2/3, sending a descending axon towards layer 5, passing through layers 4 and 6, but ramifying little or not at all in these layers (Burkhalter, 1989). In so, monosynaptic recurrent connections between layer 2/3 pyramidal cells are likely to predominate more than in any other layer (e.g. Binzegger, 2004), which has been proposed to enhance the integration of stimulus features and to broad subthreshold receptive fields (Kaur et al., 2004). Pyramidal cells in these superficial layers receive also a large proportion of trans-callosal inputs directly from the other hemisphere (Porter and White, 1986). It is also known that interconnectivity between pairs of pyramidal cells in layer 2/3 is spatially scaled. In so, it was demonstrated that connected pairs of excitatory neurons share common inputs from middle-layer 4 and within layer 2/3. When adjacent neurons are not connected to each other, there is a lack of sharing of common inputs (Yoshimura et al., 2005). On the other hand, they share common inhibitory input and excitatory input from layer 5 regardless of their connectivity. The excitatory neurons within layer 2/3 therefore create preferentially connected subnetworks embedded within the laminar and columnar functional architecture.

It is worth mentioning that, in primates, even though these superficial cortical layers are treated as one entity, there are considerable differences between the cytoarchitecture and the anatomical connections between layer 2 and layer 3. In fact, layer 2 has a dense population of small pyramidal cells in addition to a diverse group of stellate neurons, and seems to be involved mainly in local processing, since most of its input/output connections are with flanking layers. On the other hand, layer 3 has a sparser population of larger pyramidal cells, fewer stellate cells and direct connections with layer 4 (Fitzpatrick wt al., 1983). More impressive is the fact that the anatomical distinctions between layers 2 and 3 are also reflected in single cell physiological properties. In accordance it was shown recently that in macaque monkeys engaged in a fixation task to sweeping visual stimuli, layer 2 neurons had smaller spikes, higher levels of ongoing activity, larger receptive field activating regions, and less finely tuned selectivity for stimulus orientation and length when compared to layer 3 neurons (Gur and Snodderly, 2008).

3.2. Recurrent connectivity: local circuitry is the heart of cortical computation

A surprising, but consistent pattern across all areas of neocortex examined is that the majority of synaptic inputs formed on the dendritic trees of any neuron originate from nearby excitatory neurons within the same cortical area, producing local microcircuits (Braitenberg and Schüz, 1998; Douglas and Martin, 2004; White, 2007). Very few synapses are contributed by long distance connections, whether they arise from neurons in subcortical nuclei (principally the thalamus) or other cortical areas. Thus, cortical neurons are connected in a series of nested positive and negative feedback loops, in a highly recurrent local circuitry. They provide the major excitatory input to neocortical principal neurons and are critically important for information processing (Douglas et al., 1989; Douglas and Martin, 2004, 2007b; Douglas et al., 1995; Buonomano and Maass, 2009). Recently, a comprehensive attempt to assign a source to every synapse in a single cortical area was made for the area 17 of the cat (Binzegger et al., 2004). It was shown that intralaminar excitatory connections are most prominent in layers 2 and 3, where the pyramidal neurons form most of their local excitatory synapses with each other, so much that their recurrent connections involve one-fifth of all the excitatory synapses. The consequence of this is that the recurrent connections between layer 2 and 3 pyramidal neurons predominate, whereas for other layers the interlaminar recurrent connections may have a greater role (Figure 3.3).

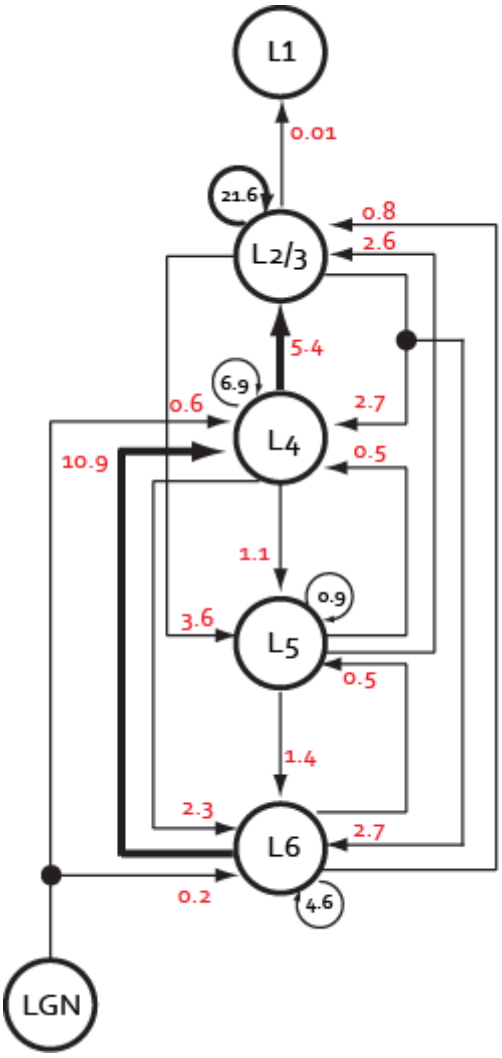

Figure 3.3. ***Quantitative map of the connections between various classes of excitatory neurons and their targets in the cortex.*** *Only the connections between the classes of the dominant excitatory neurons are shown in the diagram. Individual numbers that label each arrow indicates the proportion of all the excitatory synapses in area 17 of the cat that are formed between the various classes of excitatory neurons. A total number of synapses between excitatory neurons is estimated to be* 13.6×10^{10}*. Circles represent neurons located in different cortical layers, being "Lx" the layer in which its soma is located. LGN: thalamic lateral geniculate nucleus (adapted from Binzegger et al., 2004)*

This and other quantitative anatomical circuit data suggest a number of intriguing clues to the fundamental properties of cortical processing. The first is the dominance of local cortical synapses over the ones provided by individual afferents of a given cortical area. Overall, the vast majority of cortical excitatory synapses and virtually all inhibitory synapses originate from neurons within the local cortical space. This means that each of

the afferent projections of the cortex, either from the thalamus or other individual cortical areas, renders a surprisingly small percentage of all excitatory synapses in the target area. In fact, in the case of the visual cortex, synapses from the lateral geniculate nucleus of the thalamus form only 5-10% of the excitatory synapses, even in their main target layer 4, as seen in cats and monkeys (Usrey et al., 2000; Alonso and Swadlow, 2005). Yet these afferents clearly provide just enough excitation to drive the cortex. This raises three intriguing questions: first, why is the cortex connected to its principal thalamic nucleus by such a fragile and weak long-distance pathway? Second, how do the local cortical circuits reliably process the seemingly small input signals that arise from peripheral sensory organs, or within the cortex itself? And third, how is the fidelity of these signals retained as they are transmitted through the hierarchy of cortical areas? The answer might just lie in understanding the spatial and temporal relations of the local circuit, with its strong recurrent excitatory and inhibitory subcircuits. In fact, whether by single or by collective computation, recurrent local cortical connections provide the signal gain necessary for actively reorganizing the relatively small contributions of long-range afferents, by amplifying or suppressing those inputs (Douglas et al., 1995; Silberberg et al., 2005; Buonomano and Maass, 2009). This collective processing of transformations is thought to provide the signal restoration properties that allow significant signals to be "transformed" through many stages without detectable degradation (von Neumann, 2000). The positive feedback between neurons of one given population can be used to enhance the features of the input that match patterns embedded in the weights of the excitatory feedback connections. At the same time, the overall strength of the excitatory response of the population is used to suppress outliers via the inhibitory threshold imposed by interneurons, imposing in this way an interpretation on an incomplete or noisy input signal (Hahnloser et al., 2002; Douglas and Martin, 2007).

A second clue is the large fraction of excitatory connections made between pyramidal cells of the superficial cortical layers (Figure 3.3). Although excitatory neurons in other layers also receive input from their neighbours, it is only in the superficial layers that the pyramidal neurons make very extensive arborizations within their same layer (DeFelipe and Fariñas, 1992). Indeed, nearly 70% of excitatory input to a superficial pyramidal neuron is derived from other cells of its own type (e.g. Thomson et al., 2002). Consequently, recurrent connections between layer 2 and 3 pyramidal neurons, in which

a target neuron projects back to its source neuron in a tight positive feedback loop, are more likely than in any other layer. In so, a positive feedback might play a crucial role in cortical computation by providing gain for active selection and re-combination of the relatively small afferent signals (Douglas et al., 1995; Douglas and Martin, 2007).

The gain of a system is the (dimensionless) ratio of the magnitudes of two causally related signals. When considering a feedback system, like the one present in a given cortical layer, two different gains are usually considered. The first is the overall 'system gain'. This is measured as the ratio of the output over the input of the system. The second is the 'loop gain'. This is measured around the feedback loop, and can be expressed as the fraction of the output signal that is due to feedback. Thus, when the loop gain is zero, the system gain is entirely feedforward. As the loop gain approaches one, the system gain becomes dominated by its feedback. If the loop gain exceeds one, the system is unstable and its output diverges. The feedforward gain of individual neurons operating in rate mode is small. Typically, many input spike events must be applied to a neuron before it produces a single spike output. However, simulation studies and physiological evidence suggest that cortical circuits can generate significant system gain by the positive feedback excitation mediated by recurrent intracortical axonal connections (Hahnloser et al., 2000; Binzegger et al., 2004) (Figure 3.3). Positive feedback amplification may seem intrinsically dangerous, but neurons arranged in a positive feedback loop can be stable if the sum of the excitatory currents evoked by the afferent input and the positive feedback excitatory currents is less than the total negative current dissipated though their membrane leak conductances. It is this positive feedback amplification that allows a small input signal, like the one arriving from the thalamus, to be 'heard' in the cortex. The question is, of course, how is this small signal ever distinguished from "spontaneous" cortical activity? Artificial network models have been invaluable in providing answers for the properties of recurrent networks. One of the most prominent of these is the auto-associative or "Hopfield network" model (Hopfield, 1982). In this model it is hypothesized that recurrent networks of ideal neurons are dynamical systems whose stable patterns of activation (or attractors) can be viewed as memories, which store externally presented sensory inputs through the modification of recurrent excitatory synapses, according to a Hebbian rule (see Chapter 3.4).

Overall, the basic computation properties that a local recurrently connected circuit can perform is illustrated in Figure 3.4. The excitatory neurons receive feedforward excitatory connections that carry the input signal, feedback excitatory connections from other members of their population, and feedback inhibitory connections from the inhibitory neurons (see Figure 3.3). Often their recurrent connection strength is regular, which typically is expressed as a hill-shaped function of distance of a source neuron from its target. The properties illustrated in Figure 3.4 arise out of the interaction between the feedback excitation, which amplifies the inputs to the network, and the non-linearity introduced by the inhibitory threshold, which itself depends on the overall network activity. At the end, the important result to note here is that the positive feedback enhances the features of the input that match patterns embedded in the weights of the excitatory feedback connections, while the overall strength of the excitatory response is used to suppress outliers via the dynamical inhibitory threshold imposed by the global inhibitory neurons. In this sense, the network can actively impose an interpretation on an incomplete or noisy input signal by restoring it towards some fundamental activity distribution embedded in its excitatory connections - this is the cortical “hypothesis” (Douglas and Martin, 2007; 2007b).

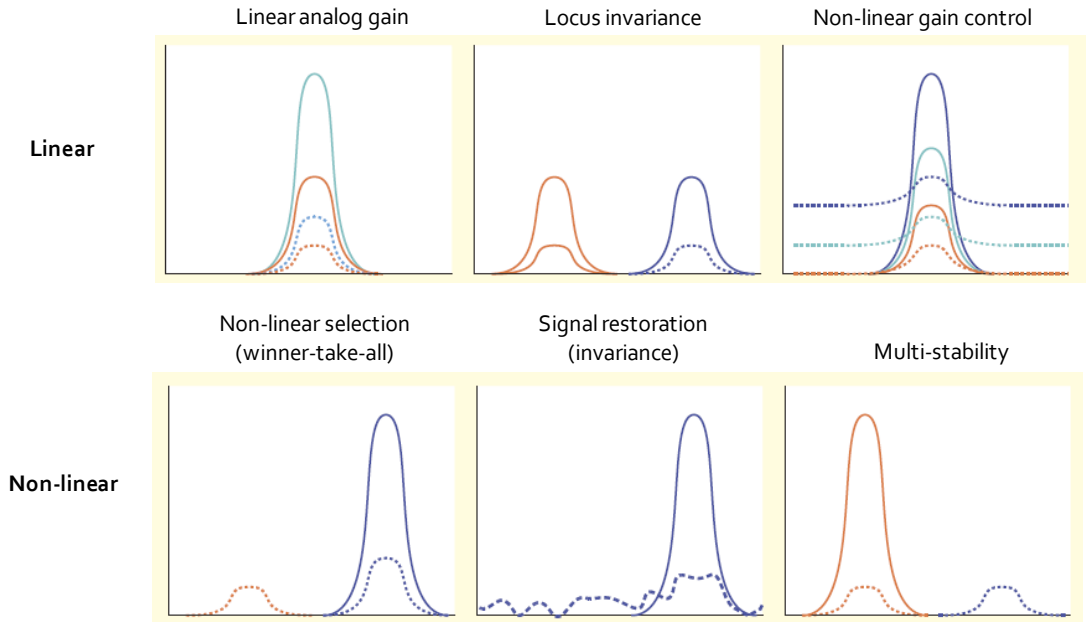

3.3. Overall anatomical model of cortical function

A cortical column represents a distinct functional module that processes electrical signals arriving from sensory inputs (Mountcastle, 1997). A simplified but comprehensive model which tries to put forward a tentative hypothesis of how the generic circuits might express themselves functionally is the following: In a laminar-temporal evolution of interactions between the main types of cortical neurons, it is generally assumed that thalamic afferents relay information onto glutamatergic spiny stellate and inhibitory small basket cells in layer 4 (Murray Sherman and Grillner, 1996). Next, the stellates activate pyramidal neurons present in both layers 2 and 3, and basket cells present in layer 3. The superficial pyramidal cells activate the pyramidal cells of layer 5, the main output layer of the neocortex, which in turn activate those of layer 6. Importantly, they also activate the vertically disposed inhibitory double bouquet cells, which could dynamically determine the input-output relations, computed by the dendrites of various layer 2/3 pyramidal neurons that they contact. The layer 6 pyramidal cells project to layer 4, where their wide arbors combine with the thalamic afferents to shape activation of layer 4 spiny stellates (see Douglas and Martin, 2004, 2007; Thomson and Bannister, 2003; Thomson and Lamy, 2007).

Figure 3.4. ***Basic computations that a recurrent circuit formed by lateral connections could perform.*** *Top left; Linear analog gain: above threshold, the network amplifies its hill-shaped input (dashed lines) with constant gain (output, solid lines). Top center; Gain invariance: this occurs when the gain remains the same across the map (provided that the connection weights are homogeneous across the array). Top right; Gain modulation: the gain of the network can be modulated by an additional constant input applied to all the excitatory neurons, and superimposed on the hill-shaped input. The gain is least when no constant input is applied (input, red dashed line; output, red solid line), and largest for a large constant input (blue lines). Bottom left; Winner-take-all: when two inputs of different amplitude are applied to the network, it selects the stronger one. Bottom center; Signal restoration: the network is able to restore the hill-shaped input, even when that input is embedded in noise. Bottom right; Bistability: when separate inputs have the same amplitudes, multistability is the operation that selects one input according to its initial conditions at the time the input is applied (adapted from Douglas and Martin, 2007; Maass, 2000; Hahnloser et al., 2000).*

Clusters of superficial pyramidal neurons receive feedforward excitatory input from subcortical, inter-areal, and intra-areal sources. In addition to their interactions with their close neighbours within their patch, the members of this patch also receive feedback from a number of sources including deep pyramidal cells immediately beneath them or in close proximity within the superficial layers, and from subcortical inter-areal connections (Thomson et al., 2002). Thus, the neurons of a superficial cluster, taken as a group, receive a sample of thalamic inputs (some preprocessed by layer 4), a sample of inputs from surrounding and remote superficial neurons, and a sample of the output of their corresponding deep pyramidal neurons. All of these inputs are processed by the dendrites of the superficial pyramids whose signal transferring properties can be adjusted dynamically by the pattern of the vertical inputs from other interneurons (e.g. double bouquet cells). The superficial pyramids collectively participate in a selection network, mediated by the horizontal inputs from inhibitory cells that control their outputs (e.g. basket and chandelier cells). The selection mechanism is a soft winner-take-all (or other integrative mechanism), which is an important element of many neuronal network models (Maass, 2000, Riesenhuber and Poggio, 1999). The outputs of the selected superficial pyramids feedback to adapt the pattern of vertical inhibitory cell activation (see Figure 3.3). In this way, the superficial layer neurons cooperate to explore all possible interpretations of input, and so select an interpretation consistent with their various subcortical inputs. The superficial layers are organized to distribute and explore possible interpretations, whereas the deeper layers are organized to exploit the evolving interpretations. The pyramidal neurons of layer 5 that drive subcortical structures involved in action (e.g. basal ganglia, colliculus, ventral spinal cord) decide the output of the cortical circuits (Kasper et al., 1994). The same layer 5 pyramidal neurons influence the ongoing input by their connection to layer 6 pyramidal cells that connect to the thalamic input layers. The explorative processing in the superficial layers is constrained via the recurrent projection from other layer 5 pyramidal cells to confirm the output that has already been decided on. These layer 5 pyramidal cells are also the origin of the feedback projections to the superficial layers of other cortical areas (Markram, 1997). In this way, they also provide additional contextual information to the evolving interpretations occurring in the superficial layers of other cortical areas.

3.4. Connectivity features of the mammalian auditory cortex

Sensory cortical maps can be freely defined as systematic spatial distributions of sensory information within a cortical region, being representations of peripheral receptor epithelia, stimulus parameters, sensory objects, or events of the external environment. Fine-tuning the thalamic inputs via a variety of functionally different synapses across the columnar six layers is the way that sensory cortices perform sensory-guided sophisticated behavior tasks.

The most widely recognized functional organization principle in mammalian primary auditory cortex (A1) is the representation of the auditory receptor surface, the organ of Corti in the cochlea (Merzenich et al., 1975) The orderly representation of frequency, sound location, amplitude, frequency modulation, or sharpness of tuning describes the tonotopic order seen in cochleotopic maps (for review see Schreiner and Winer, 2007). This systematic progression of neuronal response preferences to near-threshold pure tone frequencies across cortical space is part of a general topographic governing principle that has been also shown for other sensory modalities (e.g. visual, somatosensory) in all studied mammals so far (e.g. Wandell and Smirnakis, 2009; Petersen, 2007).

In the mouse, high frequencies are represented in the rostral part of the cortex and low frequencies in the caudal (Stiebler et al., 1997). However, because the representation of sound frequency along the cochlea is intrinsically one-dimensional, the organization of auditory cortex along the axis orthogonal to the tonotopic cortical axis cannot immediately be inferred from the organization of the sensory periphery. The auditory cortex is thus functionally anisotropic: the functional organization along the tonotopic axis is qualitatively different from the organization orthogonal to the tonotopic axis (Oviedo et al., 2010). Nevertheless, the fact that smooth and orderly maps of the periphery are preserved throughout the chain of successive nuclei up to primary cortical areas seems to argue for their general usefulness. The efficiency of a given cortical map is that it minimizes connectivity, reduces redundancy and enhances computational power by eliminating conflicting demands and coordinating multiple algorithmic transformations (for review see Chklovskii and Koulakov, 2004).

But are neurons in auditory cortex organized into functional columns as the other sensory modalities counterpats? Recently it was suggested that auditory cortex might possess a fractured tonotopy (Rothschild et al., 2010; Bandyopadhyay et al., 2010). By using in vivo two-photon calcium imaging, a method previously used to map the fine-scale organization of circuits in the visual (Okhi et al., 2005, 2006) and barrel (Sato et al., 2007) cortex, it was shown that tonotopy in A1 lacked the smooth, graded tiling, and single-cell gradations of tuning observed in visual cortex. However this does not imply that frequency is discarded as an organizing principle in A1. In fact, Rothschild et al. found that nearby neurons with similar patterns of driven, sound-evoked discharge also co-varied in their spontaneous activity. This result could be explained by the presence of partially overlapping subnetworks in A1 (Bathellier et al., 2012), or due to the presence of fine-scaled assemblies that process inputs in a different way. Such parallel and ascending auditory processing streams may be selective for different input features or specific stimulus attributes, recruiting different neuronal populations with different interconnectivity and possibly different synaptic strengths and dynamics (Bandyopadhyay et al., 2010). According to this view, similarly frequency tuned neurons (which probably receive common thalamic input) are distributed semi-randomly in local patches of A1, and interdigitated with other such populations. In addition to sharing common input, members of each subnetwork may also be strongly and selectively interconnected (see Barbour and Callaway, 2008). This interpretation is by itself consistent with *in vitro* mapping studies of visual cortex that show selective synaptic connections between layer 2/3 pyramidal neurons with common layer 4 inputs (Yoshimura et al., 2005). Another explanation might reside in the fact that although thalamocortical projections are arranged tonotopically, tonotopy in A1 becomes fractured due to intrinsic intracortical processing (see Hackett et al., 2011). Taken together these studies point to the careful conclusion that although there is some degree of gross tonotopy in the rodent auditory cortex, neurons do not seem to be organized into functional columns: nearby neurons can respond quite differently to the same stimulus (Rothschild et al., 2010; Bandyopadhyay et al., 2010; Hromádka et al., 2008).

And how is the functional anisotropy - that is, the spatial arrangement of tuned neurons - reflected at the microcircuit level? In many sensory cortices, the distinction between, for instance, pyramidal neurons in layer 2/3 are not properly made, giving rise to a misleading conception of a single homogenous functional “unit”. However in primary

auditory cortex neurons in these two layers are indeed distinct with respect to morphology, connectivity and function. Morphologically, layer 3 neurons have a classic pyramidal shape, while layer 2 neurons cells lack an elongated apical shaft, but both have dendrites that arborize in layers 2 and 1 (Barbour and Callaway, 2008). At the level of local connectivity, the pattern of intracortical synaptic input is also distinct between these layers, especially along the tonotopic axis: layer 2 receives intra-columnar input, whereas L3 received out-of-column input (Oviedo et al., 2010). Furthermore, neurons in layer 3 but not in layer 2 project to the contralateral side of the cortex, as observed in the auditory cortex of the cat and rat (Imig and Brugge, 1978; Games and Winer, 1988).

Finally, neurons in the two layers may be functionally distinct with respect to their responsiveness to simple auditory stimuli such as pure tones and white noise. Layer 2 neurons are more responsive and show well-defined frequency tuning to pure tones, whereas layer 3 neurons are largely unresponsive (Oviedo et al., 2010). This difference in responsiveness is consistent with recent results, using photostimulation-assisted identification of neuronal populations, showing that contralaterally projecting layer 3 neurons are not responsive to simple auditory stimuli (Lima et al., 2009). These observations are in agreement with the fact that nearby neurons are not driven by the same optimal stimuli, giving rise to the characteristic sparseness of representations in the auditory cortex (Hromádka et al., 2008).

Generally, A1 is characterized by strong excitatory connections from the thalamic recipient layer 4 to layers 2 and 3, where a strong intracortical recurrent excitation exists. Current anatomical and physiological observations provide evidence that the inputs and outputs of layer 4 excitatory neurons in area A1 differ from those in somatosensory and visual cortices. In particular, pyramidal neurons from layers 2 and 3 typically arborize their axons within layer 4, providing a fast intracolumnar feedback mechanism (Barbour and Callaway, 2008). Such connections may play an important role in rapidly creating auditory stimulus specificity in cortical neurons (Kaur et al., 2004) or generating specialized receptive field structures not found in other sensory areas, such as intensity tuning (Wehr and Zador, 2003). Furthermore, nearly all layer 4 spiny neurons project out of A1 to extrinsic targets, reflecting a direct feedback pathway form layers 2/3 to layer 4 that is extremely sparse or absent in other primary sensory

areas (e.g. Binzegger et al., 2004). This finding implies that these neurons provide a more direct and possibly more rapid relay between cortical input and output than layer 4 neurons in other primary sensory cortical areas, which tend to have exclusively local projections (Lund, 1984).

3.5. Optogenetics and neural circuits

Optogenetics, as the term has come to be commonly used, refers to the integration of optics and genetics to achieve gain- or loss-of-function of well-defined events within specific cells of living tissue (e.g. Scanziani and Häusser, 2009). Nowadays, proteins with engineered sensitivities to light (derived from microbial opsin genes) (e.g. Nagel et al., 2003) are infiltrating the biological mechanisms by which neurons generate and detect electrochemical signals. Encoded in DNA and active only in genetically specified target cells, these proteins provide selective optical interfaces for observing and controlling signaling by defined groups of neurons in functioning circuits, either in freely moving mammals (e.g. Huber et al., 2008) or other *in vitro* intact-system preparations (e.g. Petreanu et al., 2007;). So routinely they are, they became ubiquitous. In fact, since the initial (unrelated) identification of bacteriorhodopsin as a microbial single-component light-activated ion pump (Oesterhelt and Stoeckenius, 1973), that new members of this microbial opsin family have been discovered. These include membrane-bound ion pumps and channels such as halorhodopsins (Matsuno-Yagi and Mukohata, 1977) and channelrhodopsins (Nagel et al., 2003) that transport various ions across the membrane in response to light. However, in neuroscience research, millisecond-scale precision is essential to true optogenetics, to keep pace with the known dynamics of the targeted neural events such as action potentials and synaptic currents. This obstacle was overcome recently, when it was successfully demonstrated that the introduction of a single-component microbial opsin gene into mammalian neurons can result in reliable sustained control of millisecond-precision action potentials (Boyden et al., 2005). This primordial discovery paved the way for the perfectioning of a new set of optogenetic tools used in the investigation of neural circuits.

The variety of optogenetic spectra available at the moment contains tools for four major categories of fast excitation, fast inhibition, bistable modulation, and control of intracellular biochemical signaling in neurons and other cell types (for review see Yizhar et al., 2011). This array of optogenetic tools, which is the result of molecular engineering and genomic efforts, allows experimental manipulations focused for 1) the desired physiologic effect, 2) the desired kinetic properties of the light-dependent modulation and 3) the required wavelength, power, and spatial extent of the light signal to be deployed.

3.6. Channelrhodopsin as a tool to assess neural circuitry

Channelrhodopsin-2 (ChR2) is a seven-transmembrane-helix protein from the unicellular green algae *Chlamydomonas reihardtii* that opens as a non-selective cation channel upon the concomitant binding of *all-trans*-retinal and activation by blue light photons (Nagel et al., 2003). In dissociated hippocampal neuron cultures, the rapid light-activated photocurrents, due to the influx of cations into cells expressing ChR2, leads to depolarization and initiation of action potentials with short delay and minimal jitter (Boyden et al., 2005; Gunaydin et al., 2010). ChR2 has been successfully used in a variety of model systems to investigate the function of complex neuronal networks by stimulation of genetically targeted neurons (Boyden et al., 2005; Cruikshank et al., 2010; Petreanu et al., 2007; Adesnik and Scanziani, 2010; Choi et al., 2011).

In mouse slice physiology, namely the interrogation of neuronal circuitry, ChR2 opens the door to novel types of experiments and greatly extends the technical possibilities offered by traditional electrophysiology. In this approach, the experimenter often tries to control firing of individual action potentials with high temporal precision to investigate processes that typically operate on millisecond time scales. ChR2-based stimulation opens the possibility to stimulate distributed populations of genetically defined neurons using light, allowing drawbacks of slowness of multiple intracellular recordings (Homlgren et al., 2003; Thomson and Bannister, 2003), or even the lack of neuronal specificity when using photoactivation of groups of neurons by glutamate uncaging (Yoshimura and Callaway, 2005), to be overcome. In ChR2-assisted circuit mapping, photostimulation is combined with whole-cell recordings. Circuits are mapped between

presynaptic neurons, defined by ChR2 expression, and postsynaptic neurons, defined by targeted patching. Remarkably, even ChR2-positive axons that are severed from their parent somata can be photostimulated to fire action potentials (Petreanu et al., 2007). This means that ChR2 can be used to map long-range projections. For example, ChR2 has been used to map callosal projections linking left and right somatosensory cortex (Petreanu et al., 2007), or to map circuits from the olfactory bulb to the olfactory cortex *in vivo* (Arenkiel et al., 2007). ChR2 thus allows the mapping of synaptic connectivity over all spatial scales in the brain.

When specific ChR2 expression in neuronal populations *in vivo* (e.g. Arenkiel et al., 2007) is combined with behavioural studies, then ChR2 photostimulation allows precise tests of hypothesis about how patterns of action potential in genetically target neurons contribute to behaviour outputs. In so, the first approach to induce learning by optogenetically activating modulatory neurons has been made in *Drosophila* larvae (Schroll et al., 2006). Specific and combined activation of ChR2-expressing dopaminergic, or tyraminergic and octopaminergic neurons could be used to render an attractive / aversive behaviour towards a given odor. Recently, the behavior-reinforcing properties of dopaminergic neurons for aversive learning were demonstrated optogenetically in adult flies as well (Claridge-Chang et al., 2009). On the other hand, in mice, light-induced activation of dopaminergic neurons has been implicated in reward learning tasks (Tsai et al., 2009). Moreover, it has been shown that periform cortical neurons could be entrained to elicit different olfactory-based discrimination tasks (Choi et al., 2011), or even a sparse subset of supragranular cortical pyramidal neurons is sufficient to guide detection performances (Huber et al., 2008). Even more interesting, it was shown to be possible to elicit a freezing behaviour output by direct activation of a sparse but specific ensemble of hippocampal neurons that was previously active during learning (Liu et al., 2012). One can easily appreciate that the potential impact of ChR2 can hardly be overstated.

If ChR2 is used to elicit action potentials in neurons, light-induced depolarization has to reach the firing threshold. Owing to the small single-channel conductance of ChR2 (Bamann et al., 2008), expression levels required for reliable action potential induction are quite high. This small drawback can be overcome by substituting mammalian codons to replace algal codons in order to achieve higher expression levels (humanized

ChR2 or hChR2; e.g. Zhang et al., 2007), and this process is now typically applied to all new opsin genes. However, when ChR2 is expressed at high levels, extra spikes (for example, doublets), can occur in response to a single light pulse (Boyden et al., 2005), with potential implications as doublets may be important for neural coding. Second, many cells cannot follow ChR2-driven spiking above the gamma (~40 Hz) range) in sustained trains (Lin et al., 2009), preventing the access to a broad and important neural signaling band. Finally, rapid optically driven spike trains can cause incidental upstates with information-processing implications. The recently reported accelerated ChR2 variants, with faster recovery kinetics from inhibition, could resolve the intrinsic disadvantages of the wild-type ChR2 construct (Gunaydin et al., 2010). These novel variants should thus enable for experiments attempting to mimic natural spiking. Since accelerated ChR2 variants typically produce smaller photocurrents (Gunaydin et al., 2010), special care has to be taken to achieve high expression levels for reliable action potential induction.

At the end, an important focus of current efforts is the engineering or identification of spectrally shifted channelrhodopsins (Zhang et al., 2008). Dual or even multicolor control of different optogenetic agents will allow probing of the contributions of distinct neuronal populations to phenomena ranging from dendritic integration to behaviour. The challenge will be to alter the action spectra without compromising channel conductance, kinetics or expression levels. Moreover, would be interesting to target ChR2 to specific regions of the cell (Lewis et al. 2009) or to intracellular organelles. Given the range of possibilities, the optogenetic revolution might have only just begun.

4. Aim

The aim of the present study was to investigate the features of the excitatory synaptic local circuitry in the adult auditory cortex. Though extensive data have been produce, especially in juvenile / young animals, a hiatus of information is still present regarding the full mature cortex.

Two major questions were posed in this thesis: what are the main features that can describe local synaptic connectivity in naïve mice? And to what extent is cortical local circuitry molded by optogenetic stimulation during a learning task? Currently, electrophysiological recordings in brain slices provide the highest-resolution technique for analyzing functional interactions between individual neocortical neurons.

The aim of the first part was to provide a general quantitative description of intrinsic properties and connectivity features of pyramidal neurons in the adult mouse auditory cortex. It is important to study these features to obtain insight into possible circuit mechanisms leading to the emergence of sound-evoked activity patterns that are studied in our laboratory *in vivo*. Simultaneous quadruple whole-cell recordings from layers 2/3 and 5 pyramidal neurons were made to describe features such as intrinsic excitability, connection probability, distribution of synaptic weights, variability in synaptic transmission, and patterns of connectivity of excitatory connections.

The aim of the second part was to analyze the relative contribution of excitatory and inhibitory inputs to pyramidal neurons in the adult mouse auditory cortex. Extracellular stimulation of two independent but convergent input pathways onto layer 2/3 pyramidal neurons in combination with whole-cell voltage-clamp recordings at various holding potentials were used to disentangle excitatory and inhibitory synaptic components with high temporal precision.

The aims of the third part were twofold: first, to establish a learning paradigm in mice that is based on cues delivered by direct optogenetic stimulation of auditory cortex neurons. Second, to use this paradigm to analyze possible effects of the optogenetic stimulation on intrinsic excitability and/or synaptic transmission in brain slices prepared from optogenetically trained mice.

5. Experimental Procedures

5.1. Experimental subjects

A total of 92 in-house bred adult (8 – 12 weeks old) male C57Bl/6J mice were used for this study. After weaning on the 21st day mice were group housed (a total of 5 mice per cage), maintained on a 12 h: 12 h light/dark cycle with food and water *ad libitum*, except during the behaviour procedures. Constant background noise from radio broadcasting was present during the day. All experiments were conducted during the light phase cycle, starting time of one experiment being the same every day. All procedures were conducted in accordance with the Austrian laboratory animal law guidelines for animal research and have been approved by the Magistratsabteilung 58 of the Wiener Landesregierung, Vienna, Austria.

5.2. Slice preparation

On a given day, one mouse was sacrificed by quick cervical dislocation, decapitated and the brain rapidly removed from the skull. The brain was then immersed (approximately for 1 minute) in ice-cold oxygenated (95% O_2 / 5% CO_2) dissection solution containing (in mM) 110 choline chloride, 25 $NaHCO_3$, 1.25 NaH_2PO_4, 2.5 KCl, 0.5 $CaCl_2$, 7 $MgCl_2$, 11.6 ascorbic acid, 3.1 pyruvic acid and 25 D-glucose (final pH≈ 7.4). Two coronal cuts were made to remove a small anterior portion of the brain and the cerebellum, respectively. The brain was then fixed, anterior surface down, to the specimen plate using cyanoacrylate glue (Roti coll 1) and submerged quickly afterwards in the buffer tray filled with ice-cold oxygenated (95% O_2 / 5% CO_2) dissection solution as previously. Acute coronal whole-brain slices (300 μm-thick) were made using a vibratome (Leica VT1200S, Germany) at a speed of 0.12 mm/second. Slices were then transferred to a resting chamber filled with standard artificial cerebrospinal fluid (ACSF) composed of (in mM) 118 NaCl, 2.5 KCl, 26.5 $NaHCO_3$, 1 NaH_2PO_4, 1 $MgCl_2$, 2 $CaCl_2$ and 20 D-glucose, aerated with 95% O_2/ 5% CO_2, for 30 minutes at a temperature of 33°C, and subsequently maintained at room temperature throughout the experiments.

5.3. Electrophysiology

One individual slice was transferred to a submerged slice recording chamber where it was gently immobilized by a silver grid with attached nylon mesh. The grid was placed orthogonal to the cortical layers to prevent damaged of the dendritic trees that run perpendicular towards the pia. Excitatory layer 2/3 and layer 5 pyramidal neurons (identified according to their morphology and laminar location) localized between 50 – 70 μm below the surface of the brain slice were visualized with an upright microscope (Olympus BX51WI, Germany) equipped with infrared (IR) video microscopy and differential contrast optics, through a 40x/0,8NA water immersion objective. At this high magnification, excitatory pyramidal neurons were identified by a distinct apical dendrite that extended toward the pial surface parallel to the slice surface, indicative of a minimal damage of the dendritic arborizations during dissection. Patch pipettes were pulled from borosilicate glass (2.0mm outer and 1.16mm inner diameter glass, Warner Instruments) on a Flaming/Brown micropipette puller (Sutter Instrument, Novato, CA), yielding a final resistance of 3 – 5 MΩ. The pipette intracellular solution contained (in mM) 130 K-gluconate, 5 KCl, 2.5 $MgCl_2$, 10 HEPES, 0.6 EGTA, 4 Na_2ATP, 0.4 Na_3GTP and 10 Na_2-phosphocreatine (pH = 7.25 adjusted with KOH; 290 mOsm) and it was kept frozen for a maximum period of two weeks until use. Simultaneous whole-cell patch-clamp recordings in current-clamp or voltage-clamp modes were acquired from the somata of up to four neurons with Multiclamp 700B amplifiers (Axon Instruments, Molecular Devices, Foster City, CA). In some cases, one or two breakthroughs failed, thus yielding triple or double recordings; synaptic connections found in these cases were included in the dataset. Neurons were excluded for further analysis if, after reaching whole-cell configuration, access resistance was higher than 20 MΩ, membrane potential higher than -55 mV and if did not presented characteristic firing patterns of pyramidal neurons (Agmon and Connors, 1992; Huggenberger et al., 2009). Electrophysiological data was low-pass filtered using the 10 and 3kHz four-pole Bessel filter, sampled at 10kHz (Digidata 1440A, Axon Instruments) and collected using pClamp10 software (Molecular Devices, Inc., USA). Offline analysis of the following intrinsic neuronal properties were made using the data analysis software Clampfit 10.2 (Molecular Devices, Inc., USA): resting membrane potential (V_m), input resistance (R_i), action potential (AP) threshold, AP amplitude from threshold to peak, AP overshoot and AP half-weight width. To characterize neuronal AP firing patterns, a series of 500 ms

current pulses were applied in 20 pA steps starting at –40 up to a maximum of 340 pA. Membrane resistance (Rm) was measured at -20 pA current injection step using Ohm´s law. Membrane potential measurements were not corrected for the liquid junction potential and voltage drops across the patch pipette were compensated when recording in current-clamp mode. EPSP latency (in ms) was defined as the time difference between the presynaptic AP peak and the onset of the EPSP and the time-to-peak was taken as the time difference between EPSP maximum and its onset. All the recordings were carried out at room temperature and the slices were continually superfused in a closed circuit with ACSF oxygenated with 95% O_2 /5% CO_2.

5.4. Measurement of synaptic connection strengths

To determine whether pairs of neurons were monosynaptically connected, a precisely timed double AP was evoked in one neuron at a time by means of two suprathreshold depolarizing current pulses (2 ms pulse width, 50 ms interpulse interval, 3500 pA amplitude each), while recording the membrane potential of the other neurons. Each double AP stimulation impinged onto the neurons started 2 seconds after the end of the previous one, to avoid overlap of stimulation between the individual neurons (Figure 5.1). Mean traces were obtained by averaging 60 consecutive 8 seconds-duration trials, and all the kinetics parameters from the EPSPs were obtained from the final averaged trace (only the 1^{st} EPSP was considered for this purpose). In case of transient fluctuations of the seal, trials with depolarized traces were discarded before computing the averaged trace.

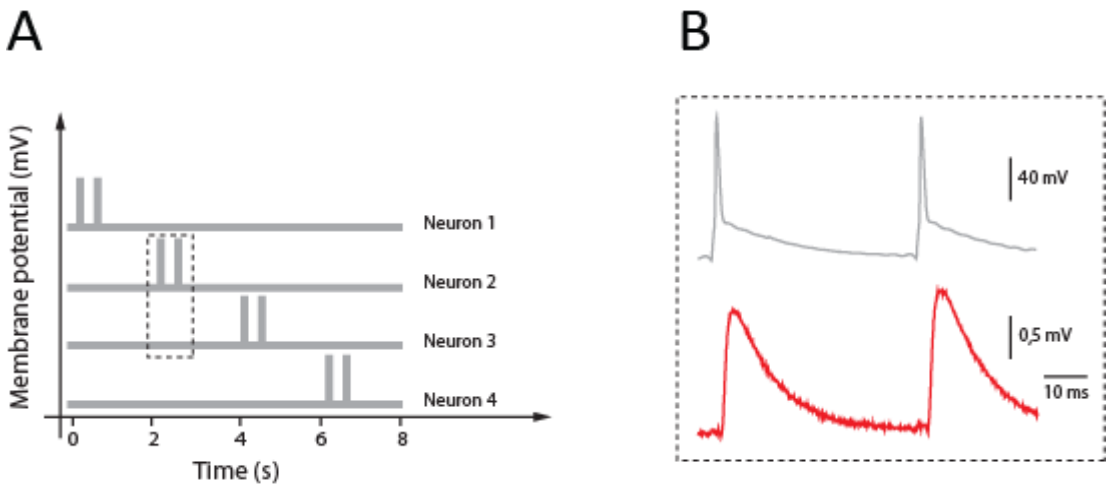

Figure 5.1. ***Stimulation and recording procedure. A)*** *Schematic representation of the waveform used to probe for synaptic connectivity. By injecting two brief 5 ms depolarizing current pulses (grey traces), 50 ms apart, a double AP is evoked in each of these neurons in turn, while recording the membrane potential of the other neurons along a 8 second-duration trial. A total of 60 consecutive trials were considered for average.* ***B)*** *Inset from panel A: time-locked EPSP (red trace) to the occurrence of the double presynaptic APs (grey trace), indicative of a pair of synaptically connected excitatory neurons. Note the difference in scale amplitude for both events.*

To assess if presynaptic stimulation successfully evoked a EPSP (and its amplitude), i.e. two neurons are connected, a comparison was made between the mean voltage across a 2 ms-long time window around the maximum peak of the EPSP and the previously computed baseline (Figure 5.2) for all the 60 individual trials. The baseline consisted as the mean value (in mV) from a 2 ms time-window placed immediately before the first current injection.

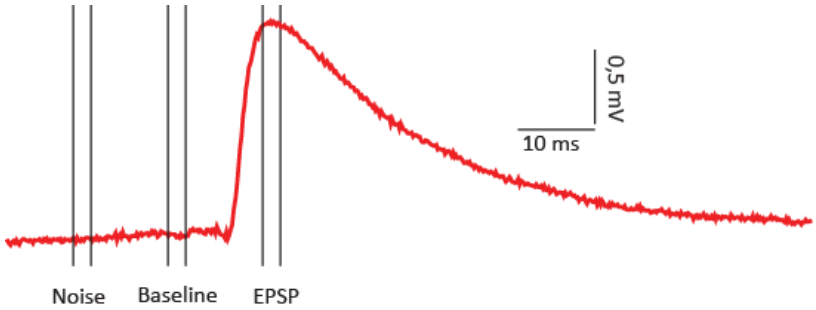

Figure 5.2. ***EPSP amplitude and reliability measurements.*** *Representative monosynaptic EPSP averaged trace (red) from an individual experiment. Three time-window events were considered for further analysis: "EPSP" denotes the maximum amplitude centered time-window; "Baseline" is placed immediately before the onset of the presynaptic AP; "Noise" denotes a time-window used for assessment of the intrinsic electrophysiological variability in the recordings. All the three time-windows have the same 2 ms-width and the same gap interval between them, and were individually assigned for each of the experiments performed. The width of all three time windows was left unchanged for the entire 60 individual trials.*

The significance of the differences between the mean values (in mV) across the 60 individual trials was evaluated by the paired Student's t-test. Values of $p < 0.02$ were considered to represent statistically significant differences and indicative of a synaptic connection between a pair of neurons. An estimation of the intrinsic variability of the recording ("noise") was assessed by another 2 ms-duration time window placed before the baseline event, and a comparison between the mean values (in mV) of both events was made. Care was taken that the time interval between baseline and the EPSP, and between baseline and the "noise" was exactly the same for both situations. When assessing about the coefficient of variation (CV; standard deviation divided by the mean) of EPSP amplitude, a comparison between the amplitude of the EPSP and the baseline was made across the individual 60 trials as well. As the averaged EPSP waveforms were time-locked to the presynaptic AP, the signal-to-noise ratio was good enough to allow for detection of synaptic connections with amplitudes as low as 0.01 mV.

The connection probability (CP), a measure of connection likelihood over all possible connections tested (assuming that they are independent events), was defined as:

where NC represents the total number of connections found, while NPC stands for the total number of possible connections, which ultimately depends on the number of neurons patched.

An analysis of single trials was also performed to determine the failure rate of a given connection. A failed event was defined as such when a presynaptic AP fails to induce a postsynaptic response. A comparison was made between each individual trial across the "EPSP" and the "noise" time windows. If for a given trial the EPSP value (in mV) was below 2 standard deviations (SD) from the mean value (in mV) of the "noise" window across the entire 60 sweeps, that trial was considered to be a failed event. Failure rate (FR) was thus defined as:

5.5. Spontaneous EPSPs analysis

An analysis of amplitude and frequency of spontaneous excitatory postsynaptic potentials (sEPSPs) was carried out using the built-in pattern-matching Template Search from Clampfit 10.2 (Molecular Devices, Inc., USA). sEPSPs events vary mostly in amplitude, but not in shape, thus are suitable for detection by the scalable shape-based algorithm. For analysis, a template was made by averaging 100 representative hand-picked spontaneous EPSPs randomly chosen (Figure 5.3). Approximately 1550–4200 spontaneous events over a period of 1.5 min were analyzed in the different experimental groups of mice, from which the frequencies of occurrence (number of events/s) and amplitude (mV) were obtained.

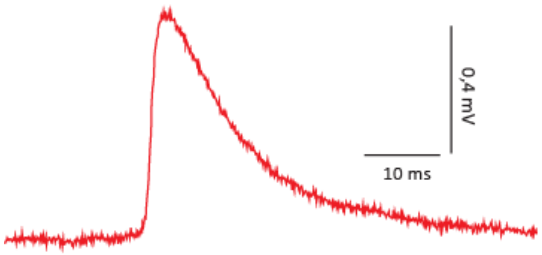

Figure 5.3. ***Spontaneous EPSP template.*** *One hundred representative and randomly chosen spontaneous EPSPs were used to built the template used for detection of neuronal spontaneous activity*

5.6. Test for overrepresentation of reciprocally connected neurons

To test for overrepresentation of reciprocal connections, a statistic was used based on how the observed counts compare with the expected counts, if an independent connection probability *p* between pairs of neurons is assumed. To generate a bootstrap distribution for the dataset with *N* total shuffled pairs of connected neurons tested, an ensemble of 10000 trials of *N* samples each from the dataset with replacement was made. The statistics from these trials formed the bootstrap distribution.

5.7. Extracellular stimulation

Postsynaptic currents (PSCs) were evoked with two bipolar platinum/iridium cluster microelectrodes (12.5 μm diameter; FHC, Bowdoin, USA), by stimulating two independent and convergent pathways into layer 2/3 pyramidal neurons. One electrode was placed vertically in relation to the recorded neuron, in cortical layer 4, while the other electrode was placed laterally, in layer 1, the upper most cortical layer consisting mostly of the distal tufts of pyramidal cell apical dendrites and many axons (Hubel, 1982) (Figure 5.4).

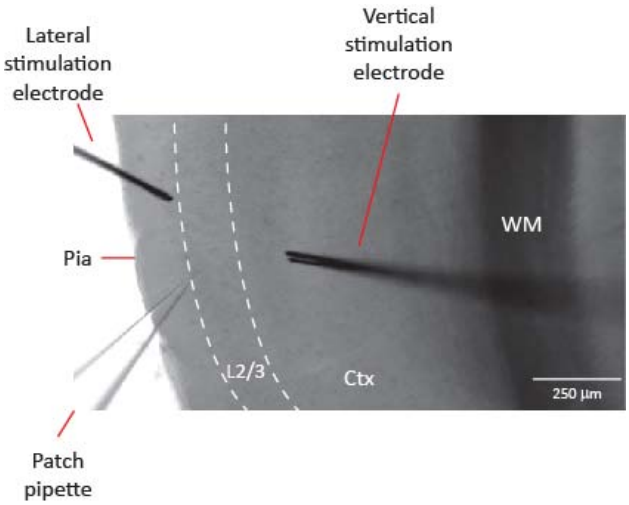

Figure 5.4. ***Extracellular stimulation configuration of two independent and convergent synaptic inputs into layer 2/3.*** *IR-DIC image from a coronal whole-brain slice partially showing the auditory cortex, along with the two extracellular stimulation electrodes used to activate a lateral and a vertical input pathways that converge into the layer 2/3 (bounded by white dashed lines). Ctx: cortex; WM: white matter.*

Electrical stimulation consisted of two 0.2 ms-long rectangular pulses (100 ms apart) delivered every 3 sec to each pathway in an alternate way, via two stimulus isolation units (ISO-STIM 01M, npi electronic, Germany). The final intensity of the stimulus (lateral input: 43.3 ± 6.5 V; vertical input: 15.4 ± 2.2 V) was adjusted in current-clamp mode in order to obtain a subthreshhold PSC, but weak enough to prevent spike contamination. When recording in voltage-clamp mode, the stimulus intensity was left unchanged. After a period of equilibration, the averages of 10 consecutive sweeps from each pathway were obtained. Off-line analysis of PSCs (Figure 5.5) was done using Clampfit 10.2 software (Molecular Devices, Inc., USA). Synaptic current amplitudes of neurons voltage-clamped through a series of holding potentials, typically from −90 to 0 mV, in steps of 15 mV increments, were measured as the difference between the amplitude during a 2 msec window including the peak of the PSC and the amplitude during a window 2 msec before the stimulus, and further used to construct current-voltage (I-V) curves. When the PSC was clearly biphasic at one or more holding potentials, measurements were made at both amplitude peaks.

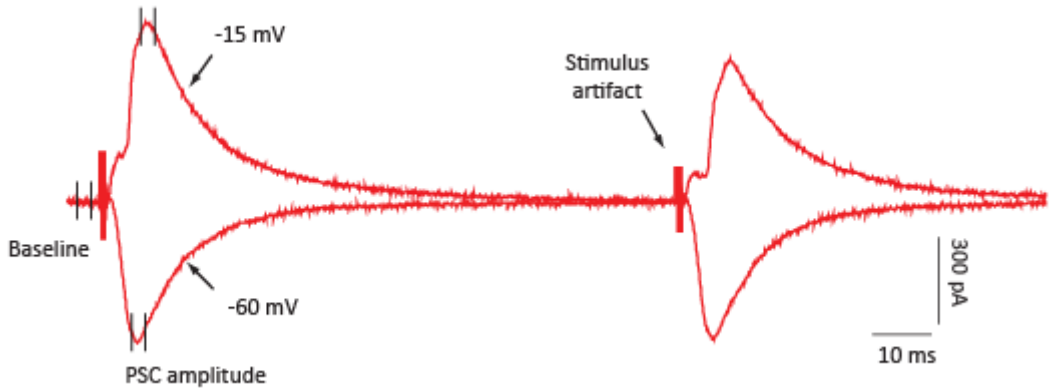

Figure 5.5. ***Postsynaptic currents measurements.*** *Two rectangular electrical pulses (denoted by the stimulus artifact; 100 ms apart) reliably evoked synaptic currents in the postsynaptic neurons specifically located in layer 2/3. Shown are representative traces from one individual neuron whose membrane potential was clamped at -60 mv (inward current) or at -15 mV (outward current). The amplitude of the postsynaptic current was measured using a 2 ms-long time-window centred on the PSC peak, in relation with a 2 ms-long time-window before the stimulus (baseline).*

In a subset of experiments, the excitatory drive onto the L2/3 recorded neuron was isolated by continuous bath application of SR-95531 (10 μM) - a γ-aminobutiric acid

(GABA) receptor A antagonist - along with tetrodotoxin (TTX; 4nM; Tocris) - a voltage-activated fast sodium channel antagonist. The inhibitory input to the recorded neurons was studied by continuous superfusion of 6-cyano-7-nitroquinoxaline-2,3-dione (CNQX; 10 μM; Sigma) - the α-amino-3-hydroxy-5-methyl-4-isoxazolepropionic acid (AMPA)/kainate receptor antagonist -, along with D(−)-2-Amino-5-phosphonopentanoic acid (AP-5; 50 μM; Sigma) – a selective N-methyl d-aspartate (NMDA) receptor antagonist. All drugs used were previously added to the ACSF in perfusion to render the proper final concentration.

5.8. Decomposition of the synaptic conductance

The method used is based on the continuous measurement of conductance changes during stimulus-evoked synaptic response. This method was successfully used before on rat primary auditory cortex *in vivo* (Wehr and Zador, 2003), as well on slices of rat visual cortex (Le et al., 2006) and mice barrel cortex (Cruikshank et al., 2007; Zhang et al., 2011). Synaptic current was determined for each holding potential. Synaptic I-V curves were plotted at each time point (*t*) following the stimulation onset, for each holding potential, and fitted with best linear fit regression. Only cells showing a Pearson correlation coefficient > 0.95 for the I-V linear regression between -90 and -30 mV were considered when calculating the conductance change of the recorded pyramidal neuron. Based on the slopes and voltage-intercepts, synaptic conductances and reversal potentials were calculated, respectively, allowing to build continuous conductance plots for a given neuron. Because these calculations were made for every time point, continuous conductance could be constructed. For validating this method, the excitatory and inhibitory conductances were measured when the excitatory or inhibitory synapses were pharmacologically blocked (see above). Excitatory synaptic reversal potential for the stimulated lateral and vertical inputs were, respectively, 43.5 and 55.9 mV (n=8 neurons). These values are considerably higher than the theoretically expected reversal potential for AMPA/NMDA PSCs of ~ 0 mV. This could be due to limited space clamp, which is particularly challenging to optimize in adult neurons with mature arborizations. The inhibitory synaptic reversal potential for the stimulated lateral and vertical inputs were, respectively, -67.0 and -65.8 (n = 5). These values for the reversal potentials are classically accepted (Wehr and Zador, 2003; Le Roux et al., 2006). The somatic reversal potential of the mixed synaptic responses, which was calculated from I-V plots, took an

intermediate value between -90 and -30 mV, and between the respective values of the excitatory and inhibitory reversal potentials. In so, the mixed reversal potentials for the lateral and vertical inputs were, respectively, -40.6 and -44.1 mV (n = 20 neurons).

5.9. Drugs

Choline chloride, NaH_2PO_4, $CaCl_2$, $MgCl_2$, ascorbic acid, KCl, pyruvic acid, K-gluconate, HEPES, EGTA, Na_2ATP, Na_3GTP, SR-95531, CNQX, AP-5 and Na_2-phosphocreatine were purchased from Sigma (St. Louis, MO). D-glucose was from Amresco (Solon, OH), $NaHCO_3$ was from Roth (France), NaCl and KOH were purchased from Merck (USA), and TTX from Tocris Bioscience (USA).

5.10. Plasmid constructs

In this study, two ChR2 constructs were used to render photosensitivity to neurons in the auditory cortex. In the first one, denoted “Syn-ChR2”, the ChR2 sequence carries the H134R point mutation, and its expression is under the control of the synapsin-1 promotor. The ChR2 is fused to an enhanced yellow fluorescent protein (EYFP) (see Figure 6.13A). The second one, denoted “CamKII-ChETA-P2A-H2B-mCherry”, the ultra-fast ChR2 variant (ChETA) carries the point mutation E123T in a H134T background. The ChETA sequence is fused to the self-cleavable peptide 2A (P2A), and to the histone 2B sequence (H2B). ChETA expression is under the control of the CamKII promoter and it is made visible by the concomitant expression of mCherry.

All plasmids (except the one for Syn-ChR2-EYFP, which was obtained from the Penn Vector Core (University of Pennsylvania, USA)) were made by Jiss John.

The double point mutation (E123T and H134R) variant in the ChR2 sequence was obtained by a Quick Change Site directed mutagenesis PCR (Stratagene) on pAAV-CamKII-ChR2-EYFP plasmid (in-house made). The primers used for the mutagenesis PCR were CAG TGG CTG CGC TAT GCA ACC TGG CTG CTC ACT TGT CC (forward) and GGA CAA GTG AGC AGC CAG GTT GCA TAG CGC AGC CAC TG (reverse). All correct clones with the proper two-point mutation were confirmed by

DNA sequencing. Next, the EYFP was replaced with a small peptide of 18 amino acids (P2A) fused to H2Bm-Cherry, using standard molecular cloning techniques, giving rise to the final construct pAAV-CamkII-ChETA-P2A-H2B-mCherry.

5.11. Preparation and delivery of adeno-associated virus

All viruses (except the one encoding for Syn-ChR2-EYFP) were prepared, purified and concentrated by Jiss John. The method for packaging plasmids in recombinant AAV was based on Stratagene's AAV Helper-Free System. Human embryonic kidney 293 cells were cotransfected with the AAV-2 terminal repeat-containing plasmid (CamKII-ChETA-P2A-H2B-mCherry or CamKII-EGFP) and packaging plasmid pDP8 (Plasmid factory). After 40 – 48 hours post transfection, cells were harvested and lysated by a series of freeze and thaw cycles which release virus particles from cells into the cell lysate. The cell lysate was further digested for 1 hour with Benzonase (Novagen) to remove unpackaged plasmid DNA and centrifuged to remove the cell debris. This clear lysate was applied to a CsCl gradient which enables the physical separation of full particles (AAV containing a genome) from empty particles based on their differences in density, and centrifuged (~23 hours, 45000 rpm, 21°C). After the centrifugation, the proper fractions containing the virus were collected and a dialysis (Pierce Slide-A-Lyzer dialysis cassette; Thermo Scientific, USA) was done using 1xPBS to remove CsCl . The AAV was then concentrated and washed using AmiconUltra Centrifugal Filter Units (Millipore; MWCO-100K). The concentrated virus is then washed 5× with 10mL of PBS. Finally, to determine the titer of the viruses, viral DNA is prepared using ViralXpress Nuclei Acid Extraction Kit (Milipore, USA), and quantitative PCR is performed suing FastStart SYBR Green Master Mix (Roche). For the AAV-2/8-CamKII-ChETA-P2A-H2B-mCherry virus the final titer used was 4.6×10^{11} viral particles/mL. For the AAV-2/8-CamKII-EGFP the titer used was 1.3×10^{12} viral particles/mL. The AAV-2/9-Syn-ChR2(H134R)-EYFP virus was obtained from the Penn Vector Core (University of Pennsylvania, USA) at a final titer of 3.7×10^{13} viral particles/mL.

5.12. Stereotaxic viral injections

Mice were anesthetized with a 0.2 mL i.p. injection of pre-made mixture of ketamine (10 mg/mL) / medetomidine (0.08 mg/L). The eyes were protected from dehydration and intensive light exposure using vaseline and a small piece of aluminium foil above it. After proper head immobilization, the scalp was washed with 70% alcohol and a flap of skin (~ $1cm^2$) covering the skull of both hemispheres was gently removed. Care was taken to expose only the temporal, pariental and parts of the occipital bones, leaving completely untouched the *musculus temporalis* covering the temporal bone. The anterior-posterior, dorsal-ventral, medial-lateral and coronal planes were adjusted after stereotaxic calibration of the alignment apparatus. Microinjections were made using pipettes (pulled from borosilicate 1.14 mm outer and 0.5 mm inner diameter, WPI) connected to a nanoliter injector (Nanoliter 2000, WPI). A stereotaxic motorized drill (Model 1911 Stereotaxic Drilling Unit, Kopf Instruments) was used to open a small hole in the mouse skull directly above the auditory cortex following the coordinates from Bregma (in mm) -2.7 posterior and +4.3 medium-lateral. Care was taken to avoid damage of the dura. A coordinate from Bregma of -2.5mm dorso-ventral was used to reach primarily the upper layers of the auditory cortex. A total volume of 80 nL of purified and concentrated AAV encoding Syn-CHR2-EYFP (or CamKII-ChETAmCherry) was used. The injections were made at a rate of 20 nL/min followed by additional 5 min in rest to allow diffusion of the viral particles away from the injection site. The micropipette was then gently removed to avoid leakage of the viral solution out of the tissue. Small drops of Vetbond glue were delivered solely on the edges of the skin to attach it to skull and thus avoiding direct infiltration of the wound. By means of a fine dentist drill the exposed skull was smoothened and two additional miniature screws were attached lateral to Bregma directly over the frontal bones to allow better adhesion of the black dental cement. A small magnetic metal round piece was embedded in the fresh and liquid dental cement layer where only the upper surface was made visible. Afterwards, the mouse was allowed to recover in its cage after a 0.02 mL i.p. injection of atipamezole (5 mg/mL; Antisedan, Pfizer).

5.13. *In vitro* characterization of ChR2-expressing neurons

Four to five weeks after viral injection, whole-brain coronal slices (300 µm-thick) were prepared as described previously. Before the beginning of the recordings, all slices were inspected with epifluorescence (Olympus BX51WI upright microscope equipped with a 100-W power range mercury short-arc lamp (USHIO, Tokyo, Japan)) to ascertain the location and the quality of the viral transfection. Only slices that showed a prominent and robust YFP expression were considered for further characterization. mCherry expression was visualised using a 575DCXR (AHF, Germany) dichroic mirror, thus minimizing channelrhodopsin activation. Recording from layer 2/3 pyramidal were made as before. To characterize the responses of ChR2-expressing neurons, current-clamp recordings were conducted in the presence of the synaptic transmission blockers CNQX (10 µM), AP-5 (50 µM) and gabazine (10 µM) (Sigma). Light stimulation was delivered using full-field epifluorescence through a fluorescence mirror unit (U-MWIB3, Olympus) equipped with a blue excitation bandpass filter (460 – 495 nm) via a water immersion objective (40x/0,8NA, Olympus). The timing, duration and frequency of the individual light stimulus were controlled via a shutter driver (model VCM-D1, UniBlitz, USA) and triggered using Clampex 10.2 software (Molecular Devices). Light-evoked APs were induced by a train of five light pulses, 5 ms duration each, at different frequencies (from 1 to 80Hz, in some cases up to 200Hz). The percentage of successful APs that a given neuron could reliably fire upon a given train of light pulses was defined as follows:

$$\frac{\text{number of APs evoked by a train of light pulses}}{\text{number of light pulses}} \times 100$$

where 100% corresponds to 5 time-locked APs induced by 5 individual blue light pulses. It was observed that in all tested Syn-ChR2-expressing neurons (n = 10), and in a minor subset of CamKII-ChETA-positive neurons (3 out of 9), photostimulation induced doublets or triples of APs, per each light pulse. For sake of clarity these doublets or triplets were considered as one AP. The average of ten consecutive sweeps (5 sec long) was considered for further analysis. Photocurrents were evoked by delivering one 1 sec-long light pulse in voltage-clamp mode at -65 mV holding potential. Two consecutive sweeps were separated by a gap of 3 seconds. The average

of 10 consecutive sweeps was considered for further analysis. The amplitude of the photocurrents was measured in the stationary portion of the trace, taking as comparison the baseline immediately before the delivery of the light pulse.

5.14. Chronic cranial window implantation

After 3 weeks post-injection, mice were anesthetized with a 0.2 mL i.p. injection of ketamine/medetomidine mixture. Dexamethasone (4 mg/mL dose) was administered by an intramuscular injection (0.02 mL) to the quadriceps for reducing the cortical stress response during the surgery and preventing cerebral edema. A 0.2 mL i.p. injection (from a 0.50 mg/mL stock) with carprofen prior to surgery was given to reduce inflammation. The eyes were protected from dehydration and from intensive light exposure as before. After washing the remaining scalp with 70% ethanol a flap of skin covering the right lateral part of the head was removed. The right temporal bone was unveiled by gentle removal of a small part of the *musculus temporalis* (previously injected with 1% Xylanest (lidocaine with epinephrine 1:200.000)) with a blunt spatula. Using a fine motorized drill, the bones were smoothened, and a part of the zygomatic process was removed and covered with a thin layer of 3M Vetbond glue as well as the remaining *musculus temporalis* to prevent blood capillary seepage. A thin layer of black dental cement (Lang Dental) was applied on top of the glue after it has dried, avoiding the area over the temporal bone. Next, a rectangular groove in the skull around the part of the brain containing the auditory cortex was made using a dental drill, leaving an island of skull (~2 mm × 3 mm dimensions) intact in the centre. The island of remaining temporal bone was carefully removed with blunt a forceps to expose a part of the brain containing the auditory cortex. Special care was taken to leave the dura intact. Small focal bleeding, due to the rupture of superficial cranial capillaries, was controlled by applying Gelfoam (Pfizer) previously soaked in a buffer of solution containing (in mM) 125 NaCl, 5 KCl, 10 D-glucose, 10 HEPES, 2 $CaCl_2$ and 2 $MgSO_4$ (pH = 7.4). The exposed dura was then kept wet by the use of a soaked Gelfoam as well. Optical cranial window was completed by covering the craniotomy with a drop of pre-warmed liquid 1.2% agarose (Sigma, St Louis, Misouri) followed by a small circular cover glass (5mm diameter, Electron Microscopy Sciences). The cranial window was afterwards sealed

with black dental cement over the cover glass´s contour and exposed skull. At the end, a small round metallic piece was placed, using dental cement around its periphery, on top of the mouse head for later magnet attachment of the miniature blue LED (see section 5.15.3).

5.15. Behaviour procedures

All components of the behaviour setup were controlled by a personal computer with Windows XP (Microsoft) operating system running custom Matlab software (Mathworks) written by Dr. Brice Bathellier. Naïve mice with implanted LEDs had free access to food but had restricted drinking water availability. Water was only available during and immediately after the behaviour sessions for a maximum of 10 minutes. The behavioural box consisted of a white Plexiglas chamber (25×25×42cm dimensions, model H10-11M-TC, modified, Coulborn Instruments), a removable metal grid floor and a single rectangular water delivery port mounted in one wall. The port was equipped with a water delivery tube (connected to a water reservoir placed outside the behaviour box, above the port) and placed in front of an infrared (IR) phototransistor-photodiode pair that signalled the interruption of the infrared beam when the mouse entered its snout. Water was delivered due to gravitation and the drop size was controlled with solenoid valves. Before the initiation of the daily experiment, the water valve connecting the water reservoir and the licking tube was open to prevent the formation of any air bubble in the licking tube and thus clogging it. The excessive water was then thoroughly cleaned, making the port completely devoid of water prior to the behavioural session. A bright blue masking light (high-power LEDs) was mounted immediately above the port to mask any scattered light potentially reaching the retina of the mouse. The masking light consisted of a 225 ms pulse of bright blue light illuminating the entire port and was presented during every trial independently of whether photostimulation was presented or not. The behavioural box was inserted in a sound- and light-proof cabinet which was equipped with white LEDs as constant house light (placed above the behavioural box), and a CCD KB-R3138 camera with infrared LEDs (LG electronics) which was connected to a Cronos framegrabber (Matrox).

Training consisted of two phases, and the transition from the first, - Habituation – to the second, - Perceptual task -, was only allowed if mice performed at least at 75% correct or above. A total of two sessions were performed daily, 30 minutes maximum duration each. After each session, the mice were put back to their home cages. Within a session a given trial is initiated when the mouse snout enters the port and starts licking the water delivery tube. Immediately after the IR beam-break, a photostimulation (PS) trial (delivered by the LED place above the cranial window) or a no-photostimulation (NPS) trial is initiated in a random way along the entire session. After successful training, the mice are expected to continue licking at the tube and break the IR beam during a certain period of time (Reward Delay; 2.5 sec duration) after the end of the NPS trial to collect a water reward (Reward Duration; 0.5 sec), or to leave the port after the end of the PS trial to avoid a time out (7 sec duration) that can be accompanied by an aversive air puff (pressure = 10psi; Air Compressor, Silent Air Technology, Germany) (Figure 5.6).

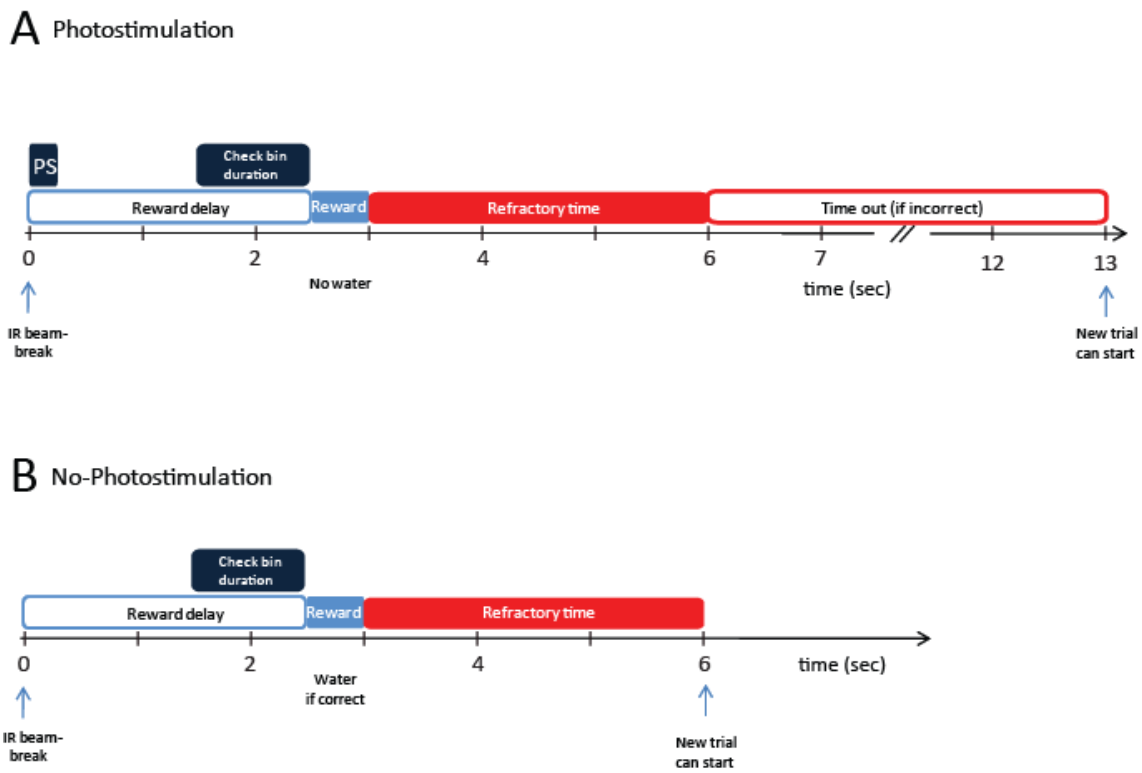

A positive trial (NPS) is considered correct if the mouse licks during more than 75% of the Check bin duration (1 sec-long), and a negative trial (PS) is correct if the mouse

licks less than 75% of the Check bin duration. No reward is delivered for a correct negative trial (head retraction upon photostimulation) and no other punishment is given for an incorrect positive trial (water available and no lick). No further trial can be restarted before the end of the Refractory Time (3 sec duration).

5.15.1. Habituation

Naïve mice that have been water deprived for 24h prior to the first habituation session were put individually in the behaviour box inside the sound- and light-proof cabinet. Mice were then trained in order to get water from the water port by breaking the IR beam inside the port. A drop of water was made available for every trial initiated after a given Refractory Time (3 seconds) for every time the mouse entered his snout in the port. Neither acoustic cue, neither photostimulation event was presented during the habituation sessions. In order to faithfully train the mice to perceive that there's a time window (Reward delay) between the initiation of the trial and the delivery of the water reward, the Reward delay and the Check bin duration are automatically augmented during the habituation session every time the mouse has been able to receive 10 successful rewards. After a certain number of consecutive steps (6), the final Reward delay (2.5 s) and Check bin duration (1 s) are reached. The Habituation sessions were repeated until mice had on average 75% chance of getting the water reward on the last step (i.e. with 2.5 s Reward delay) and get approximately 100 rewards in one session.

Figure 5.6. ***Timeline of the trials in the Perceptual task****. When a given mouse enters its snout in the water port and starts licking at the water delivery tube, it is detected by an infrared (IR) beam placed in front of the tube. Immediately after this event, either a* ***A)*** *train of 5 light pulses (5 ms width pulse) at 20 Hz is presented (Photostimulation, PS), or* ***B)*** *no light signal is delivered (No-Photostimulation). After successful training, the mice are expected to continue licking at the tube and break the IR beam during a certain period of time (Reward Delay) after the end of the NPS to collect a water reward, or to leave the water port after the end of the PS to avoid a time out that can be accompanied by an aversive air puff*

The water Reward duration consisted of 500ms time window, formed by 100 ms of valve opening followed by a 400ms time period when the valve is closed. In some cases, mice that eventually obtained the least number of rewards were put together in the same behaviour box with the ones which obtained the most. This was done to improve the number of visits to the water port in less motivated (or frightened) mice. On average, a total of 4 to 5 habituation sessions were performed before allowing the mice to transit to the Perceptual task.

5.15.2. Perceptual task

After chronic window implantation and LED assemblage, mice were allowed to recover for 24h before going into the Perceptual task. On a given day, mice were put individually in the same behaviour box as during the previous Habituation phase. The LED was connected to the behaviour control system before the mouse was placed in the box. The cable to the LED controller ran freely through the roof of the box, but care was taken to prevent tangling of the wires. After the initiation of a given trial, a no-photostimulation or a photostimulation (5 light pulses, 5ms width pulse, 20Hz) event was presented in a pseudo-random order with a 0.5 probability Mice are expected to continue licking at water tube during the Check bin duration for a (positive) no-photostimulation (No-PS) trial, and to retract their head from the water port if a (negative) photostimulation (PS) trial occurs. If in a PS trial the mouse continues licking at the water tube during the Check bin duration time window an aversive air-puff (1 bar pressure) delivered via an air-pump (Silent Air Technology, Germany) directly to the mouse's snout. At the end, mice are expected to perceive the photostimulation event as predictive for a punishment and retract their head in order to prevent it in time. After the end of a given Detection task session the LED assemblage was detached from the mouse head and the animal was put back in his home cage.

5.15.3. *In vivo* photostimulation

One day after cranial window implantation mice were anesthetized using an isoflurane-oxygen mixture (1.4% isoflurane/O_2 by volume) delivered by an anaesthesia regulator (Univentor 400 Anaesthesia Unit, High Precision Instruments) and mounted on a

stereotaxic apparatus over a heating pad to keep body temperature. Eyes were again protected against dehydration by using a layer of vaseline. A sheet of cellophane paper was placed above the mouse head (acting as a physical barrier between the mouse head and the dental cement forming the LED cap), and a miniature blue high power light-emitting diode (LED, 470 nm peak wavelength, NFSB036BT, Nichia, Tokyo, Japan) was mounted centred on the cranial window. An extra layer of vaseline was place aver the cellophane coverage to allow its later detach from the LED-dental cement assembly. A round magnet was then placed above the metallic piece previously placed above the mouse skull (see section 5.14). The assembly was then covered with black dental cement to prevent leakage of light. After complete drying of the dental cement the assembly was carefully lifted from the mouse head and the animal was allowed to recover in its cage. The photostimulation consisted on the delivery of five light pulses, 5 ms duration each at 20Hz. All LEDs (average light intensity ~ 30 mW) were tested before implantation and before initiation of the individual behaviour training.

6. Results

A total number of 92 inbred wild-type C57Bl/6J mice were used, with 8 to 12 weeks of age, a period where full brain development has been achieved (Kobayashi, 1963), including adult-like hearing abilities (Song et al., 2006). Recordings were made specifically from pyramidal neurons in supragranular layer 2/3 and infragranular layer 5. To target for these individual neurons, 300 µm-thick coronal whole-brain slices were prepared, and the primary auditory cortex was identified in the slice according to the coordinates given in recent literature (Paxinos and Franklin, 2001). Care was taken to record from neurons that presented a prominent apical dendrite oriented towards the pia, indicative of minimal dendritic arborization damage, as confirmed by DIC microscopy beforehand. On a first approach, the neurons were selectively targeted for recording based on their pyramidal-like shaped soma. The boundaries of the supragranular layer 2/3 and infragranular layer 5 were assigned based on high-contrast infrared pictures taken during the electrophysiology experiments (Figure 6.1). Starting from the slice pial surface, layer 2/3 was identified as being the first level of the slice that contains identifiable neuronal somata below layer 1, a cell-sparse layer containing mostly non-pyramidal neurons (Hestrin and Armstrong, 1996). On the other hand, the identification of infragranular layer 5 was made by the size of the soma of the neurons present in this region, which when compared with layer 2/3 are noticeable larger (see Introduction). Overall, and based in previous comparable studies made in the mouse somatosensoty cortex (Lefort et al., 2009; Oswald and Reyes, 2008), the following subpial distances for the layer lower boundary was taken into account when identifying the layers of interest: 300 µm for layer 2/3 and 850 µm for layer 5. Moreover, the intrinsic excitability of the recorded neurons was also used as an additional criterion to distinguish between the precise laminar locations of the neurons. In so, it is known that neuronal excitability of layer 5 pyramidals is prominently influenced by the hyperpolarization-activated inward cation current (I_h), which contributes to several basic physiological processes including resting membrane conductance and stabilization of resting potential (Magee, 1998). I_h is a prominent current with increasing channel density along the dendrites of layer 5 pyramidal neurons, as compared with layer 2/3 neurons (Kole et al., 2006; Larkum et al., 2007). This current makes itself “visible” as a prominent “sag” in the voltage trace as a result of a subthreshold current injection step (see Magee, 1998; Kole et al., 2006; Huggenberger et al., 2009). This “sag” in the voltage trace was then used to confirm that

a given neuron was indeed properly located in infragranular layer 5 (see Figure 6.2).

6.1. Features of local cortical connectivity in the adult naïve mice

In the first part of this study, one main question was made: what are the properties that characterize local synaptic connectivity in the auditory cortex from adult naïve mice? To probe for local synaptic connectivity between pairs of pyramidal neurons, somatic whole-cell patch-clamp recordings in current clamp mode were made from two to four neurons simultaneously. In this way, one neuron is stimulated in turn while recording intracellularly from another three neurons that potentially receive input from the stimulated neuron. With this approach, one can have a full handle on the intrinsic electric properties of the targeted neurons, and an evaluation of their synaptic connectivity. In the example experiment seen in Figure 6.1, four pyramidal neurons were successfully recorded simultaneously. By injecting two brief 5 ms-duration depolarizing current pulses, a double action potential (AP) is evoked in each of these neurons in turn, while recording the membrane potential of the other neurons. For monosynaptically connected neurons, a presynaptic AP evokes release of the excitatory neurotransmitter glutamate, which opens ionotropic glutamate receptors present in the postsynaptic neuron, resulting in a time-locked unitary excitatory postsynaptic potential (EPSP) for each of the evoked AP. For every presynaptic neuron in a local microcircuit containing 4 neurons, there are 3 possible target neurons, giving a total of 12 possible synaptic connections. The recording of several individual pairs of potentially connected excitatory neurons enables the comparison of the overall pattern of functional connectivity between neurons in two cortical layers in the adult auditory cortex in a statistically meaningful way. Care was taken to record from excitatory neurons close to each other (< 50 µm apart).

.

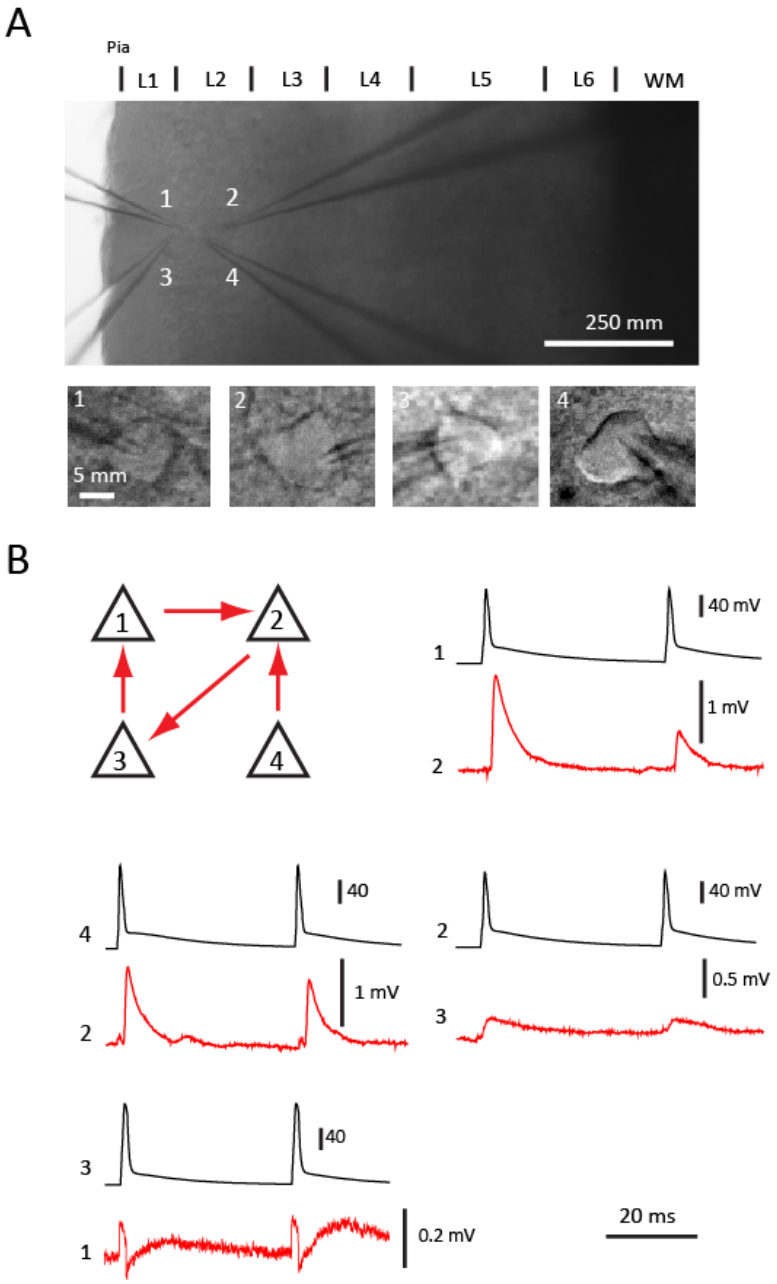

Figure 6.1. ***In vitro whole-cell recordings targeted to the adult mouse auditory cortex. A)*** *IR-DIC images from a coronal whole-brain slice partially showing the auditory cortex and four individual patch pipettes (top; numbered 1 to 4) and the corresponding four individual neurons (bottom; numbered 1 to 4) present in layer 2/3 that were targeted for a simultaneous quadruple patch-clamping experiment.* ***B)*** *Schematic synaptic connectivity diagram from a representative experiment. Each red arrow represents an observed monosynaptic connection between a pair of neurons (triangles). Membrane potential traces are shown for each of the 4 connections found (in a total of possible 12), showing presynaptic APs (black) and EPSPs (red) in the depicted synaptically connected neurons. The EPSPs exhibited a remarkable variability in terms of their amplitudes. Lx indicates the individual x cortical layer; WN, white matter.*

6.1.1. Intrinsic electrophysiological properties of pyramidal neurons in the adult mouse auditory cortex

As shown in Table 6.1, the resting membrane potential (Vm) and the membrane resistance (Rm) of the recorded neurons differed significantly between both cortical layers ($p < 0.001$). Neurons that needed to be injected with a compensatory current to maintain a constant Vm level were rejected from this particular analysis. On average, layer 2/3 pyramidal neurons (n = 289) had, when compared with layer 5 neurons (n = 215), a significant lower Vm value (average ± s.e.m.: -74.2 ± 0.88 *versus* -67.7 ± 0.56 mV, respectively). Moreover, the Rm value for layer 2/3 (126.2 ± 5.7 MΩ) was also smaller when comparing with the Rm for neurons in layer 5 (176.1 ± 9.81 MΩ). These observations are in accordance for what has been reported either in the developing mice (L2/3: Vm = -81 mV; Rm = 139 MΩ; Oswald et al., 2008) and adult rat auditory cortex (L2/3: Vm = -76 mV; Rm = 55 MΩ; L5: Vm = -74 mV ; Rm = 114 MΩ; Huggenberger et al., 2009), as well as in other sensory cortical areas (L2/3: Vm = -72 mV ; Rm = 188 MΩ; L5: Vm = -63 mV ; Rm = 162 MΩ; Lefort et al., 2009). In summary, pyramidal neurons in layer 2/3 are in a more hyperpolarized physiological state and have lower membrane resistance values - a measure of the overall contribution of the membrane ion channels and transporters to the movement of ions across it - when compared with its layer 5 neurons counterparts. These intrinsic properties seem to be fully achieved already 2 weeks postnatal in mice (Oswald et al., 2008; Lefort et al., 2009).

To assess about AP intrinsic properties, a brief 5 ms-duration suprathreshold depolarizing current step was injected somatically in the recorded neurons (the same experimental procedure used to assess about synaptic connectivity). A random sample of neurons was considered for analysis. Neurons that needed to be injected with a compensatory current to maintain a constant Vm level were rejected from this analysis. The APs elicited in neurons from both cortical layers were virtually indistinguishable (Table 6.1).

Table 6.1. ***Intrinsic membrane and action potential properties of the recorded pyramidal neurons.*** *Values are mean ± standard error of the mean (s.e.m.); Vm, resting membrane potential; Rm, membrane resistance; n, number of neurons; Statistically significant differences (*p < 0.05) between cortical layers were assessed by using the unpaired Student´s t test.*

	Layer 2/3	**n**	**Layer 5**	**n**
V_m (mV)	-74.2 ± 0.88	289	-67.7 ± 0.56 *	215
R_m (MΩ)	126.2 ± 5.70	289	176.1 ± 9.81 *	215
AP threshold (mV)	-32.4 ± 1.69	52	-33.0 ± 1.21	60
AP amplitude (mV)	91.8 ± 1.13	52	95.9 ± 0.82 *	60
AP overshoot (mV)	58.8 ± 1.99	52	61.8 ± 1.60	60
AP half-height width (ms)	1.6 ± 0.04	52	1.7 ± 0.03 *	60

AP threshold (the membrane potential that must be achieved for AP burst to occur) was not statistically different ($p > 0.05$) between pyramidal neurons in either layer 2/3 (n = 52) and layer 5 (n = 60). The overshoot (defined as the peak relative to 0 mV) was also similar between both cortical layers. On the other hand, the average AP amplitude (measured from AP threshold to peak) and the AP half-height width (width at half-maximal AP amplitude) were different between cortical layers ($p < 0.05$). On average the amplitude of the APs elicited in layer 5 was higher (95.9 ± 0.82 mV) when compared with the APs elicit in layer 2/3 (91.8 ± 1.13 mV). Contrary, the average AP in layer 2/3 was narrower (1.6 ± 0.04 ms) than its counterparts in layer 5 (1.7 ± 0.03 ms). These observations are in line with what has been seen for other glutamatergic pyramidal neurons in other cortical areas in the brain slice preparation (for review see Bean, 2007).

In the plots of the number of APs (mean ± s.e.m.) as a function of injected current (input/output curve), a significant difference was also observed between neurons from either cortical layers (Figure 6.2). The number of APs that on average pyramidal neurons from layer 5 (n = 206) could fire was significantly higher ($p < 0.05$) in the majority of the input current range used, as compared with pyramidal neurons form layer 2/3 (n = 201). A minor number of neurons were rejected from this particular analysis due to unreliable count of AP numbers in the most depolarized current injection steps. In the range from 60 to 280 pA of injected current, an average difference of 2.7 ±

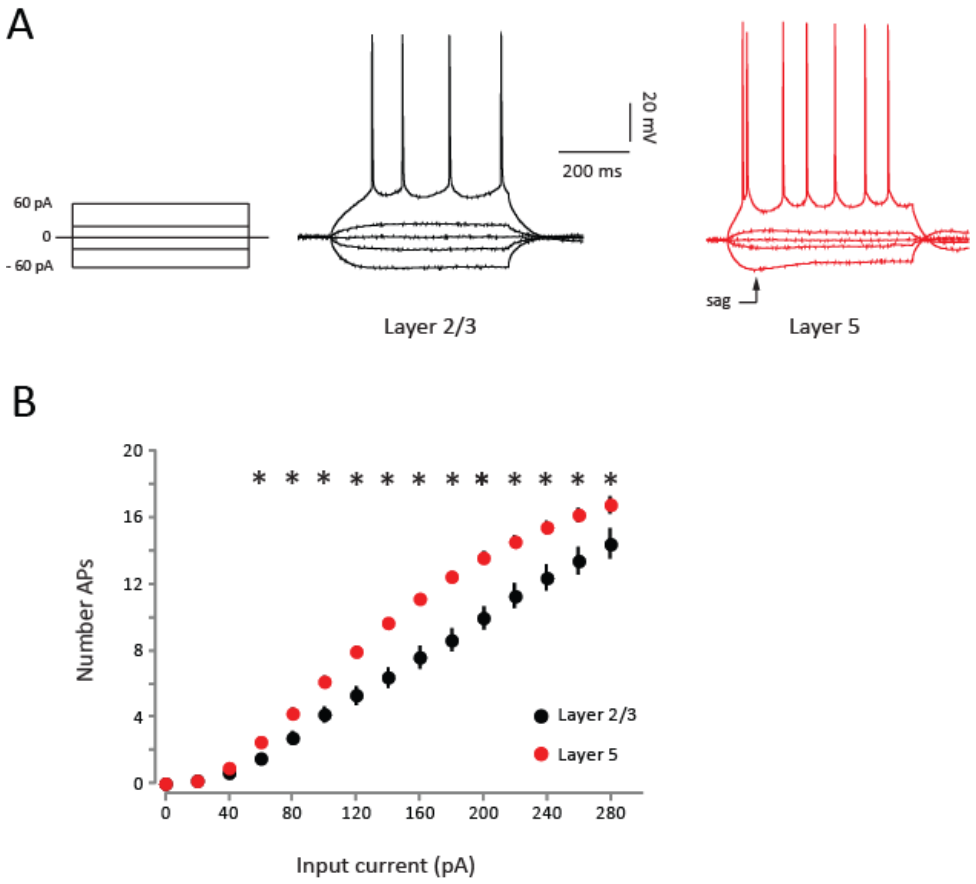

Figure 6.2. ***Differential intrinsic excitability features of auditory cortex pyramidal neurons.*** ***A)*** *Left: schematic diagram depicting the injected current steps (-60, -20, 0, 20 and 60 pA); Middle and right: Representative voltage traces evoked by the injected command steps from individual pyramidal neurons located in layer 2/3 and layer 5. APs were virtually indistinguishable when comparing both cortical layers. Note the marginal "sag" in the control trace as an indication of* I_h *activation.* ***B)*** *Relationship between the number of APs that neurons from layer 2/3 (n = 201; black circles) or layer 5 (n = 206; red circles) could fire upon increasing input current (input/output curve). On average, it was observed that layer 5 neurons revealed high firing rates for the majority of input current when compared with layer 2/3 neurons. Values are mean ± s.e.m.. Statistically significant differences (*p < 0.05) were assessed using the two-way ANOVA test.*

0.25 APs was observed between layer 2/3 and layer 5 neurons. Since the AP threshold does not vary between both cortical layers (see Table 6.1), these changes in intrinsic excitability likely reflect the differences observed in resting membrane potential and membrane resistance between layer 5 and 2/3 neurons, namely the more depolarized state and high membrane resistance that layer 5 pyramidals have, making them more

prone to fire on a given input current. Interestingly, the observed differences in intrinsic excitability between layer 2/3 and layer 5 neurons are in accordance to the reported differences in spontaneous and evoked population activity in the rat auditory cortex *in vivo* (Sakata and Harris, 2009).

6.1.2. Features of EPSP amplitudes, kinetics and reliability

As stated in Table 6.2, there was a significant ($p < 0.05$) difference between several EPSP intrinsic properties recorded in the two cortical layers. The EPSP amplitudes observed in layer 2/3 ranged from 0.02 to 3.37 mV (see also Figures 6.1 and 6.3), whereas in layer 5 this interval was remarkably shorter (from 0.01 to 0.9 mV). There was also a significant difference in the average EPSP amplitude between layer 2/3 (0.38 ± 0.06 mV; n = 80) and layer 5 (0.21 ± 0.06 mV; n = 15). Using developing rodents generally higher average EPSP amplitudes have been observed (L2/3: 0.2 – 1 mV, Holmgren et al., 2003; L2/3: 0.71 mV, L5: ~ 0.7 mV, Lefort et al., 2009; L2/3: 0.6 mV, Oswald et al., 2008; L5: 0.3 – 0.5 mV, Song et al., 2005). These discrepancies might reflect a characteristic feature of the mature cortex towards low amplitude synaptic connections. The latency (defined as the time difference between the presynaptic AP peak and the onset of the EPSP) and the average time-to-peak of the EPSPs (taken as the time difference between EPSP maximum and its onset) were also distinct ($p < 0.05$) between neurons in layer 2/3 and layer 5 (Table 6.2). The average EPSP latency in layer 2/3 was 1.6 ± 0.1 ms (n = 80), while for layer 5 was significantly higher (2.3 ± 0.44 ms; n = 15). This discrepancy was also observed for the EPSPs time-to-peak (compare 4.2 ± 0.32 and 7.8 ± 1.46 ms for layer 2/3 and layer 5, respectively). Similar features in the mouse developing barrel cortex were reported previously (Lefort et al., 2009).

Table 6.2. ***Excitatory synaptic connectivity features and kinetics of EPSPs.*** *Values are mean ± s.e.m.; P, probability of connection; CV, coefficient of variation; n, number of found EPSPs; Statistically significant differences (*p < 0.05) between cortical layers were assessed using the unpaired Student´s t test*

	Layer 2/3	n	Layer 5	n
P (found /tested)	11.7 % (80/682)		3.01 % (15/498)	
Mean EPSP amplitude (mV)	0.38 ± 0.06	80	0.21 ± 0.06 *	15
Range (mV)	0.02 – 3.37	80	0.01 – 0.9	15
Latency (ms)	1.6 ± 0.1	80	2.3 ± 0.44 *	15
Time-to-peak (ms)	4.2 ± 0.32	80	7.8 ± 1.46 *	15
CV	1.3 ± 0.08	80	3.0 ± 0.83 *	15
Failure rate	0.61 ± 3.3	80	0.64 ± 7.7	15
Paired-pulse ratio	1.1 ± 0.16	80	0.8 ± 0.14 *	15

Across the entire data set, few large-amplitude connections were found, but many small amplitude ones, which gives rise to a skewed distribution of EPSP amplitudes in layer 2/3 and layer 5 (Figure 6.3) (Brunel et al., 2004; Frick et al., 2008; Lefort et al., 2009; Song et al., 2005; Ikegaya et al., 2012). Plotting the dataset for layer 2/3, which has a sufficient number of detected connections, on a semilog scale, it can be well approximated by a normal distribution (Figure 6.3) (Song et al., 2005; Ikegaya et al., 2012).

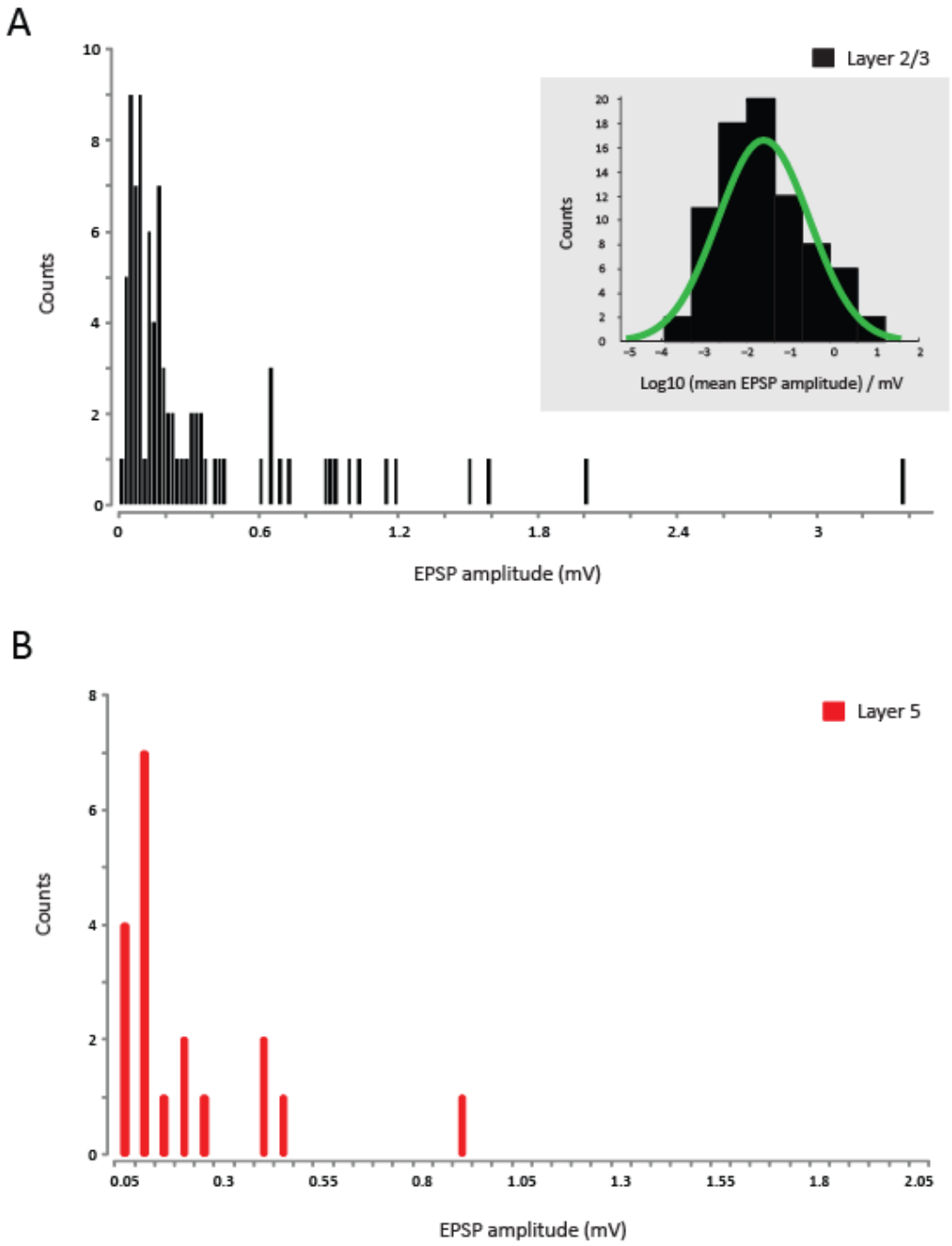

Figure 6.3. ***Long-tailed distribution of EPSP amplitudes. A)*** *Distribution of the average EPSP synaptic connection amplitudes found across the entire data set for layer 2/3, binned at 0.02 mV intervals. Note the long tail, indicating rare high-amplitude synaptic connections. Inset: the data set can be well approximated with a normal function (green curve) when plotted on a semilog scale (Lilliefors test for normality ($p < 0.05$)).* ***B)*** *Distribution of the average EPSP amplitudes for layer 5, binned at 0.05 mV intervals. Due to the limited amount of connections found ($n = 15$), a reasonable fit is not possible.*

6.1.3. Variability in postsynaptic transmission

It is known that for individual central synapses, identical presynaptic electric stimulations results in variable evoked postsynaptic potentials. This fact is due mainly to the probabilistic exocytosis of glutamate and the variable timing and amplitude of the postsynaptic response itself (see Ribrault et al., 2011). On a trial-to-trial basis, in a single experiment, it was observed variable EPSP responses due to the same presynaptic AP stimulation. As can been appreciated in one example experiment shown in Figure 6.4 (and see also Figure 6.1) - which depicts two independent connections recorded from two layer 2/3 neurons -, a double presynaptic AP can evoke both a high and reliable EPSP in another layer 2/3 pyramidal, as well as a smaller and highly variable EPSP.

To further characterize the variability of EPSP amplitude across the 60 trials in a single experiment, the coefficient of variation (CV = standard deviation/mean) was calculated. As can be seen in Table 6.2, the CV of EPSP amplitudes (defined as the standard deviation of peak amplitudes divided by the average amplitude) differed significantly ($p < 0.05$) from a value of 1.3 ± 0.08 in layer 2/3, to 3.0 ± 0.83 in layer 5, which indicates a lower trial-to-trial variability of the EPSPs in layer 2/3 as opposite with a much higher variability of the synaptic connections found in layer 5. Another feature that can be appreciate easily in Figure 6.5 (and Figure 6.4) is the very low trial-to-trial variability of high-amplitude EPSPs compared with the highly variable responses found for small-amplitude synaptic connections. This remarkable relationship between the decreases in CV with increasing synaptic strength can be better visualised and quantified by plotting the CV as a function of mean EPSP amplitudes for both cortical layers (Figure 6.5). The increased reliability of high-amplitude EPSPs, measured as a reduction in the CV, held true for both cortical layers tested.

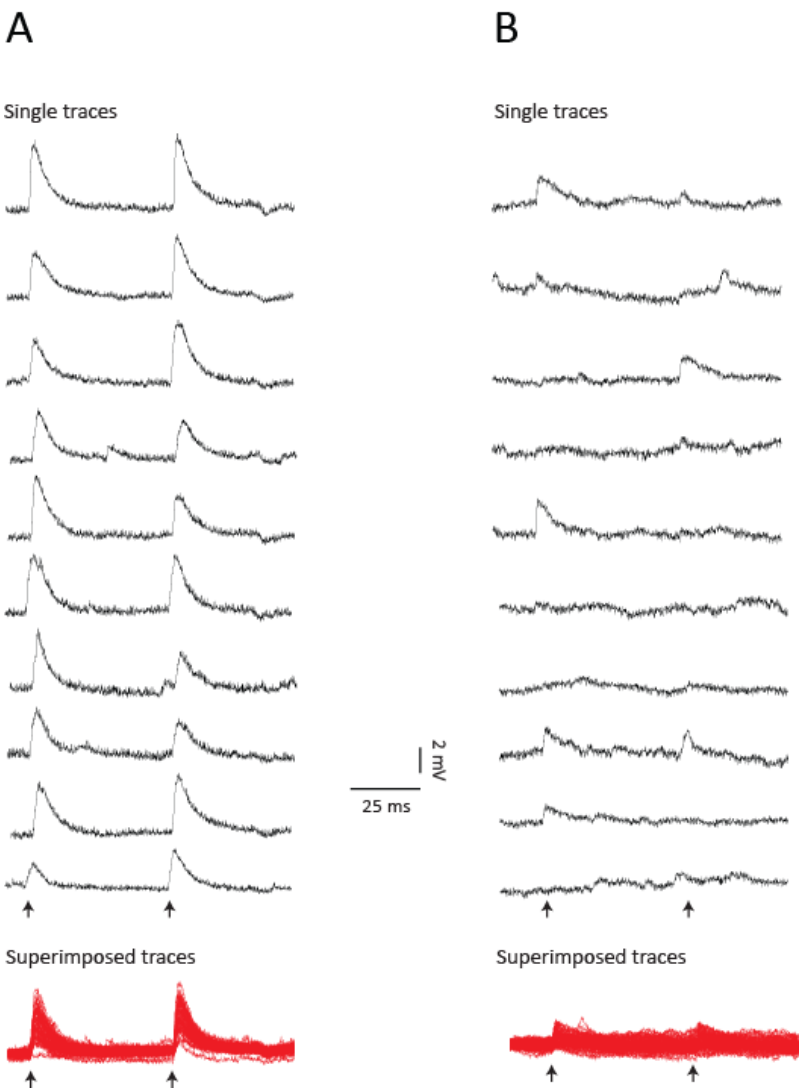

Figure 6.4. ***Variability in EPSP amplitudes on a trial-to-trial basis. A)*** *Ten representative individual and consecutive traces (black) from the highest EPSP amplitude found across the entire data set (3.37 mV) showing negligible trial-to-trial variability in a single experiment.* ***B)*** *Ten individual and consecutive traces (black) from one low amplitude EPSP connection (0.89 mV) showing considerable trial-to-trial variability. Depicted in red for both panels are the superimposed 60 traces for each connection. Both examples are from pyramidal neurons recorded in layer 2/3. Arrows indicate the time points of presynaptic stimulation.*

Moreover, the failure rate (number of trials that failed to evoke an EPSP, divided by the total number of trials) was evaluated for each of the functional connections found. As shown in Table 6.2, the average failure rate for layer 2/3 (0.61 ± 3.4) and layer 5 (0.64 ± 7.7) was not statistical different from each other ($p > 0.05$). Interestingly also to note the decrease in failure rate with the increase of the individual EPSP amplitudes (Figure 6.5), which indicates that synapses with low failure rates (and low CV) tended to be the ones

with high-amplitude EPSPs than those with high failure rates (and high CV). In summary, although rare, these high-amplitude reliable synaptic connections may dominate the entire network activity, assuming a critical role in the formation of interconnected clusters of neurons, as has been also suggested previously (Song et al., 2005).

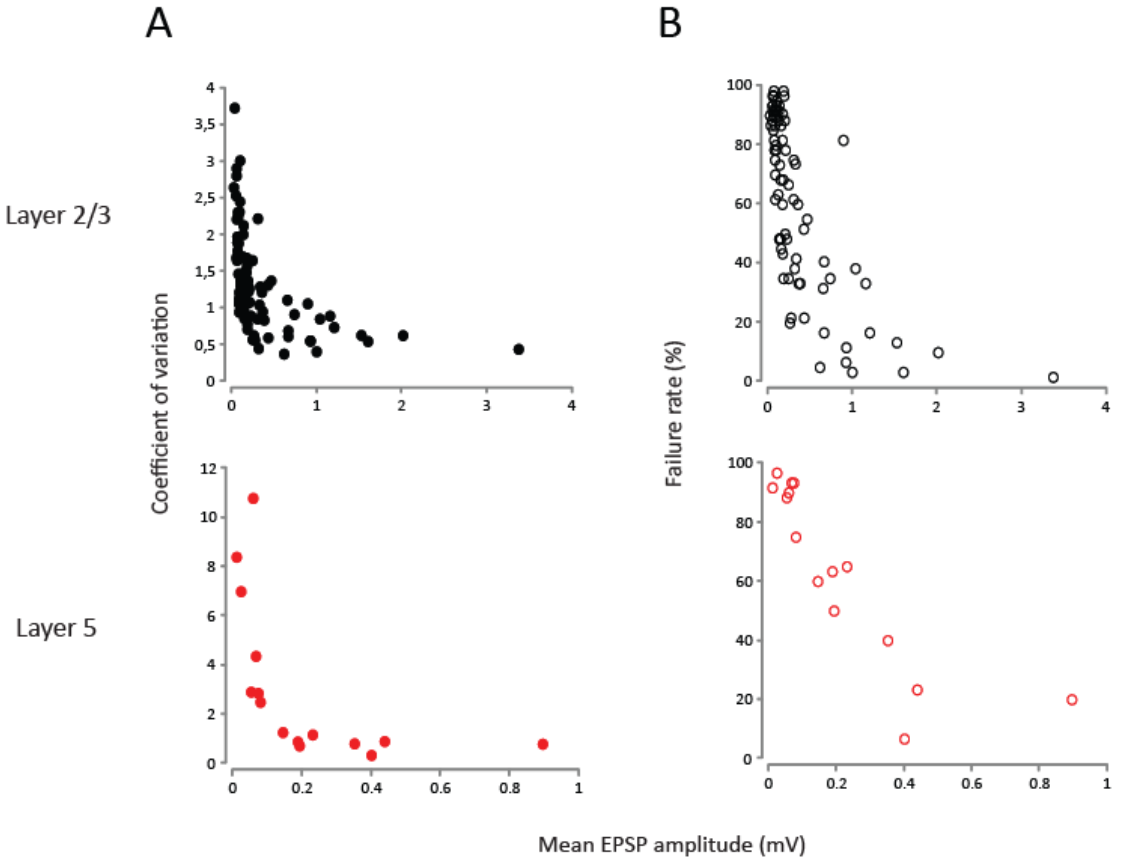

Figure 6.5. ***Rare high-amplitude connections are more reliable than low-amplitude ones. A)*** *Distributions of coefficient of variation (CV) as a function of mean EPSP amplitude (only 1st EPSP pulse shown) of each single connection found in this study for neurons from layer 2/3 (top; black) and layer 5 (bottom; red).* ***B)*** *Distribution of percentage of failure rates as a function of the mean ESP amplitude for every functional detected connection. Note that although rare, the high-amplitude connections are the more reliable and less variable ones which may have important role in the overall network connectivity. Each circle represents a single functional connection (layer 2/3: n = 80; layer 5: n = 15).*

It is known that central synapses differ considerably in their response to repetitive and closely spaced afferent stimulation, some showing synaptic depression and others showing facilitation (for review Zucker and Regehr, 2002). These phenomena are

believed to depend on residual calcium concentrations in the presynaptic terminal, and/or the depletion of readily releasable vesicles. As stated in Table 6.2, the paired-pulse ratio to two consecutive 50 ms-apart pulses across both cortical layers was marginally different ($p < 0.05$). On average, the second EPSP showed a smaller amplitude as compared with the first EPSP, which resulted in synaptic depression in layer 5 (0.8 ± 0.15; n = 15). On the other hand, synapses from layer 2/3 did not show significant short-term plasticity (paired-pulse ratio: 1.1 ± 0.16; n = 80).

6.1.4. Explanation of the variability in mean connection strengths with a binominal model of transmitter release

The wide range of EPSP amplitudes observed (L2/3: 0.03 – 3.37 mV; L5: 0.01 – 0.9 mV) could potentially be accounted for by differences in all three parameters of the quantal model of synaptic transmission, i.e. the number of synaptic contacts (n), probability in the neurotransmitter release (p) and the size of the postsynaptic response to a quantum of transmitter (q) (del Castillo and Katz, 1954). In this quantal model of synaptic release, a synaptic connection is assumed to be composed of n independent release sites, from where a single vesicle, at most, is released with a probability p upon the arrival of an AP, thus contributing with a quanta q to the postsynaptic response. If one assumes that the intrinsic variability of synaptic transmission can be described by a binomial distribution, then synaptic amplitudes could potentially be explained by differences in all three parameters, in the following manner:

However, can the wide range of observed average EPSP strengths be largely explained by the variability in only one of the above parameters, as has been previously suggested (Loebel et al., 2009)? In order to assess what characterizes synaptic connections in the adult auditory cortex, several simulations were made, where two of the above parameters were kept constant, while varying the third one. The outcome of this binomial distribution for the several tested scenarios was then compared with the original relation between CV (and failure rates) and mean EPSP amplitude for both cortical layers. For a binomial process, the following equations apply:

As showed in Figure 6.5, one can easily appreciate that changes in *q* alone cannot explain the dependences of both CV and failure rates with mean connection strengths (Figure 6.5A, left); in essence, when varying the size of the quantal units, there is only a scaling along the mean EPSP amplitude axis, not remotely representing the actual data. However, changing only the release probability (*p*) from small to high values, while keeping *q* and *n* constant, can account for much of the variability observed in the dataset (Figure 6.5A, middle). Moreover, changing *p* was not the only way of capturing the variability in the dataset: fixing *q* and *p*, and only changing *n*, could also lead to an appreciable fit (Figure 6.5A, right), which implies that for the observed high amplitude connections (with low failure rate and low CV) a very large number of presynaptic release sites need to be accounted for - approximately 100 -, which is in accordance with has been previously reported in somatosensory cortex (range 1 – 170 release sites; Loebel et al., 2009). However, this good fit, was only possible when *p* was fixed to a low value (0.08), as this was essential to capture the high CV (and high failure rates) values associated to low mean amplitude connections.

In summary, it was observed that differences in the number of release sites and in probability of release can both explain the observed systematic decrease in response variability, as the synaptic efficacy increases. This observation also held true for the data in cortical layer 5 (Figure 6.5B).

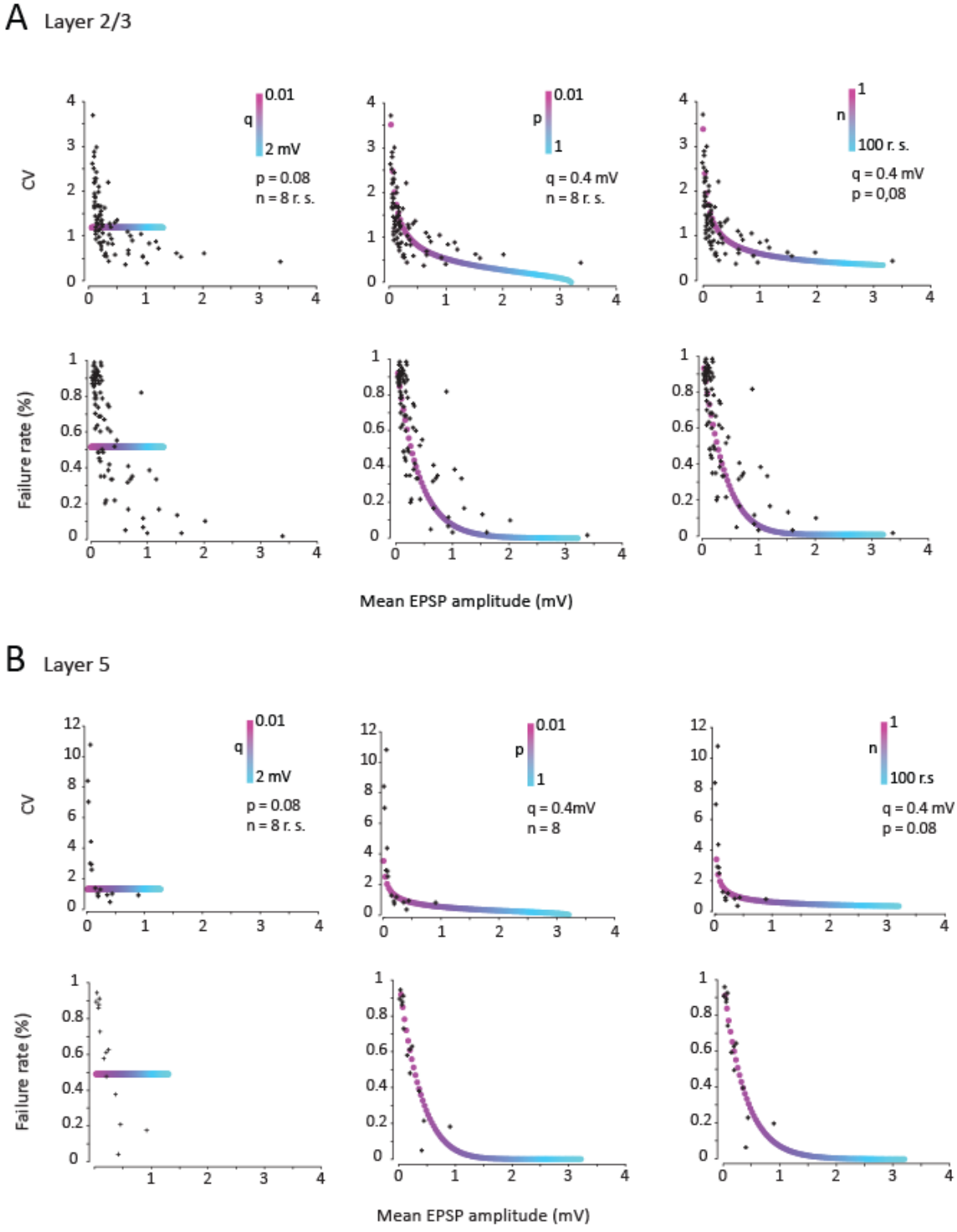

6.1.5. Patterns of synaptic connectivity

The probability of connectivity (total number of functional connections divided by the total number of connections tested) suffered from variability when comparing individual experiments and so, in order to obtain significant quantitative information, it was of utmost importance to record from many pairs of neurons. A total number of 340

neurons from layer 2/3, and 290 neurons from layer 5 were recorded. For the supragranular layers 2/3 a total of 682 possible synaptic connections were tested, among which 80 were functional ones, giving a value of 11.7% as the average probability of any two excitatory layer 2/3 neurons being monosynaptically connected. For infragranular layer 5, a connection probability of 3.01% was found, which represents a total of 15 functional connections among 498 possible ones (Table 6.2). One can easily appreciate that local synaptic connectivity was not uniform: in layer 2/3 the connectivity is higher when compared with layer 5. Similar observations were reported previously for the rat layer 2/3 (P = 9%; Holmgren et al., 2003; in the range of 9 to 12%; Lefort et al., 2009) and layer 5 (P = 9.2%; Thomson et al., 2002; P = 11.6%; Song et al., 2005) somatosensory cortex.

A given simultaneously recorded pair of neurons can be generally classified into three different classes: unconnected, unidirectionally connected, or bidirectionally connected. Assuming that the existence of a connection between any two neurons is independent of each other, that P defines the connection probability and N the total number of pairs of neurons tested, then the expected number of unconnected pairs should be $N(1 - P)^2$, the unidirectionally connected pairs should be $2NP(1 - P)$, and the expected number of bidirectionally connected pairs is defined by NP^2. In layer 2/3, a total of 40 pairs of connected neurons were found. Among those, 31 were connected unidirectionally and 9 via a bidirectional connection.

By assuming independent connection probabilities between pairs of neurons, one can appreciate that the observed number of bidirectionally connected pairs of neurons is

---

Figure 6.6. ***Low probability of neurotransmitter release and small quantal units account for the variability in individual connections in the adult auditory cortex.*** *Top row: plot of CV in dependence of mean EPSP amplitude in* ***A)*** *layer 2/3 or* ***B)*** *layer 5 for binomial distributions with increasing* q *(left),* p *(middle) or* n *(right), while keeping the other two quantal parameters unchanged (stated in each panel).; Bottom row: plot of failure rate (%) in dependence of mean EPSP amplitude in layer 2/3 for binomial distributions with increasing* q *(left),* p *(middle) or* n *(right), while keeping the other two quantal parameters unchanged (stated in the corresponding panel above); For every graph, black crosses correspond to one individual functional connection described before (layer 2/3: n = 80; layer 5: n = 15)*

twice of the expected one (4.7) from a randomly wired network (given by 0.117 × 0.117 × 341; Figure 6.7). On the other hand, the observed number of neuronal pairs that are unidirectionally connected is significantly less ($p < 0.05$) when compared with the expected one (265.9). These observations argue for an overrepresentation of reciprocally connected pairs of neurons in layer 2/3 in the mouse adult auditory cortex, confirming also previous reports for the rat somatosensory cortex (Holmgren et al., 2003; Song et al., 2005). Not enough data was gathered from layer 5 to make any reliable analysis.

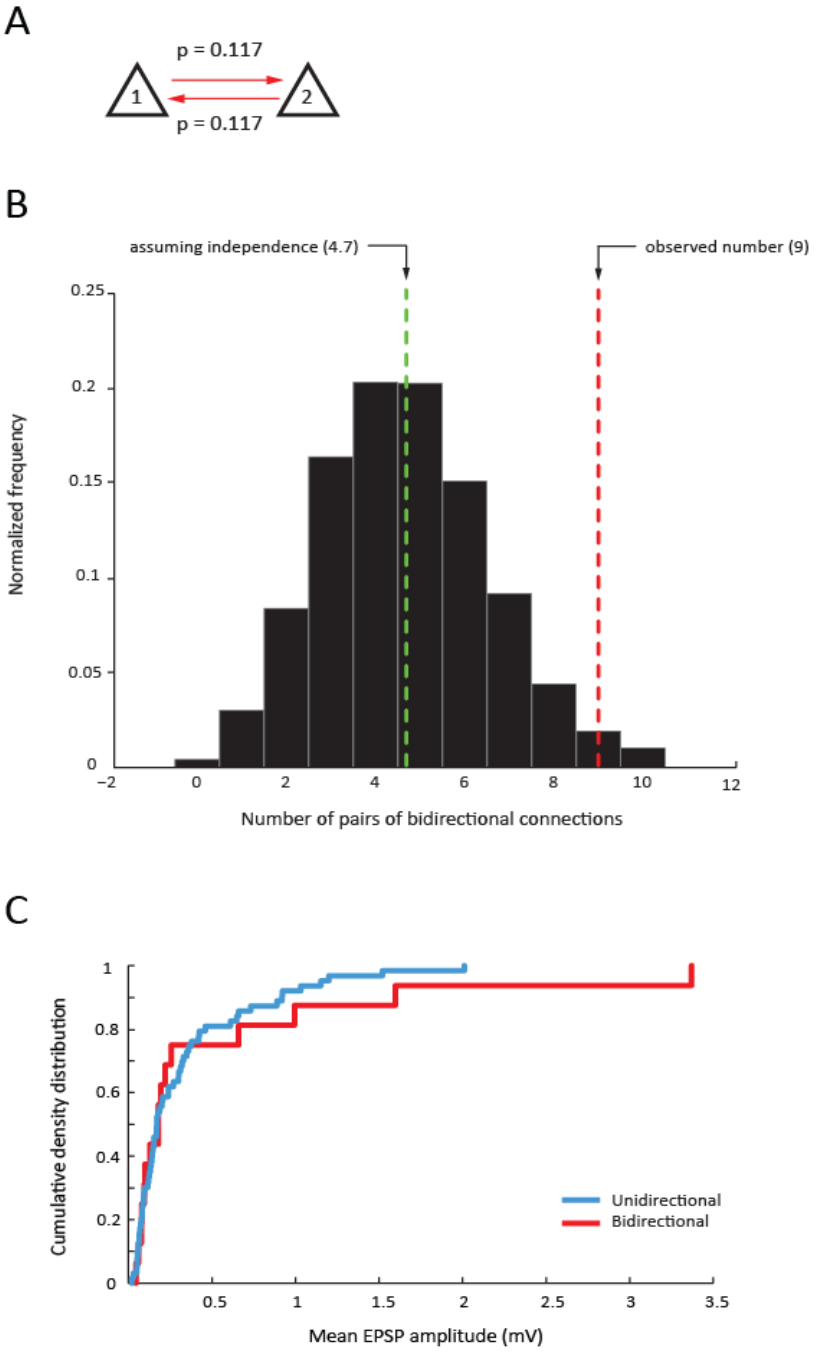

There was no significant difference ($p > 0.05$; unpaired Student's *t* test) between the mean EPSP amplitude for the bi- and unidirectional connections (compare 0.50 ± 0.19 and 0.34 ± 0.05 mV, respectively), nor there was a significant linear correlation between the EPSP amplitudes for either the connections in a given pair (R = 0.13). This is in contrast with previous reports done with developing animals where reciprocity of connections is greater for stronger connections (Markram et al., 1997; Holmgren et al., 2003; Song et al., 2005). Nonetheless, it holds true that if neuron A synapses onto neuron B, then the probability of B synapsing onto neuron A is several times greater than chance. As cortical excitatory synapses are weak and stochastic, a neuron cannot fire an AP unless it receives a significant number of synaptic inputs in a narrow time window. In so, what is the minimal number of presynaptic inputs that a neuron needs to receive to reach AP threshold? Knowing the range of AP threshold, and EPSP amplitudes (including the unconnected (EPSP amplitude = 0 mV) connections tested) for both cortical layers (Tables 6.1 and 6.2), it is possible to assess how many randomly chosen EPSPs should be added up to reach a given AP threshold. Assuming random firing and independent connection probabilities between pairs of neurons, an average of ~900 presynaptic neurons (Figure 6.8A; point *a*) are require to drive a postsynaptic neuron to fire an AP in layer 2/3. This estimation is significantly higher for layer 5 (~2400 presynaptic inputs; Figure 6.8B, point *a*). Interestingly, and taken into account the strongest connection found for either layer 2/3 (3.37 mV) and layer 5 (0.9 mV), the AP threshold could also be reached by a minimal number of ~25 presynaptic neurons for L2/3 (Figure 6.8A, point *b*), and ~100 presynaptic inputs for L5 (Figure 6.8B, point *b*).

Figure 6.7. ***Overrepresentation of bidirectional connection in cortical layer 2/3. A)*** *Independent probabilities of connections within a given pair of recorded neurons (triangles) are assumed.* ***B)*** *Distribution of counts of bidirectional connected pairs of neurons estimated by the bootstrap method. To notice that reciprocal connections are two times more likely to occur (red line) than predicted if independent probabilities of connections are assumed (green line);* ***C)*** *Cumulative density distribution of the mean EPSP amplitudes of the uni- (blue) and bidirectionally (red) connected pairs of neurons.*

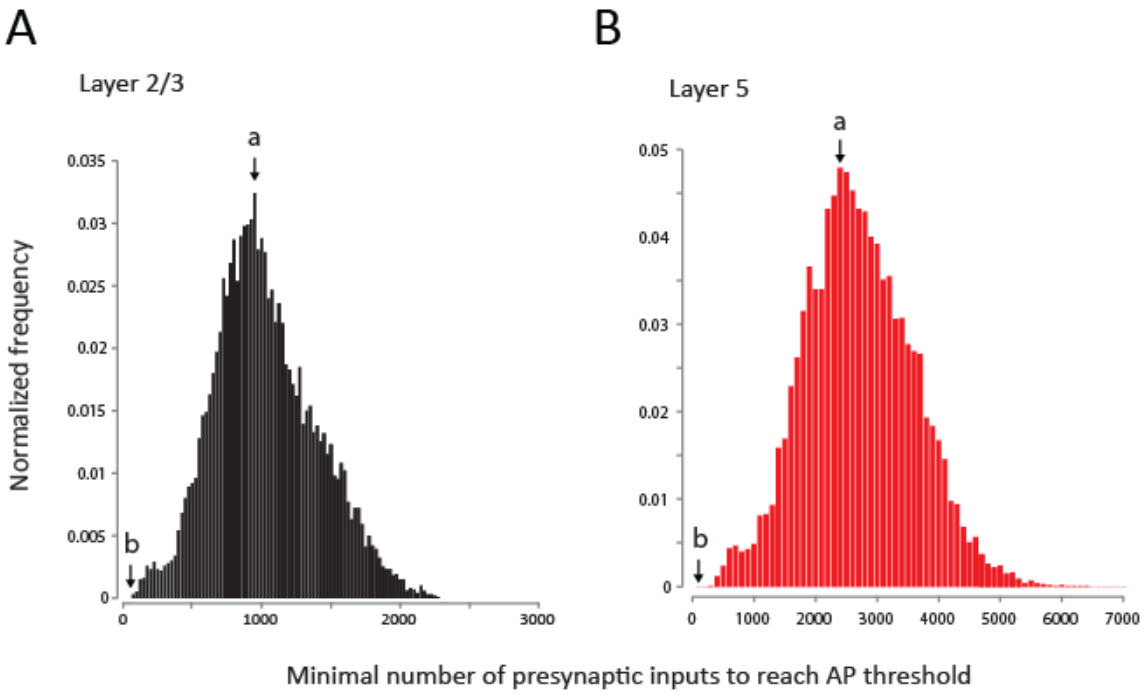

Figure 6.8. ***Estimation of the number of randomly chosen presynaptic inputs required to reach AP threshold.*** *Normalized distribution of number of presynaptic inputs required to drive a given postsynaptic neuron to reach action potential threshold in* ***A)*** *layer 2/3 (black; binned at 25 intervals) and* ***B)*** *layer 5 (red; binned at 100 intervals), estimated by the bootstrap method. Random firing and independent connection probabilities between pairs of neurons were assumed. Points* ***a*** *and* ***b*** *in both panels indicate, respectively, the average and the minimal (taken into account the largest EPSP amplitude found in both datasets) number of required presynaptic inputs to reach AP threshold.*

6.1.6. Cortical differences in spontaneous neuronal activity

One useful tool in assessing about the basic mechanisms of neurotransmission is the study of the spontaneous excitatory postsynaptic events. Due to the infrequent spontaneous spiking by cortical neurons (Hromádka et al., 2008; O'Connor et al., 2010) and their highly asynchronous states (Ecker et al., 2010; Renart et al., 2010), some of these events occur spontaneously in an AP-independent manner. The properties of these events, in particular frequency of occurrence and relative amplitude, offer a means to study the otherwise inaccessible presynaptic and postsynaptic terminals (e.g. Ribrault et al., 2011). The analysis of spontaneous excitatory postsynaptic potentials (sEPSPs) was made for both cortical layers, using a Template-based search method (see Methods). For

this purpose, the frequency of occurrence and the sEPSPs intrinsic amplitudes were assessed in parallel during the local connectivity experiments in only a subset of randomly chosen neurons (except for the ones where compensations in Vm had to be done). As can be observed in Figure 6.9, there was significant difference ($p < 0.05$) in the average frequency of these spontaneous events between layer 2/3 (1.4 ± 0.2 events/s; n = 34 neurons) and layer 5 (2.3 ± 0.2 events/s; n = 18 neurons). Moreover, there was a significant ($p < 0.05$, unpaired Student's *t* test) difference between the number of spontaneous events recorded in the individual neurons across layers (L2/3: 123.3 ± 15.4 events / neuron; L5: 207.8 ± 16.7 events / neuron). As showed in Figure 6.9C, the sEPSP amplitude was significantly higher in pyramidal neurons from layer 2/3 (0.83 ± 0.06 mV / neuron), as compared with layer 5 pyramids (0.44 ± 0.03 mV / neuron) ($p < 0.001$; unpaired Student's *t* test). Alterations in both the frequency and amplitude of sEPSPs suggest a bidirectional contribution of both presynaptic release and postsynaptic responsiveness mechanisms in global neurotransmission within these cortical layers.

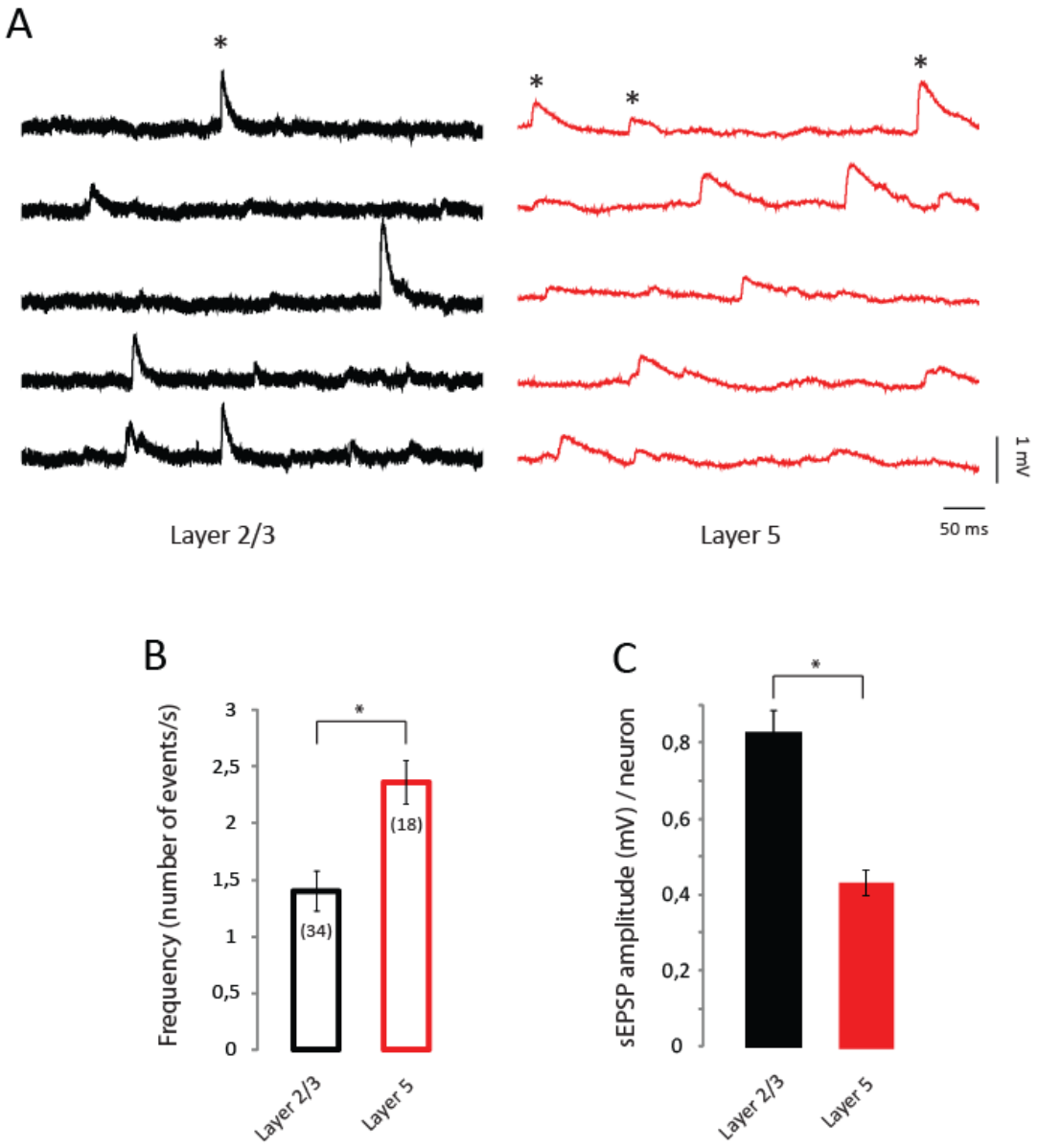

Figure 6.9. ***layer 2/3 and layer 5 sEPSs features. A)*** *Five representative whole-cell current-clamp recordings of sEPSPs from one layer 2/3 (left) and one layer 5 pyramidal neuron (right). Asterisk (*) denotes sEPSPs in either traces.* ***B)*** *Average sEPSP frequencies (number of neurons in brackets) and* ***C)*** *sEPSP amplitudes in layer 2/3 and layer 5. For all panels, colour scheme: black (layer 2/3), red (layer 5); All values are mean ± s.e.m.; * p < 0.001, unpaired Student's t test.*

6.2. Relative contribution of excitation/inhibition drive onto layer 2/3 pyramidal neurons with temporal resolution

In the second part of this work, the relative contribution of excitatory and inhibitory drives that impinge onto pyramidal neurons, with precise temporal resolution, was assessed. It is known that mature neocortical neurons form a dense mosaic that contains lateral and vertical connections travelling within and between the cortical layers (e.g. Douglas and Martin, 2004; see Introduction), where cortical excitability is determined by the influence of both excitatory (glutamatergic) and inhibitory (GABAergic and glycinergic) synaptic inputs that originates in dynamic local recurrent networks (e.g Binzegger et al., 2004). A delicate balance between excitation and inhibition that a neuron receives is thus maintained within a narrow window to avoid excessive excitation, or neuronal quiescence, in response to alterations in ongoing neuronal activity. In sensory cortices, a balance between feedback or feedforward inhibition and recurrent excitation reduces the randomness of cortical operation and increases temporal precision (e.g. Wehr and Zador, 2003; Le et al., 2006; Zhang et al., 2011).

In order to characterize the relative contribution of synaptic excitatory and inhibitory conductances onto layer 2/3 pyramidal neurons, synaptic currents were evoked by minimal intracortical extracellular electrical stimulation of two independent and convergent cortical pathways. One stimulation electrode was placed vertically to the targeted neuron directly in layer 4 in order to stimulate the known strong vertical columnar input from layer 4 neurons, while the second electrode was situated laterally to the recorded neuron to selectively activate the robust lateral recurrent intracortical input which is known to shape layer 2/3 pyramids responsiveness (see Introduction). Both pathways were alternatively stimulated with a double squared pulse, 100 ms apart (see Methods). Whole-cell recordings under voltage-clamp mode at varying holding potentials (from -90 to -30 mV, in some cases up to -15 mV holding potential; Figure 6.10) were made, followed by the determination of the associated excitatory and inhibitory conductances using previous linear methods (see Methods for details; Monier et al., 2003; Wehr and Zador, 2003; Le et al., 2006; Shu et al., 2003; Cruikshank et al., 2007).

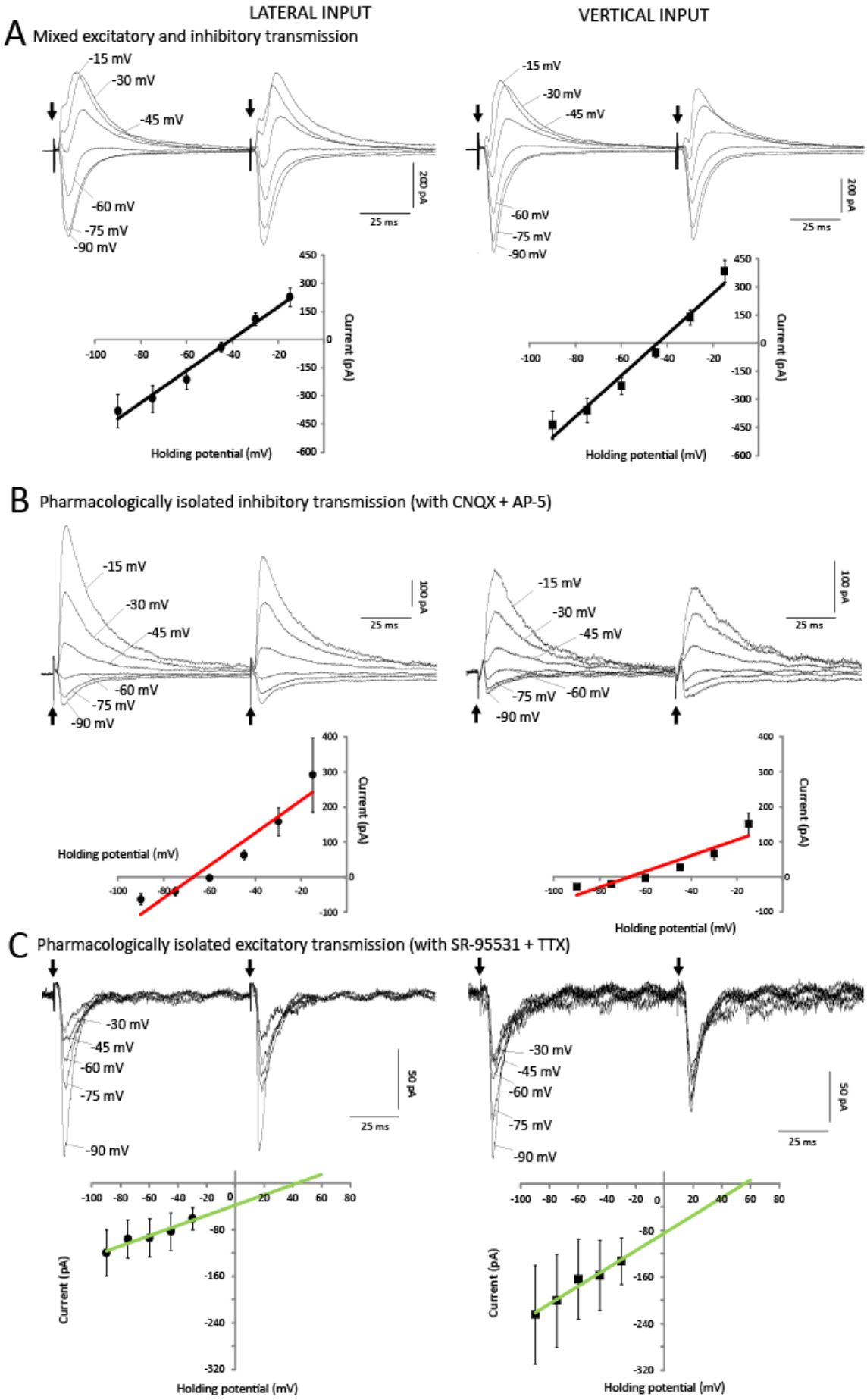
LATERAL INPUT
VERTICAL INPUT
A Mixed excitatory and inhibitory transmission
-15 mV
-30 mV
-45 mV
-60 mV
-75 mV
-90 mV
200 pA
25 ms
Current (pA)
Holding potential (mV)
B Pharmacologically isolated inhibitory transmission (with CNQX + AP-5)
100 pA
C Pharmacologically isolated excitatory transmission (with SR-95531 + TTX)
50 pA

The responses of the recorded pyramidal neurons to the stimulation of the lateral and vertical inputs had a weak excitatory conductance (G_e), followed by a statistically significant ($p < 0.05$; n = 20) stronger inhibitory conductance (G_i), as can be appreciated for an example in Figure 6.11A. On average, the maximum G_e and G_i for the lateral stimulated pathway were, respectively, 2.08 ± 0.6 and 7.22 ± 1.4 nS. For the vertical input the observation was similar (G_e = 2.0 ± 0.4 nS; G_i = 8.11 ± 1.6 nS). This discrepancy between G_e and G_i maxima was also observed for the 2nd pulse situation (Figure 6.11B). Moreover, it is known that in adult cortices, the ratio of excitatory and inhibitory conductances (E/I ratio) is presumably balanced across a wide variety of stimulus conditions. The establishment of E/I balance in adult cortical neurons may result from developmental and experience-dependent co-regulation of developing glutamatergic and GABAergic synapses (see Turrigiano and Nelson, 2004). In so, the

---

Figure 6.10. ***Determination of the synaptic excitatory and inhibitory reversal potentials. A)*** *Top: representative synaptic postsynaptic currents (PSCs) evoked by two 1ms-duration (100 ms apart) pulses extracellular stimulation of a lateral and vertical independent and convergent intracortical synaptic pathways to layer 2/3 pyramidal neurons at six different holding membrane potentials (from -90 to -15 mV). At depolarized holding potentials (from -45 mV, i.e. between reversal potentials for excitation and inhibition) the response was biphasic: initially inward, then turning outward in a few milliseconds. The overall synaptic currents amplitudes for a given individual neuron were similar when comparing both stimulated pathways. Bottom: corresponding synaptic current-voltage (I-V) curves for both stimulated inputs (n=20). The linear regression slope and x-intersect give, respectively, the synaptic conductance and mixed synaptic reversal potential.* ***B)*** *Top: representative pharmacologically isolated inhibitory PSCs (bath perfusion of CNQX (10 μM) and AP-5 (50 μM)) recorded at different holding membrane; Bottom: corresponding I-V plot used to calculate the inhibitory reversal potential for both stimulated inputs (n=5).* ***C)*** *Top: representative pharmacologically isolated excitatory PSCs (bath perfusion of SR-95531 (10 μM) and TTX (4nM)) recorded at several holding potentials. Bottom: corresponding I-V plot used to calculate the excitatory reversal potential, by linear extrapolation of the regression line (n=8). For all the panels, arrows indicate the double-pulse extracellular stimulation, and each PSC trace corresponds to the average of 10 consecutive repetitions at the same holding potential; (●), lateral input; (■) vertical input. Each point in the I-V curve corresponds to the averaged (± s.e.m.) PSCs amplitudes for the 1st pulse only, plotted against the holding potential.*

E/I ratio was directly measured for the layer 2/3 pyramidals when the two cortical inputs were stimulated. Overall, the E/I ratios for the lateral and vertical inputs were low (lateral: 0.33 ± 0.04; vertical: 0.5 ± 0.17), consistent with the notion of a general decrease in E/I ratio after the critic developmental period (Zhang et al., 2011), and were not significantly different from each other, arguing for a constant E/I ratio within and across cortical layers. Similar conclusions can be drawn for the 2nd pulse situation.

Furthermore, to test if there was a significant difference in excitatory-inhibitory delays for both stimulated pathways, the latencies between G_e and G_i peaks were measured (Figure 6.11C). For this purpose, the first derivative was applied to either the excitatory and inhibitory individual trace conductances, in order to assess about points of maximum conductances. On average, it was observed that the separation of excitation and inhibition (i.e. the delay of inhibition from excitation; n = 20 neurons) was 1.62 ± 0.8 ms for the lateral stimulated pathway, and 0.78 ± 0.4 ms for the vertical input. When analyzing the 2nd pulse situation, the observation was similar (Figure 6.11D). These excitatory-inhibitory delays were similar when compared both stimulated pathways (p > 0.05). The very narrow range of latencies between G_e and G_i (less than 2 ms) argues for a monosynaptic nature of the stimulated intracortical projections onto the recorded layer 2/3 pyramidal neurons (Cruikshank et al., 2007; Zhang et al., 2011).

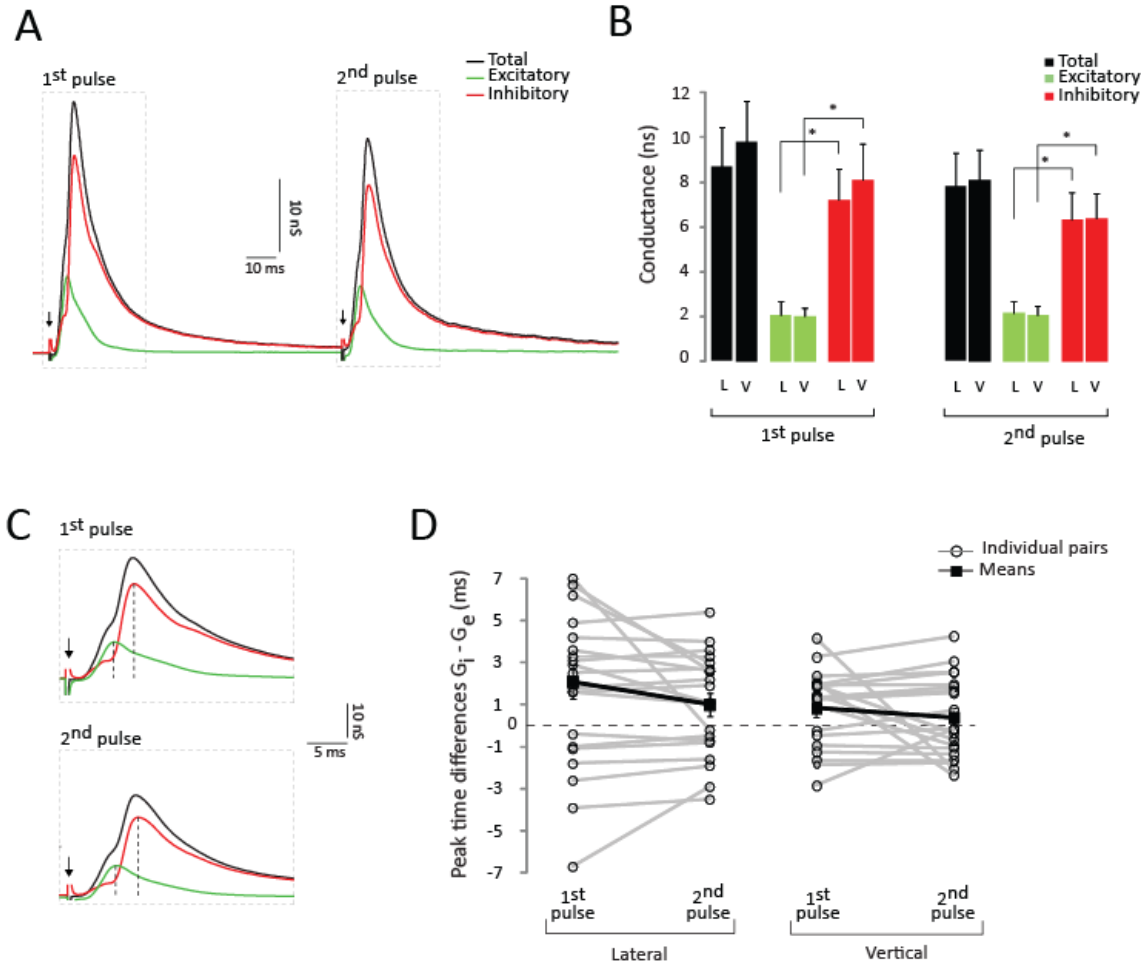

Figure 6.11. ***Temporal resolution of vertical and lateral excitation/inhibition drives onto layer 2/3 neurons. A)*** *Representative example of the temporal evolution of the underlying excitatory (green) and inhibitory (red) conductances after decomposition of the total conductance (black), from the same neuron as in Figure 6.10A. The decomposition of the total conductance was done by comparing the measured reversal potential for the mixed synaptic conductance to the previously calculated reversal potentials for excitation and inhibition, using conventional linear methods (e.g. Cruikshrank et al., 2007).* ***B)*** *Quantification of the average (± s.e.m.) maximum excitatory (green) and inhibitory (red) conductances after decomposition of the total trace (black), for both stimulated pathways (L, lateral; V, vertical) and for both delivered pulses.* ***C)*** *Expanded traces of the initial time period highlighted in panel A (dashed boxes), showing the time latency between the inhibitory peak conductance and the excitatory conductance (vertical dashed lines), after the stimulation onset, in both pulses delivered.* ***D)*** *Quantification and comparison between the peak time differences between inhibitory and excitatory conductances for both stimulated pathways. Thin grey lines connect the 1st and 2nd pulse for a given recorded cell, while the thick black line connects group means. For all the panels, arrows indicate the double-pulse extracellular stimulation; (*), $p < 0.05$, paired Student's t test.*

In addition to the amplitudes of the intracortical conductances, the kinetics of these conductances was also examined. As showed before, on average, excitatory conductances preceded inhibitory conductances by less than 2 ms. Interestingly, however, and in opposition with previous reports (e.g. Wehr and Zador, 2003; Le et al., 2006; Cruikshank et al., 2007; Zhang et al., 2011), in almost half of the recorded neurons (8 out of the total 20 neurons), the inhibitory trace presented a two-wave barrage conductance, which can be fully appreciated in Figures 6.12A and 6.12B. It was observed that, on average, in these cases, the first inhibitory wave came on average 1.4 ± 1.0 ms before the maximum of the excitatory conductance peak for the lateral input, and 0.12 ± 0.6 ms for the vertical input (Figure 6.12C). Similar finding was observed for the 2^{nd} pulse situation. It was also observed that the latencies of the inhibitory second wave were surprisingly bigger: 3.4 ± 1.7 ms for the lateral pathway, and 6.0 ± 1.4 ms. Similar latencies were also seen for the 2^{nd} pulse situation for both stimulated pathways. This surprisingly finding is consistent with a view of a possible disynaptic feedback or feedforward inhibitory mechanism (Cruikshank et al., 2007; Zhang et al., 2011; see Discussion, section 6.5).

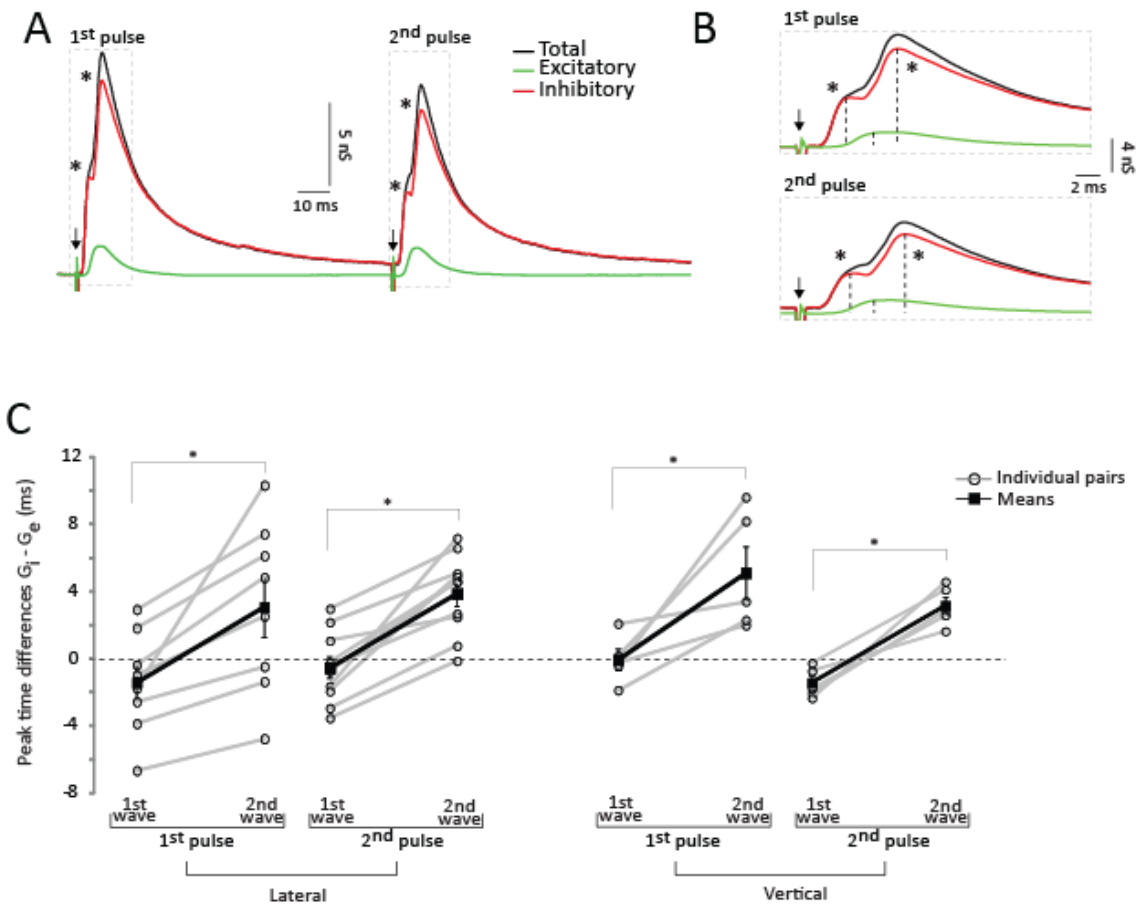

6.3. Features of local cortical connectivity upon the acquisition of an artificial-driven behaviour

In the third part of this study, one final question was made: how is neuronal connectivity affected after the acquisition of a learned behaviour? It is known that learning and perceptual guided behaviours in mammals can be driven by artificial activation of cortical neurons (Houweling and Brecht, 2007; Huber et al., 2008; Wang et al., 2012). In fact, the induction of perception-guided behaviours (Huber et al., 2008; Otto et al., 2005; Wang et al., 2012) can be achieved by the activation of a relative small number of neurons (e.g. ~700, Huber et al., 2008; ~300, Choi et al., 2012), and that decision making occurs in the timing of the intrinsic cortical activity (as short as 3 ms; Yang et al., 2008).However, to address the initial question, one should develop a strategy to precisely control and activate defined groups of neurons, assess about their relevance in driving a given behaviour and finally to determine if a given acquired behaviour is translated in alterations in synaptic connectivity between those specific

neurons that were engaged in the task. Although cortical electrical microstimulation can establish possible relationships between the activity of groups of neurons and perceptual and discriminatory behaviours (e.g. Houweling and Brecht, 2008; Otto et al., 2005; Rousche et al., 2003), it encompasses several disadvantages, namely, it excites local and long-range axons non-discriminately. Therefore, the cell types and precise cell locations that drive behaviour in classical microstimulation experiments are poorly defined. This drawback can at least partially be overcome by direct photostimulation of genetically defined neural populations.

6.3.1. Characterization of light-induced responses in channelrhodopsin-expressing pyramidal neurons

In this strategy, groups of neurons are genetically rendered with photosensitivity by means of expression of the transmembrane light-gated algal channel channelrhodopsin-2 (ChR2). The activation of ChR2 with blue light (~470 nm wavelength) is sufficient to produce rapid light-activated cationic photocurrents (Nagel et al., 2003), which allows neurons to be engaged in single and in complex trains of action potentials in a precise

---

Figure 6.12. ***Two-wave inhibitory patterns. A)*** *Representative example of the temporal and kinetic evolution of the underlying excitatory (green) and inhibitory (red) conductances after decomposition of the total conductance (black) For a total of 8 (out of the 20 neurons total; Figure 6.11), a two-wave inhibitory pattern barrage was observed, as a two distinct inhibitory peak conductances (denoted by asterisk).* ***B)*** *Expanded traces of the initial time period highlighted in panel A (dashed boxes), where vertical dashed lines indicate the time of maximum conductances for the inhibition and excitation, after the stimulation onset. Two inhibitory peak conductances were clearly observed, with different latencies towards the excitation maximum conductance.* ***C)*** *Quantification and comparison of the peak time differences between the two-wave barrage inhibition and excitation, across the stimulated pathways, and the double extracellular stimulation pulses. For all cases, the first wave of inhibition came before the excitatory peak conductance, while the 2nd wave always followed the excitation. Thin grey lines connect the 1st and 2nd inhibitory waves for a given recorded cell. A thick black line connects group means For all the panels, arrows indicate the double-pulse extracellular stimulation; (*), $p < 0.05$, comparison between means; paired student's t test.*

temporal mode (Boyden et al., 2005).In the present study, two ChR2 constructs were tested for their ability to render light sensitivity to neurons, and possible suitable use during *in vivo* photostimulation-driven behaviour (see later). In the first construct used, denoted "Syn-ChR2", the H134R mutation present in the ChR2 sequence can give rise to larger stationary photocurrents in comparison to the wild-type ChR2 (Zhang et al., 2007). In this case, the expression of the ChR2, and the reporter fluorescent protein (EYFP), were under the control of the synapsin-1 promoter (Figure 6.13A), which allows the exclusive expression of ChR2 to neurons (Kügler et al., 2002). By using confocal microscopy, it was possible to conclude that ChR2-EYFP invaded the soma, dendrites and axons of neurons (Figure 6.13B). In the second construct used (denoted "CamKII-ChETA"), neurons were rendered photosensitive with an ultra-fast ChR2 variant (ChETA). This fast kinetic mutant of ChR2 carries the point mutation E123T in a H134T background and it is engineered to render a more precise temporal resolution in the light-induced APs over sustained trains of light due to its intrinsic faster deactivation kinetics (Gunaydin et al., 2010). The ChETA sequence was fused to the self-processing peptide 2A (P2A), and to the histone 2B sequence (H2B), and further to the red fluorescent protein mCherry (Figure 6.13D). After P2A self-cleavage (Tang et al., 2009), ChETA-specific membrane expression is made "visible" by the correspondent nuclear red label, which has the advantage of proper visualization of infected neurons in the brain slice (Figure 6.13E), while minimizing ChETA activation with a different light wavelength. The genetic construct was under the control of the α-calcium/calmodulin-dependent protein kinase II (CaMKII) promoter, allowing specific targeting of excitatory neurons (Burgin et al., 1990).

By means of stereotaxic injections, in separate mice, of recombinant adeno-associated virus (AAV), which carries the different ChR2 constructs, it was possible to target for neocortical neurons present in the upper cortical layers of the auditory cortex (Figure 6.13B and 6.13E; see Methods). To characterize the responses of the ChR2-expressing neurons to photostimulation, coronal brain slices from naïve mice were made, 4-5 weeks post-viral injection. A specific and prominent fluorescent expression was observed in the primary injection site in the auditory cortex (Figure 6.13B and 6.13E), as well in axonal callosal projections into the contralateral side, and even retrograde projections into the auditory thalamus for the Syn-ChR2 construct (Figure 6.13B). This indicates the correct targeting of auditory cortex for viral infection.

Whole-cell recordings were made specifically from ChR2-positive layer 2/3 cortical pyramidal neurons, as before. Photosimuli consisted of trains of 5 individual light pulses (5 ms width pulse), delivered at different and increasing frequencies (from 1 to 80Hz), via full-field epifluorescence microscopy (bandwidth 460 - 495 nm using a blue excitation bandpass filter U-MWIB3 and 100W mercury lamp; 12.02 mW light-intensity). Light-induced APs were pharmacologically isolated by continuous superfusion of the synaptic transmission blockers CNQX (10 μM), AP-5 (50 μM) and gabazine (10 μM). This characterization had the purpose to assess up to which light-pulse frequency a ChR2-positive layer 2/3 pyramidal neuron could reliably follow the light train. On average, it was observed that neurons expressing Syn-ChR2 (n = 10), or CamKII-ChETA (n = 9), can fire one AP in response to each of the single light pulses reliably in the range between 1 to 20 HZ of light frequency (Figures 6.13C, 6.13F and 6.13G). However, there was an improved performance from CamKII-ChETA-expressing neurons over a broader frequency range (up to 40Hz), also in accordance with previous reports (Gunaydin et al., 2010). In this regard, ChETA-expressing neurons considerably outperformed the Syn-ChR2-positive neurons (Figures 6.13G).

Furthermore, the photocurrents amplitudes elicited by one long (1 sec) pulse of blue light were recorded from neurons expressing both genetic constructs. It was observed robust inward photocurrents in Syn-ChR2-positive neurons (655.4 ± 92.0 pA measured at the steady-state level; n = 15) with rapid kinetics (Figure 6.13H). These photocurrents initially peaked, then decreased to a sustained level, and lasted only during the light pulse duration. In all Syn-ChR2-expressing pyramidal neurons recorded from (15/15) it was possible to observed light-induced APs mediated by inward photocurrents, which argues that possibly all the neurons infected in the primary injection site are ChR2-positive neurons, with minor differences in ChR2 expression levels due to the narrow range of photocurrent amplitudes across individual neurons. On the other hand, the ChETA-mediated photocurrents were statistically ($p < 0.05$) smaller (82.5 ± 7.6 pA; n = 9/9) when compared with the photocurrents in Syn-ChR2-expressing neurons (Figure 6.13H), and also compared with previous reports in hippocampal cultures, where photocurrents of ~ 650 pA were observed (Gunaydin et al., 2010). Although ChETA-expressing excitatory neurons outperformed their Syn-ChR2-expressing counterparts in the undeniable ability to reliably fire APs in a broader frequency range (from 1 to 40Hz), the significant lower amplitude of its photocurrent could in part explain the

inefficacy of the use of ChETA for in vivo photostimulation-dependent task. In fact, originally intended to pursue behaviour photostimulation experiments, it did not prove to be the best suitable approach to do so. One possible explanation might be an incomplete cleavage of the linking self-processing peptide 2A, resulting in insufficient ChETA expression at the neuron's membrane, which would result in low amplitude photocurrents. No major differences ($p > 0.05$) were observed in resting membrane potential and membrane resistance in neurons expressing either of the channelrhodopsin variants (Syn-ChR2: -59.0 ± 2.7 mV and 248.2 ± 21.4 MΩ, n = 15 neurons, respectively; ChETA: -61.0 ± 2.4 mV and 252.5 ± 39.7 MΩ, n = 9 neurons, respectively).

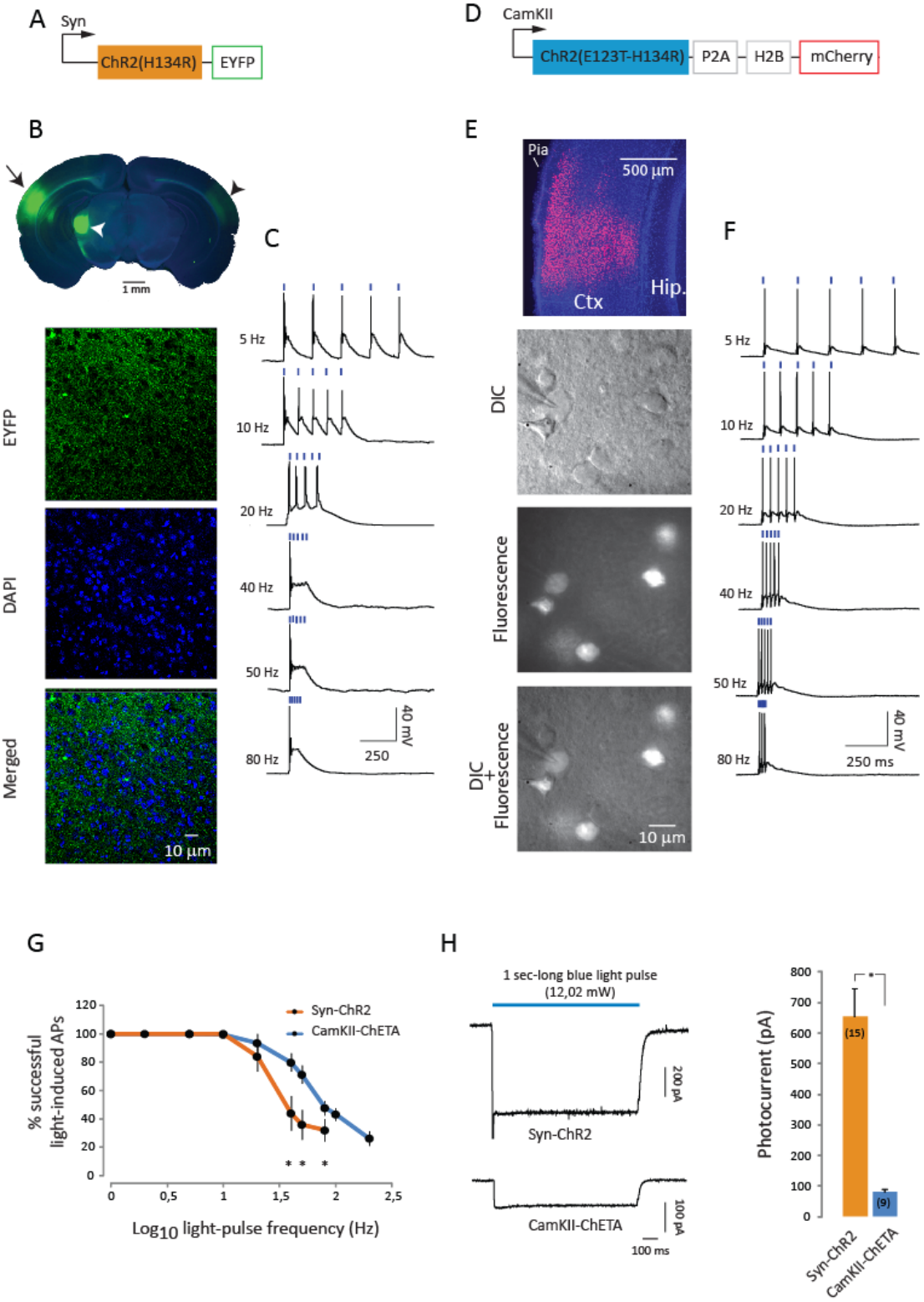
A
Syn
ChR2(H134R)
EYFP
D
CamKII
ChR2(E123T-H134R)
P2A
H2B
mCherry
B
1 mm
C
EYFP
DAPI
Merged
10 µm
5 Hz
10 Hz
20 Hz
40 Hz
50 Hz
80 Hz
40 mV
250
E
Pia
500 µm
Ctx
Hip.
DIC
Fluorescence
DIC + Fluorescence
10 µm
F
5 Hz
10 Hz
20 Hz
40 Hz
50 Hz
80 Hz
40 mV
250 ms
G
% successful light-induced APs
120
100
80
60
40
20
0
Syn-ChR2
CamKII-ChETA
* * *
0
0,5
1
1,5
2
2,5
Log10 light-pulse frequency (Hz)
H
1 sec-long blue light pulse
(12,02 mW)
200 pA
Syn-ChR2
CamKII-ChETA
100 pA
100 ms
Photocurrent (pA)
800
700
600
500
400
300
200
100
0
(15)
(9)
*
Syn-ChR2
CamKII-ChETA

Figure 6.13. ***Rendering of photosensitivity to neurons in layer 2/3 by expressing ChR2. A)*** *Drawing of the genetic construct used to express ChR2 into neurons. ChR2 carrying one point mutation (H134R), fused to an enhanced yellow fluorescent (EYFP) marker, and under the control of the synapsin-1 promoter.* ***B)*** *Top: Full-field epifluorescence coronal slice image showing the primary injection site (arrow), as well as contralateral colossal axonal projections (black arrowhead) and thalamic projections (white arrowhead). Green: EYFP expression; Blue: nuclear marker DAPI; Bottom: Confocal microscopy pictures of ChR2 expression (EYFP fluorescence; green) in the primary injection site of slice depicted above, revealing somatic, dendritic and axonal specific expression.* ***C)*** *Current-clamp recordings illustrating light-induced APs in one representative Syn-ChR2-EYFP-expressing neuron, in response to trains of 5 light pulses (5 ms pulse width; blue mini-bars on top of the traces) at varying frequencies (left).* ***D)*** *Schematic drawing depicting the construct used to expressing the ultra-fast ChR2 version (ChETA) into neurons. ChETA, carrying the point mutation E123T in H134T background was fused to the auto-cleavable peptide 2A (P2A), histone 2B (H2B) sequence and the red fluorescent protein mCherry, under the control of the CamKII promoter.* ***E)*** *Top: Full-field epifluorescence image depicting the primary injection site for ChETA expression (mCherry fluorescence; red) specifically in the auditory cortex of a mouse previously injected with the construct depicted in C); Blue: nuclear marker DAPI as a counterstaining; Ctx: cortex; Hip.: hippocampus; Bottom: Representative DIC and fluorescence images of individual layer 2/3 neurons taken from the slice depicted above.* ***F)*** *Same as C), for a representative neuron expressing CamKII-ChETA. Note the reduced AP's plateau potential which allows the neuron to reliably follow the light train up to 50Hz, as compared to the example in C).* ***G)*** *Summary of the percentage of successful light-evoked APs as a function of light-pulse frequency (1, 2, 5, 10, 20, 40, 50 and 80Hz) for the recording neurons expressing Syn-ChR2 (orange; n = 10) or CamKII-ChETA (blue; n = 9). Note that above 40Hz, on average, neurons cannot reliably follow the light trains.* ***H)*** *Left: photocurrents induced by 1 sec-long blue light pulse (horizontal bar) in representative pyramidal neurons expressing Syn-ChR2 (top trace) or CamKII-ChETA (bottom trace). Neurons were voltage-clamped at -65 mV; Right: quantification summary of the photocurrents amplitudes in Syn-ChR2 (orange) and CamKII-ChETA (blue) expressing neurons, represented by mean ± s.e.m. Values in brackets are the total number of recorded neurons. (*) $p < 0.05$, unpaired Student's t test.*

6.3.2. Optical photostimulation in auditory cortex can drive behaviour in freely moving mice

The next main question is: can freely moving mice learn to report photostimulation of layer 2/3 neurons in the auditory cortex? To answer this, light-pulses were delivered to Syn-ChR2-expressing neurons in awake and freely moving mice. For this purpose, a small and permanent cranial window was implanted above the auditory cortex, which provided optical access for further photostimulation via a miniature blue LED placed in the centre of the window (Huber et al., 2008; Figure 6.14A). The miniature LED was further connected to a controller during the entire behaviour session. When there was a deterioration of the optical path due to thickening of the dura, and bone growth, among others, over the long time spans required for the behavioural training, the mice were immediately removed from the experiments, and were not considered for further analysis.

Mice were initially habituated to the training chamber, for a period that on average lasted 4 to 5 days (Figure 6.14B). During the habituation, no photostimulation was delivered (see Methods). Afterwards, mice were trained in a task to associate photostimulation of Syn-ChR2-expressing neurons in the auditory cortex (one train of 5 light-pulses, 20Hz, 250 ms total duration) to an aversive stimulus (air puff), or to a water reward when no photostimulation was delivered. In such a task, mice should be able to retract its head from the water delivery port upon auditory cortex photostimulation, and thus avoiding punishment, or get a water reward by not removing its head in the non-photostimulation situation (Figure 6.14C). It was observed that on average, after five to ten training sessions, a subset of mice (7 out of a total of 13 mice) expressing Syn-ChR2 in the auditory cortex reliably reported photostimulation; in the presence (absence) of a photostimulus, mice retracted (stayed in the port) its head form the water port (Figures 6.14C and 6.14E, range 69.7 – 96.5% correct performance). Moreover, mice reached a plateau of 90 to 160 trails per session. Asymptotic correct performance levels were reached only after the 30^{th} session, in contrast with previous reports (4^{th} to 7^{th} session, Huber et al., 2008). Control mice (n = 3), previously injected with a genetic construct that does not render photosensitivity to neurons (expression of EGFP only), performed only at change levels (50%), even after 35 sessions (Figures 6.14D and 6.14E). In the future, it is of utmost importance to increase the number of

Syn-ChR2-injected mice that are due to be trained. Nevertheless, these experiments demonstrate that photostimulation of supragranular layers of the auditory cortex can drive perceptual-guided behaviour. Due to the light scattering effects in the brain tissue, it argues that cortical upper layers are mainly activated in detriment of infragranular ones (Huber et al., 2008).

6.3.3. Impact of artificial-guided behaviour in local synaptic connectivity

To assess how patterns of local synaptic connectivity are affected by the learned acquisition of the previous photostimulation-guided task, *in vitro* whole-cell recordings were made from mice that reached asymptotic correct performance levels (n = 7; see Figure 6.14D). For this purpose, mice were trained in a last behaviour session and, less than 24 h after, coronal whole-brain slices were made as previously described from those specific mice. For all the mice that were used for electrophysiology recordings, it was possible to observe a remarkable Syn-ChR2 expression (via EYFP fluorescence) in approximately 2 to 3 slices that contained the auditory cortex. As a control, mice were used which did not go along the training procedures (n = 7), and so, were not subject of any behaviour contingency. These non-trained mice were only subjected to the virus-mediated Syn-ChR2 expression, and care was taken to choose mice with similar virus expression timelines for proper comparison. On average, for both trained and non-trained mice, the age of the animals was in the range of 12 – 13 weeks, and 6 to 8 weeks after virus injection. As can be appreciated in Table 6.3 and Figure 6.15A, the neurons from trained and non-trained mice were virtually indistinguishable from each others, presenting comparable resting membrane potential, membrane resistance, and several AP features, including spiking threshold, AP amplitude and overshoot ($p > 0.4$; unpaired Student's *t* test).

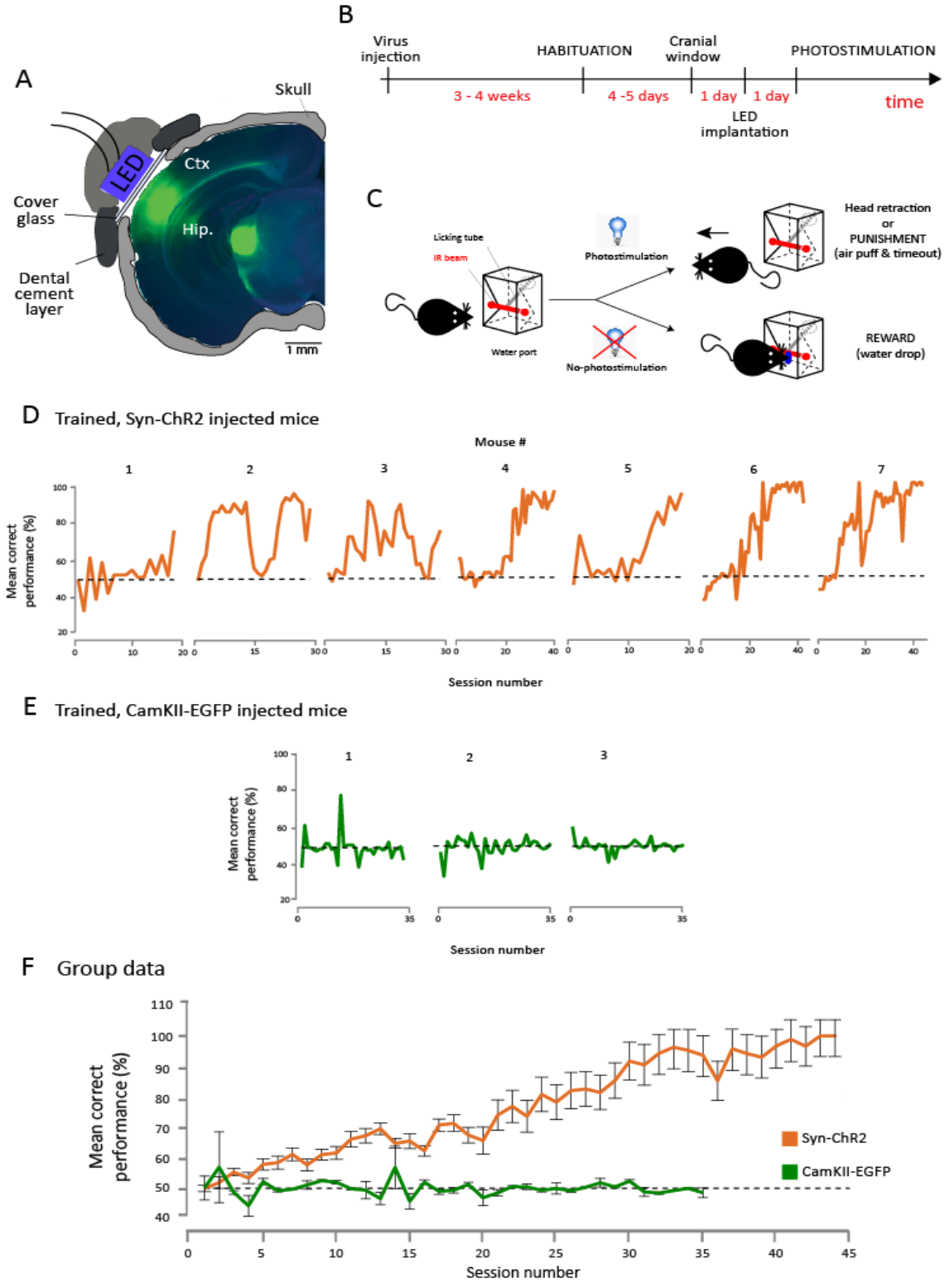
A
Skull
LED
Ctx
Hip.
Cover glass
Dental cement layer
1 mm
B
Virus injection
HABITUATION
Cranial window
PHOTOSTIMULATION
3 - 4 weeks
4 -5 days
1 day
1 day
LED implantation
time
C
Licking tube
IR beam
Water port
Photostimulation
No-photostimulation
Head retraction or PUNISHMENT (air puff & timeout)
REWARD (water drop)
D
Trained, Syn-ChR2 injected mice
Mouse #
Mean correct performance (%)
Session number
E
Trained, CamKII-EGFP injected mice
Mean correct performance (%)
Session number
F
Group data
Mean correct performance (%)
Syn-ChR2
CamKII-EGFP
Session number

Figure 6.14. ***Photostimulation of the auditory cortex in freely moving mice performing a perceptual task. A)*** *Schematic of the photostimulation apparatus. After a small craniotomy, a small cover glass is apposed to the exposed cortical area previously injected with Syn-ChR2 construct (green), and stably fixed with dental cement. A removable miniature blue LED is placed over the cranial window to selectively activate neurons expressing Syn-ChR2. Ctx: cortex; Hip.: hippocampus.* ***B)*** *Detailed timeline of the experimental procedure.* ***C)*** *Schematic of the behaviour apparatus and reward contingencies. The mouse initiates a trial by introducing its snout into the water port and breaking the infrared (IR) beam. Photostimulation (PS) consists of one train of 5 blue light pulses (5ms pulse width), delivered at 20Hz. The mouse then decides to either retract its head to avoid a punishment (air puff and 7s timeout period), or to wait for a water reward by licking the water delivery tube. For every trail initiated, a blue masking light placed immediately above the water port is presented (one light pulse; 250ms duration) to mask possible scattered light into the retina by the removable blue LED. PS and non-photostimulation (NPS) trials were presented pseudo-randomly with a probability of 0.5 throughout the entire 30 minutes behaviour session.* ***D)*** *Individual behaviour performance data from 7 mice previously injected with Syn-ChR2. Represented is the percentage of average correct performance (orange lines) throughout individual sessions. Note the variability in the time (sessions number) that a given mouse needs to perform correctly task. Dashed line corresponds to change levels (50%).* ***E)*** *Behaviour performance (green lines) in 3 mice previously injected with CamKII-EGFP virus.* ***F)*** *Group data for the behaviour performance for mice injected with Syn-ChR2 (orange; n = 7) and with CamKII-EGFP (green; n = 3) along individual behaviour sessions. Thick line: mean ± s.em; dashed black line: chance levels (50%).*

Table 6.3. ***Intrinsic membrane and connectivity properties of the recorded pyramidal neurons in trained and non-trained mice.*** *Values are average ± s.e.m.; Vm, resting membrane potential; Rm, membrane resistance; n, number of neurons*

	Trained	n	Non-trained	n
V_m (mV)	-66.1 ± 1.9	26	-64.2 ± 2.0	16
R_m (MΩ)	262.5 ±27.1	26	289.3 ± 45.8	16
AP threshold (mV)	-29.1 ± 3.5	26	-25.3 ± 4.0	16
AP amplitude (mV)	97 ± 1.8	26	98.6 ± 2.4	16
AP overshoot (mV)	67.2 ± 3.9	26	72.8 ± 5.9	16
AP half-height width (ms)	1.7 ± 0.03	26	1.6 ± 0.07	16
P (found /tested)	7.0 % (6/86)		2.8 % (2/72)	
Mean EPSP amplitude (mV)	0.23 ± 0.07		0.31	
Range (mV)	0.03 – 0.39		0.04 – 0.59	

Neurons that needed to be injected with a compensatory current to maintain a constant Vm level were rejected from this particular analysis. Interestingly, it was observed that, on average, ChR2-expressing neurons from trained (n = 26) and non-trained (n = 16) mice, were more depolarized and had higher membrane resistance values when compared with their counterparts from naïve mice that were not injected with ChR2 (Naïve: Vm = -74.2 ± 0.88 mV, Rm = 126.2 ± 5.70 MΩ; $p < 0.05$, one-way ANOVA; see Tables 6.2 and 6.3). Moreover, there was no significant difference in the AP threshold between groups (Trained: -29.1 ± 3.5; Non-trained: -25.3 ± 4.0; Naïve: -32.4 ± 1.69; $p = 0.2135$; one-way ANOVA). However, ChR2-positive neurons from trained and non-trained mice presented APs with higher amplitudes and overshoots, as compared with layer 2/3 neurons from non-injected mice (Naïve: AP amplitude = 91.8 ± 1.13 mV, AP overshoot = 58.8 ± 1.99 mV; $p < 0.012$, one-way ANOVA).

Furthermore, when the number of APs that a given neuron from trained and non-trained mice groups were plotted in relation with the input injected current (Figure 6.15B), it was observed that in general, neurons from the trained group have a tendency to fire less APs (for the same input current level) as compared with its non-trained counterparts neurons ($p = 0.01$; two-way ANOVA).

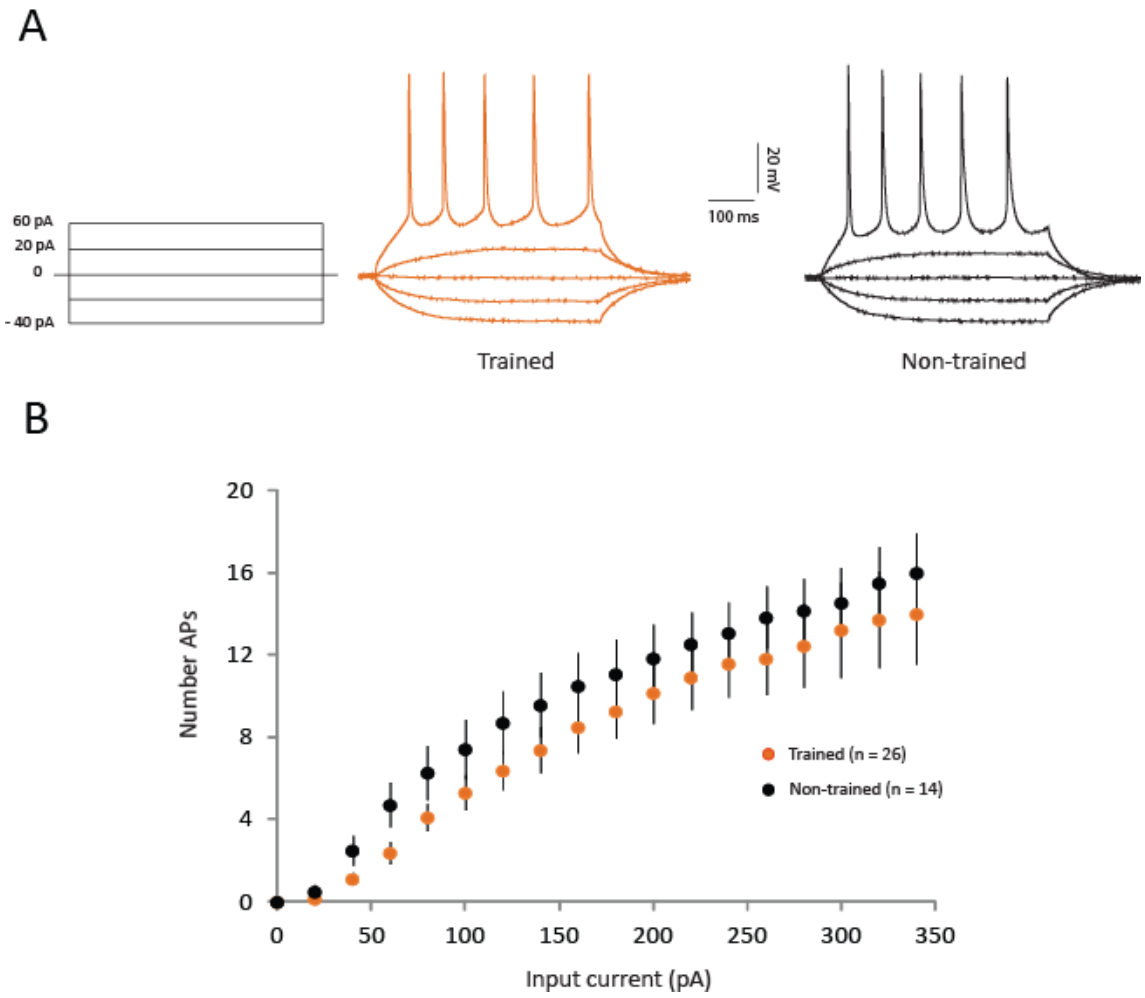

Figure 6.15. ***Intrinsic excitability features of pyramidal neurons from trained and non-trained mice. A)*** *Left: schematic diagram depicting the injected current steps (from -40 to 100 pA); Middle and right: Representative voltage traces evoked by the injected command steps from individual pyramidal neurons from a trained and non-trained mouse. APs were virtually indistinguishable when comparing both behaviour situations.* ***B)*** *Relationship between the number of APs that neurons from trained (n = 24 neurons; 7 animals; orange circles) or non-trained mice (n = 16 neurons; 7 animals; black circles) could fire upon increasing input current (input/output curve). A significant difference was observed between trained and non-trained mice (p = 0.01; two-way ANOVA test). All values are mean ± s.e.m*

As shown in Table 6.3, there was not a significant difference in the average EPSP amplitude between trained and non-trained mice (and even when comparing with naïve mice data; Tables 6.2 and 6.3). Synaptic connectivity between pairs of Syn-ChR2-positive neurons was assessed as described before. It was observed that the probability of a given pair of ChR2-expressing neurons of being connected was, on average, for

trained and non-trained mice, low (Table 6.3). A total number of 48 neurons from trained and 40 neurons from non-trained mice were recorded from. A total of 86 possible synaptic connections were tested, among which 6 were functional ones, in the sum of trained mice used (n = 7), giving a value of 7.0% as the average probability of any two excitatory layer 2/3 neurons being monosynaptically connected. For the non-trained mice a connection probability of 2.8% was found, which represents a total of just 2 functional connections among 72 possible ones. No significant difference was found between probability of connection among trained and non-trained mice (tow-tail Fisher's exact test; p = 0.292). Due to the technically demanding nature of the experiments, it was not possible to obtain a data set that would be large enough to adequately pursue proper analysis.

6.3.4. Comparable spontaneous neuronal activity in trained and non-trained mice

The analysis of spontaneous excitatory postsynaptic potentials (sEPSPs) was made in layer 2/3 pyramidal neurons from trained and non-trained mice, using a Template-based search method (see Methods). As before, the frequency of occurrence and the sEPSPs amplitudes were assessed in parallel during the connectivity experiments in a subset of randomly chosen neurons (except for the ones where compensations in Vm had to be done). As shown in Figures 6.16A and 6.16B, it was observed that the average frequency of these spontaneous events was similar ($p > 0.05$, unpaired Student's *t* test) between these two groups of mice (Trained: 2.3 ± 0.3 events/s; n = 11 neurons; Non-trained: 2.2 ± 0.4 events/s; n = 10 neurons). Moreover, the number of spontaneous events recorded in the individual neurons from trained (200.6 ± 28.2 events / neuron) and non-trained (155.6 ± 26.7 events / neuron) mice were also similar ($p > 0.05$).. Furthermore, as showed in Figure 6.16C, the sEPSP amplitude was as well similar ($p > 0.05$) between both groups of mice (Trained: 0.41 ± 0.03 mV / neuron; Non-trained: 0.49 ± 0.08 mV / neuron). It is concluded that the active engagement of a mouse in a behaviour task do not have any effect on the on-going neuronal activity in pyramidal neurons in layer 2/3.

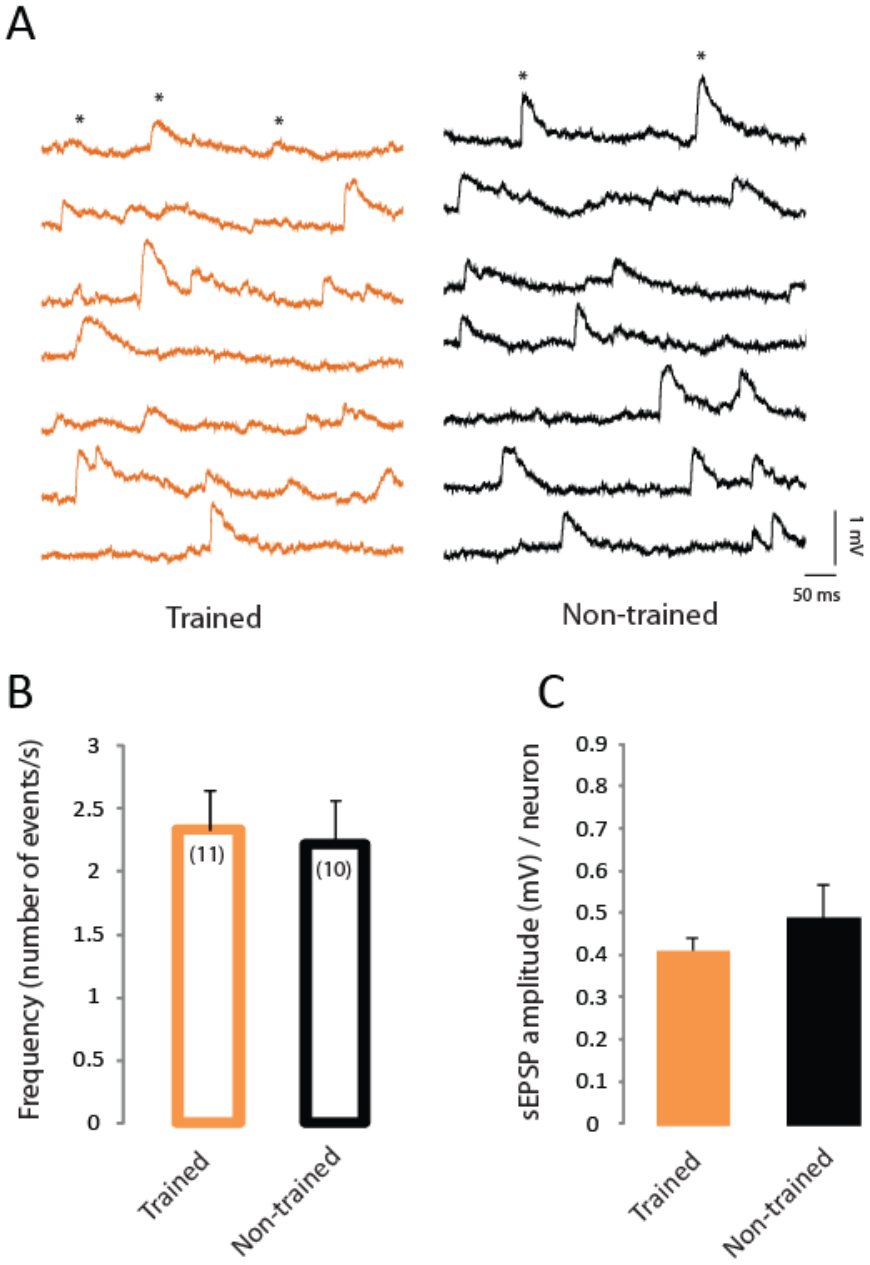

Figure 6.16. ***Increase in layer 2/3 sEPSP frequencies and decrease in sEPSP amplitudes in Syn-ChR2-expressing layer 2/3 neurons in trained/non-trained mice. A)*** *Seven representative whole-cell current-clamp recordings of sEPSPs from one layer 2/3 pyramidal neuron in trained (left) and non-trained (right) mice. Asterisk (*) denotes sEPSPs in either traces.* ***B)*** *Average sEPSP frequencies (number of neurons in brackets) and* ***C)*** *sEPSP amplitudes (number of events in brackets) in trained and non-trained mice. For all panels, colour scheme: orange (trained), black (non-trained). All values are mean ± s.e.m.*

7. Discussion

The main goal of this study was the characterization of local synaptic connectivity in the adult mouse auditory cortex, a brain region critically involved in the proper encoding of external auditory cues. For this purpose, two initial questions were made: 1) which features can describe local connectivity in the adult auditory cortex, and 2) does cortical local circuitry changes upon artificial activation during a learning task? To answer these questions, multiple simultaneous quadruple whole-cell recordings were made *in vitro* from excitatory pyramidal neurons from supragranular layer 2/3 and infragranular layer 5, either in naïve or in trained mice. These two cortical layers have distinct local processing features, which allow shaping the flow of information in the canonical columnar auditory microcircuit (Atencio and Schreiner, 2010). This electrophysiological method has the advantage of incorporating information about the intrinsic properties of specific neurons and the signs and strengths of the synapses that connect them (e.g. Thomson and Bannister, 2003).

7.1. Sparse connectivity and long-tailed distribution of synaptic weights

The majority of the studies that made attempts to characterize and quantify the synaptic circuits within well-defined cortical columns (e.g. Binzegger et al., 2004; Yoshimura et al., 2005; Ohki et al., 2006; Lefort et al., 2009; Mao et al., 2011), or within specific cortical layers (e.g Holmgren et al., 2003; Song et al., 2005; Barbour and Callaway, 2008; Oswald and Reyes, 2008; Avermann et al., 2012), relied on developmentally immature cortical neurons (animals with 10 to 31 days of age). The question arises: can that body of information be reliably transposed to the adult and fully mature cortex? Are the features that characterize local synaptic circuitry universal throughout development? Adult mice have the advantage that they can be engaged in several training and learning paradigms, from which post-weaned mice are kept away due to their on-going development changes in sensory processing. Although the developmental maturation of cortical neurons has been analysed (Oswald and Reyes, 2008), it never reached adult stages. Here, it was made a first attempt to characterize and quantify the excitatory local circuitry at a single-cell resolution in the adult mouse (with more than 8 weeks of age). The major findings of this study are related with several nonrandom features of synaptic

connectivity. It is concluded that the network consists of sparse synaptic connections characterized by low synaptic weights that tend to cluster together in the form of overrepresented bidirectional motifs. This sparseness of the network is in good accordance with recent experimental evidence showing sparse cortical activity *in vivo* (Ecker et al., 2010; O'Connor et al., 2010; Renart et al., 2010).

The distribution of connection strengths - which can be fitted by a lognormal distribution - has a heavy tail and implies that synaptic weight is concentrated among few, but powerful, synaptic connections. These recurrent networks with a long-tailed distribution of synaptic weights exhibit stability and flexibility among diverse activity patters (Ikegaya et al., 2012). In fact, a computational study has shown that spontaneous self-organization of a recurrent neuronal network through spike timing-dependent plasticity leads to many weak synapses and a few synapses that produce > 5 mV depolarization (Izhikevich et al., 2004). Moreover, the lognormal distribution of spine sizes is reported to emerge spontaneously when the magnitude of the changes in spine size during synaptic plasticity is proportional to the size of the spine (Loewenstein et al. 2011). Therefore, the long-tailed distribution of synaptic weights is likely a natural consequence of neuronal networks with synaptic plasticity. Consistent with this notion, the long-tailed distribution dominates among synapses in various regions that exhibit synaptic plasticity, including the neocortex (Markram et al., 1997; Holmgren et al., 2003; Song et al. 2005; Lefort et al. 2009), hippocampus (Hanse and Gustafsson, 2001), and cerebellum (Brunel et al. 2004). However, a point should be made that a great sum of the excitatory axons and dendrites are likely to be truncated during slicing, affecting in this way connection probabilities, but also the true estimation of synaptic weights between pyramidal neurons, especially in distant pairs. This phenomenon can be minimized by recording deep in the coronal slice. Nonetheless, it is noteworthy that the large range of EPSPs found in the dataset could also be easily approximated with a lognormal distribution, as well as it was the case for acute slices (Song et al., 2005; Lefort et al., 2009) or slice cultures (Ikegaya et al., 2012).

7.2. Network of few "strong" and many "weak" excitatory connections

Another major conclusion was that the adult local recurrent circuitry is formed by a few large amplitude connections embedded among an overwhelming large number of low

amplitude synaptic connections. In line with previous reports (Binzegger et al., 2004; Song et al., 2005; Lefort et al., 2009; Ikegaya et al. 2012), it seems that also in the adult cortex, the map of the recurrent excitatory connectivity can be described as being formed of many "weak" and a very few "strong" excitatory projections. The large-amplitude EPSPs observed in the present dataset can be explained by 3 plausible (not exclusive) mechanisms. First, the large EPSPs could be generated by structurally large synapses. The size of dendritic spines correlates with synaptic strengths (Matsuzaki et al., 2001) and is lognormally distributed (Loewenstein et al., 2011). Second, the large EPSPs could occur at dendrites proximal to the soma. Indeed, larger EPSP had faster waveform kinetics (~2 ms time to peak), consistent with cable theory. Finally, large EPSPs could arise from multiple synaptic sites between pairs of connected neurons (Sorra and Harris, 1993; Markram et al., 1997). In so, the few low-variance and large-amplitude EPSP found in the dataset, could be envisaged as linking neurons into strongly connected functional cell assemblies, where the dynamic strengthening of synapses through correlated activity in presynaptic and postsynaptic neurons (Hebb, 1949; Markram et al., 1997; Feldman, 2000; Sjöström et al., 2001; Song et al., 2005; Lefort et al., 2009) is likely to contribute to the formation of these large synaptic connections. The many unreliable small-amplitude EPSPs might primarily offer neuronal networks opportunities for synaptic plasticity. Indeed, weaker connections can be strengthened easily through a variety of activity-dependent learning rules (e.g. Sjostrom et al., 2001). Therefore, in a network formed by a great number of weak connections, a few strong connections could define stable trajectories through which the majority of information might flow. Future studies are required to see if stronger connections are distributed uniformly among neurons, of if they belong to "hub" neurons. Also, studies involving larger networks of cortical neurons will be needed to provide a more complete understanding of the network structure and function itself.

Moreover, it is known that spontaneous spiking by the majority of cortical neurons *in vivo* is infrequent, usually with a frequency of less than 1 Hz (Hromádka et al., 2008; O'Connor et al., 2010), and highly asynchronous (Ecker et al., 2010; Renart et al., 2010). This sparseness of recurrent network might be stabilized by the reliability of large amplitude connections in eliciting spikes in the postsynaptic neuron, thus stabilizing sparse spiking and augmenting the power of single neurons (Ikegaya et al., 2012). In a computational analysis, it was concluded that a key feature that might

maintain infrequent activity seems to be a highly inhomogeneous distribution of synaptic weights (Ikegaya et al., 2012). Namely, a network provided with large amplitude EPSPs could be maintained at low network activity level, through a mechanism where the strongest fraction of synapses could trigger APs in postsynaptic neurons, in the critical presence of the dominant weak amplitude synaptic connections (London et al., 2010; Ikegaya et al., 2012). In this view, weak synapses could be envisaged as a background noise provider that modulates the efficiency of spike transmission by changing the overall activity level and thereby defining the network state. Moreover, such sparse network dynamics mediated by rare large-amplitude EPSPs are compatible with observations in the somatosensory cortex of awake, behaving mice (Poulet and Petersen, 2008). Finally, it would be interesting to assess about the functional role of these potent synaptic connections in the freely learning mice (Barkat et al., 2011), especially to examine any potential subnetworks, which might for example link neurons with the same tonotopic preferences (Bandyopadhyay et al., 2010; Rothschild et al., 2010).

7.3. The variability in mean connection strengths can be largely captured by differences in neurotransmitter release probability and number of release sites

According to the quantal hypothesis (del Castillo and Katz, 1954), the efficacy of a given connection can be described by the product of the presynaptic neurotransmitter release probability (*p*), the number of release sites (*n*), and the size of the postsynaptic response to a quantum of transmitter (*q*). Describing the mechanisms underlying synaptic transmission is thus crucial to understand the neural code. One such property which is repeatedly observed in the neocortex and across cortical layers, and also confirmed in the present study, is the wide distribution of synaptic efficacies (Markram et al., 1997; Holmgren et al., 2003; Song et al., 2005; Feldmeyer et al., 2006; Lefort et al., 2009). The wide range of EPSP amplitudes observed in the data set could potentially be explained by differences in all three parameters. In this study, synaptic connections within layer 2/3 pyramidal neurons, with EPSP amplitudes ranging from 0,02 and 3,37 mV, as well excitatory connections within layer 5 pyramidal neurons (0,01 – 0,9 mV EPSP range) were observed. By means of selectively keeping one parameter of the quantal model constant, while varying the remaining two, one question was made:

which of the parameters best explains the wide EPSP ranges observed in both cortical layers? In the neocortex, it has been observed that though excitatory connections at layer 2/3 present a high release probability (~0.8), yet they are maintain by a uniquantal release mechanism (Silver et al., 2003). Moreover, it has been proposed, in theoretical arguments, that the distribution of synaptic efficacies in layer 5 pyramidals can be explained by just attributing increasing numbers of release sites to the stronger amplitude connections, suggesting the involvement of simultaneous release of several vesicles (Loebel et al., 2009). From the two examples stated above, it seems that synaptic neurotransmission cannot be universally confined to a single model, even within cortical layers in the same cortical column.

In the present thesis I observed, similarly as in the above mentioned studies, a wide range of mean connection strengths for the various pairs of connected neurons. The mean connection strength of a given connection was strongly correlated with the trial-to-trial variability (CV), as well as with the failure rate. To test if the wide range of the connection strengths in the dataset, as well as their relationship to CV and failure rate, could be explained by variation of only one of the three parameters *n*, *p*, or *q*, the theoretical mean connection strength was calculated in dependence for only one of the parameters while keeping the others fixed (see Figure 6.6). The variability of mean connection strengths could be well approximated either by assuming a wide range of different release probabilities with a fixed relatively low number of release sites (~8) or it could be approximated well with a fixed low release probability of ~0.08 and a wide range of release sites ranging from very few to several tens. Changes in quantal size only were not able to capture the distribution of mean connection strengths.

It is believed that, in the neocortex, excitatory connections between pyramidal neurons make on average 5 functional synaptic contacts (Markram et al., 1997; Silver et al., 2003; Feldmeyer et al., 2006; Bremaud et al., 2007) and that their synaptic contacts could have more than one active zone, each of which charged with 5 to 15 readily releasable docked neurotransmitter vesicles (see Ribraut et al., 2011). Moreover, stronger synaptic connections between pyramidals have more synaptic contacts than weaker ones (Markram et al., 1997; Feldmeyer et al., 2006; Loebel et al., 2009). The results stated here do in fact confirm this observation, in the sense that since the majority of connections that build up the network have low efficacy (low EPSP

amplitude / high-variance), these are in fact characterized by a low number of release sites (up to 10). Moreover, one should add the low probability of release as a general feature that might describe the recurrent connectivity in the adult auditory cortex.

Modulating the synaptic efficacy via the release probability has a limited range, as it is constrained by the number of available vesicles. Furthermore, modulating synaptic efficacy via the number of release sites has a potentially wider range, and it preserves the temporal response structure, for instance, to a train of incoming APs (Le Be and Markram, 2006; Loebel et al., 2009). That one found in the present study between the synaptic efficacy and the estimated number of release sites, as well as with the release probability, might suggest that both modulatory mechanisms interact together in giving synapses multiple possibilities to adjust to incoming inputs, as has been described for other highly plastic synapses (e.g. Oertner et al., 2002). In the future, would be interesting to understand the functional implications of such differences in synaptic transmission reliability on the neural code, especially in such infrequent firing rate cortical neurons.

7.4. Large fraction of presynaptic inputs required to reach spiking threshold

It is known that cortical neurons form a dense network that contains horizontal and vertical connections traveling within and between the cortical layers (Szentagothai, 1978; Douglas and Martin, 2004). These connections are both convergent and divergent, such that the response of any individual neuron is believed to be determined by the constant bombardment of synaptic inputs (DeFelipe et al., 2002; Binzegger et al., 2004). Moreover, the total number of synapses that a neuron receives can be quantified by summing the synaptic inputs from axons in the cortical layers through which its dendrites pass. For instance, in the area 17 of the cat, in general the total number of synapses on a given neuron type can range between 2981 and 13075 (Beaulieu and Colonnier, 1985; Binzegger et al., 2004). Pyramidal neurons in layer 5 are the ones presenting the highest number of synapses due to their extensive dendritic branching along the cortical column: in layer 2/3, the dendrites of layer 5 pyramidals receive a total of ~1400 synapses, and in layer 5 soma and dendrites they receive a total of ~4900 synapses. Also, a massive number of synapses these dendrites receive come from layer

1 (~5600). On the other hand, pyramidal neurons in layer 2/3, due to a lesser extent of their dendrites (mainly confined to layer 2/3 itself and into upper layer 1), receive a smaller number of synaptic inputs: each neuron in layer 2/3 receives on average 2094 synapses from other pyramidal in layer 2/3, the major source of synaptic input in this cortical layer. On the other hand, a recent report on juvenile rats (Feldmeyer et al., 2006) concluded that a single layer 2/3 pyramidal receives synaptic inputs from only 270 other layer 2/3 pyramidals. In the dataset presented here, the largest depolarization that could be observed was up to 3 mV in layer 2/3, and 0,9 mV in layer 5, which are both significantly smaller than the largest postsynaptic depolarizations observed in the immature cortex, which in rare cases reached 8 to 12 mV amplitudes (Holmgren et al., 2003; Song et al., 2005, Lefort et al., 2009), and in agreement with a general decrease of EPSP amplitudes with age (Reyes and Sakmann, 1999). Moreover, in juvenile animals, the average EPSP amplitudes can easily reach 1 mV (Feldmeyer et al., 2006). The immediate functional implication is that for a given postsynaptic neuron to reach AP threshold it requires a larger fraction of convergent presynaptic inputs, as compared with immature cortex. In the present study it was confirmed that in the adult auditory cortex, pyramidal neurons in both cortical layers do require a larger extent of presynaptic inputs to reach threshold, do to their intrinsic low EPSP amplitudes. These findings and the differences observed between layers 2/3 and 5 are not surprising. Intracellular recordings from multiple neurons have shown that different types of neurons have different connection probabilities and different numbers and distributions of synapses (Thomson et al., 2002; Thomson and Bannister, 2003; Thomson and Lamy, 2007). Furthermore, as stated and verified in the present study, connection probabilities between neocortical neurons also vary according to the layer in which they reside (e.g. Bannister et al., 2002; Holmgren et al., 2003; Yoshimura et al., 2005; Song et al., 2005; Lefort et al., 2009), the brain regions to which they project, and the brain regions from which they receive input (e.g. Kasper et al., 1994; Anderson et al., 2010).

7.5. Excitatory / inhibitory balance in the adult auditory cortex

A recent body of evidence has lead to the conclusion that the concomitant occurrence of synaptic excitation and inhibition in primary sensory cortices can be accounted even by the simplest sensory stimulus like a whisker deflection (Okun and Lampl, 2008), a brief

acoustic tone (Wehr and Zador, 2003), an odor (Poo and Isaacson, 2009), or a grading bar in the visual field (Monier et al., 2003). The combination of these two synaptic conductances, namely their relative strength and temporal relationship, can critically influence cortical function in space and time. In general, studies have greatly relied on pharmacological blockade of those two synaptic conductances in controlled voltage-clamp experiments (e.g. Wehr and Zador, 2003). However, acute experimental manipulations that selective decrease either inhibition or excitation, have the ultimate outcome to shift cortical activity to a hyperexcitable (epileptiform) or silent (comatose) state, which precludes an reliable assessment of which cortical properties (e.g. tuning) are being affected by the shutdown of inhibition or excitation. In so, many reported studies rely on correlative evidence substantiated by computation models (e.g. Cruikshank et al., 2007; Luz and Shamir, 2012).

In this thesis, the relative contribution of synaptic excitatory and inhibitory conductances, with precise temporal resolution, that impinge onto excitatory principal neurons in layer 2/3 was made. These pyramidal neurons project their axons laterally within their own layer, as well vertically, toward layer 5, and present biased signal flow: in a recent report, it was shown that activity of layer 2/3 principal neurons generates an excitatory/inhibitory (E/I) ratio that differs between layers, being inhibition favored within its own layer but is biased toward excitation in layer 5 (Adesnik and Scanziani, 2010). However, in the present study, the determined E/I ratios between the vertical and lateral stimulated inputs were similar between both pathways. It should be noted that so far, studies have been focused on developing, immature sensory cortices, where a great degree of synaptic plasticity occurs, and where both excitatory and inhibitory synapses are still under development, opening the possibility that during maturation, phenomenon as biased signal flow towards a given cortical layer, might be an intrinsic event helping shaping future excitatory and inhibitory connections.

Since in this study the afferents to layer 2/3 pyramidals were stimulated via extracellular electrodes, one cannot make a reliable argument on which type of inputs are being stimulated, not even on the specificity of the presynaptic neurons (inhibitory and excitatory neurons cells) that are being recruited to the observed synaptic events. Based solely on the average latencies differences between the excitatory and inhibitory peak conductances (< 1ms), one can convincingly report that cortical transmission onto layer

2/3 pyramidals via ascendant and lateral axonal projections is extremely fast, in a direct monosynaptic pathway. It is known that within individual neurons, the ratio between incoming excitation and inhibition can change rapidly and dynamically according to behavior demands, on a millisecond basis. This basic cortical operating principle controls not only the neurons participation in networks but also define the networks themselves. In principal neurons of the rodent auditory cortex, brief tones can lead to an increase in synaptic excitation that is followed by a surge of inhibition (Wehr and Zador, 2003; Wu et al., 2008). Similarly, whisker deflections lead to a rapid sequence of excitation followed by inhibition in neurons of the somatosensory cortex (Okun and Lampl, 2008). Hence, in these cortical areas, in response to impulse-like stimuli, inhibition and excitation occurs in a precise and stereotyped temporal sequence: an initial barrage of excitatory input is rapidly quenched by inhibition, truncating the spiking response within extremely brief temporal window, increasing temporal precision and thereby reducing the randomness of cortical operation (Pouille and Scanziani, 2001). Interestingly, and in opposition with has been reported before (Wehr and Zador, 2003; Chruikshank et al., 2007; Zhang et al., 2011), it was observed for a subset or recorded neurons, that the excitatory conductance was flanked by a two-wave separate inhibitory barrages (see Figure 6.12). To one's knowledge, this observation has never been previously documented. In contrast to their counterparts glutamatergic principal cells, GABAergic interneurons do not generally form long range axonal projections (however see exception e.g Melzer et al., 2012). In so, the main interaction between these types of cortical neurons happens locally: individual interneurons can inhibit >50% of pyramidal cells located within ~100 μm and receive excitatory input from a large fraction of them (e.g. Holmgren et al., 2003; Silberberg et al., 2005; Yoshimura and Callaway, 2005; Yoshimura et al., 2005; Packer and Yuste, 2011). Thus not only are interneurons excited in proportion to the level of local network activity, but they directly influence it through their inhibitory feedback recurrent inhibition (Figure 7.1A), a connectivity pattern that is ubiquitous in the cortex. On the other hand, cortical cells can receive excitatory inputs via long-range axons originating from other cortical or subcortical areas; these inputs can then diverge onto both excitatory cells and interneurons, giving rise to feedforward inhibitory circuits (Buzsaki, 1984) (Figure 7.1B). Moreover, it is know that in layer 2/3, at least four different types of interneurons have been found to form reciprocal connections with pyramidal neurons, that a

pyramidal cell might be simultaneously connected with more than one type of interneuron, and importantly, the properties of pyramidal–interneuron synaptic transmission differ considerably depending on the interneuron type (see Markram et al., 2004 for review). Taken all of this information into account, it is reasonable to speculate that the first (and faster) inhibitory barrage that preceded the excitatory conductance, might be due to the local recruitment of interneurons positioned in the immediate vicinity of the recorded layer 2/3 pyramid neurons, consistent with the general notion that pyramidal neurons may form functionally distinct microcircuits with various types of local interneurons. The specific identity of such interneurons that contributed for the observed two-wave inhibitory pattern is, at this point, unknown. Moreover, the specific postsynaptic target of a given interneuron onto the pyramidal neuron (either the soma, or the axon initial segment, or even the apical dendrites) and its role in shaping cortical inhibition is obscure. In the future, powerful genetic tools (Luo et al., 2008) can be deployed to singly isolate each subtype of interneurons and investigate not only their identity, but also the role how synaptic inhibition could play, for instance, in the tuning of cortical neurons in the adult brain (e.g. O'Connell et al., 2011).

The time gap between these two opposing conductances is not the only way in which the ratio between excitation and inhibition can be relevant for cortical processing. In the rodent auditory cortex the E/I ratio in a given cortical neuron also depends on the property of the sensory stimulus, like its frequency. It was shown that intracortical local inhibition can laterally sharpen the frequency tuning of neurons, ensuring their highly selective representation (Wehr and Zador, 2003; Wu et al., 2008). It is known that local populations in the auditory cortex are highly heterogeneous in their gradient of frequency selectivity (tonotopy), in which neighboring neurons are not necessarily tuned to the same frequency (Bandyopadhyay et al., 2010, Rothschild et al., 2010), and due to that, the E/I ratio between nearby neurons vary significantly. In this study, the E/I ratios of the individual layer 2/3 pyramidal neurons recorded from are very similar among them, arguing for a homogenous population of neurons that may receive similar inputs. The two-wave barrages of inhibition that was observed in almost half of the recorded neurons cannot be assigned to a supposed heterogeneity in the local population, but due to differential ways of synaptic communication that impinge onto cortical supragranular layers.

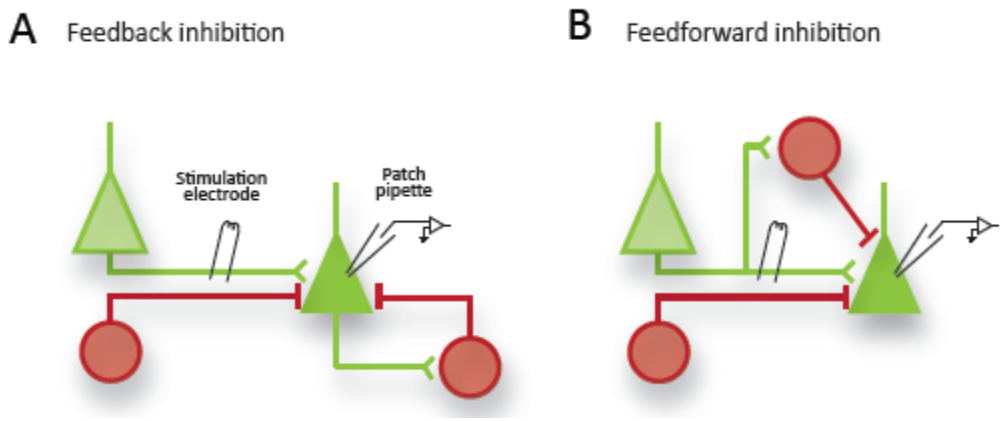

Figure 7.1 ***Feedback and feedforward inhibitory mechanisms that can account for the observed two-wave barrages. A)*** *Simplified schematic representation of a feedback inhibitory. Extracellular stimulation drives activation of both pyramidal principal cells (green triangles) and interneurons (red circles) that impinge their axons into the recorded L2/3 neuron. The first-wave of inhibition is faster when compared with its excitation counterpart. Delayed feedback inhibition arises when cortical L2/3 pyramid makes excitatory contact (green lines) with local interneurons that in turn makes inhibitory synapses (red lines) on the same pyramidal neuron.* ***B)*** *Feedforward inhibition is generated when stimulated long-range excitatory afferents diverge onto both principal cells and local interneurons.*

7.6. Optical stimulation of the auditory cortex can drive behaviour in the adult mouse

Casual relationships between the activity of groups of neurons and a given behavioural output are abundant. In monkeys, perception of skin flutter (Romo et al., 1998), perceptual judgments on motion direction (Salzman et al., 1990), or even face perception (Afraz et al., 2006), all could be accomplished by selective somatosensory microstimulation. Moreover, electrical stimulation of single neuron in the barrel cortex (Houweling and Brecht, 2008), or small populations in the auditory cortex (Otto et al., 2005), have been proven to be sufficient to drive behaviours in rats, in the millisecond time-scale that neural activity operates (Yang et al., 2008). With the possibility of selectively expressing channelrhodopsin in a limited subpopulation of cortical neurons, optical microstimulation has been used to dissect the impact of precisely timed APs in guiding behaviour and learning in a diversity of model organisms (see Introduction).

In the present study, auditory cortical neurons in the adult mouse were also rendered with light sensitivity by means of AAV-mediated ChR2 expression. The high titer virus production allows the long-term gene expression without significant toxicity effects in the non-dividing neurons – a critical feature for use in the nervous system (Kootstra and Verma, 2003). AAV vectors were produced using helper virus-free systems, which insure that they act as delivery vehicles for genetic material without the potential to replicate or express genes that induce cytotoxic effects. This method allowed expression of ChR2 in a broad population of neurons along the cortical column, especially in the supragranular layers. The ChR2 expression was confined to the injection site and could be broadly detected (due to the concomitant EYFP expression) under the cranial window. Although the use of light-mediated stimulation of sensory cortices in driving behaviour has been proven as a suitable approach (see above), here in the present study one also was able to recapitulate previous reports (e.g. Huber et al., 2008), and extended those considerations towards the auditory cortex, namely the advantage of using ChR2-based optical stimulation to study the impact of precisely defined APs in cortical neurons in guiding behaviour. After reaching stable and functional expression of ChR2 (confirmed by the reliable light-evoked responses from layer 2/3 neurons in slices), mice were entrained in a perceptual task. At the end, mice were able to report photostimulation of the auditory cortex as a signal for an aversive stimulus, as demonstrated by their later acquired avoidance behaviour. Though extremely labor intense, one could observe that Syn-ChR2 injected mice reached asymptotic correct performance levels (above 95%) by the end of the last training session Although the time required to reach correct performance levels above chance was highly variable from mouse to mouse, and the fact that only half of the mice were able to correctly report cortical photostimulation, this should not obscure the effectiveness of such behaviour training. In the future would be interesting to assess the specific impact of activating only a small subset of cortical neurons of a given tonotopic area of the auditory cortex, since the results presented here are due to a broad, indiscriminate activation of several tonotopic areas of the cortex.

However, in a group of preliminary experiments, the use of an ultra-fast ChR2 variant (ChETA; Gunaydin et al., 2010) to render photosensitivity only in excitatory neurons (via the CamKII promoter; see Figure 6.13) proven not to be suitable for behavioural trainings, since no mice expressing ChETA was able to report cortical photostimulation,

as opposite with the mice injected with Syn-ChR2. Speculations on why this was the case might be the ChETA-mediated photocurrents elicit in slices were of considerable smaller amplitude as compared with previous studies (Gunaydin et al., 2010), and even compared with the amplitude of photocurrents in Syn-ChR2-expressing pyramidal neurons (see Results, Figure 13), though both constructs were very effective in inducing reliable and time-precise APs in the recorded pyramidal neurons.

7.7. Intrinsic properties of optogenetically stimulated neurons *in vivo*

Neurons possess homeostatic mechanisms which integrate activity levels and alter network and cellular properties to counteract long-term perturbations (Turrigiano et al., 1998; Desai et al., 1999). Several reports have described changes in intrinsic excitability after chronic alteration in activity, such as long periods of depolarization (Desai et al., 1999; Kim et al., 2008; Goold and Nicoll, 2010; O'Leary et al., 2010), which ultimately have the goal to stabilize neuronal firing. Here, one could appreciate that ChR2-expressing pyramidal neurons, as compared with non-infected control neurons from naïve mice, did not present statistical differences in AP threshold, though a small and clear trend for higher threshold levels could be seen in ChR2-positive neurons. This is indicative that ChR2-expressing neurons, regardless of the past training history of the mouse, could have comparable depolarization levels to fire APs. However, recent reports have found opposite effects (Goold and Nicoll, 2010). Nevertheless, pyramidal neurons expressing ChR2 possess higher AP amplitude and AP overshoots. This observation is in line with a recent report (Goold and Nicoll, 2010) that found that chronic cell-autonomous optogenetic depolarization of CA1 pyramidal cells results in changes in intrinsic AP properties of ChR2-expressing neurons. This change in AP features such as threshold (Goold and Nicoll, 2010), or even amplitude and overshoot (present study) agrees with a recent study (Grubb and Burrone, 2010) in which it was observed that a change in the axon initial segment position during burst patterns of activity, which in turn correlates with changes in APs features. This phenomenon is related to the active relocation of sodium and calcium voltage-dependent channels upon intense depolarization epochs, influencing in this way the overall neuronal ionic conductances (O'Leary et al., 2010; Kim et al., 2008).

As stated before, network-wide (Turrigiano et al., 1998) as well as cell-autonomous (Goold and Nicoll, 2010; Grubb and Burrone, 2010) increases in excitation initiates homeostatic synaptic changes, which is translated in alterations in all of a neuron's excitatory synaptic strengths to compensate for deviations from optimal levels of neural activity (Turrigiano, 1999). More specifically, in chronic depolarization events, mediated by the constant activation of ChR2 with blue light in pyramidal neurons, a compensatory synaptic depression of both AMPA and NMDA response amplitudes has been reported, with concomitant elimination of synapses (Goold and Nicoll, 2010). In the present study, it was observed that the average EPSP amplitude between pairs of connected ChR2-expressing neurons, from both trained and non-trained mice, is comparable to their non-expressing neurons from naïve mice. On average, mice that were engaged in behaviour trainings were subject to 2 training sessions per day, one hour duration total. These episodes of ChR2-mediated depolarization were thus not enough to cause any synaptic depression mechanism between neurons.

Finally, it is widely accepted that midbrain dopaminergic neurons can encode reward prediction errors, by supposedly computing temporal differences between the values of current and previous states/actions (Schultz, 1998; Claridge-Chang et al., 2009). Since in the present study mice learned to perceive direct cortical photostimulation with an aversive stimulus, and the absence of it with a positive water drop reward, it is feasible to speculate about the role of such dopaminergic neurons is the overall perception-guided behaviour. The selective activation by ChR2 expression of subsets of dopaminergic neurons in different brain regions, combined with a Cre-dependent viral strategy (Kravitz et al., 2012), would be possible to tackle how dopamine signaling is implicated in perceptual-drive reinforcement learning, as well as the specific cortical substrates targeted by the dopamine signals.

At the end, the main question is no longer about the necessity or sufficiency of cortical neuronal groups in eliciting behaviours, but rather inside the properties that govern the (re)arrangement of groups of individual neurons that can give rise to such remarkable output.

7.8. Local synaptic connectivity features upon photostimulation-driven behaviour

Can local cortical circuitry be changed by the active acquisition of a learned behaviour? According to Hebb's neuronal plasticity rules (Hebb, 1949), yes. Donald Hebb was among the first thinkers who tried to put in motion a hypothesis in which there would be a correlation between neuronal function and psychological processes. He stated (Hebb, 1949) that the brain's ability to generate coherent thoughts derives from the spatiotemporal orchestration of neuronal activity, and that a discrete, strongly interconnected group of active neurons, the "cell assembly", would represent a distinct cognitive entity. Because of their supposed high degree of interconnectivity, the stimulation of a sufficient number of assembly members can activate the entire assembly. The temporal evolution of such assemblies by some internal mechanisms (Hebb's "phase sequences"), would, in turn, provide the basis by which complex cognitive processes, such as memory recall, thinking, or even decision making, could flow independently of direct control from external sensory inputs (e.g. Harris, 2005). At the end, Hebb's cell assembly is essentially a graph of synaptically interconnected excitatory neurons, in which a readable output should be possible to accomplish (Wennekers et al., 2003). Hebb's cell assembly hypothesis is a prominent hypothesis that attempting to comprehensively link internal cognitive and physiological processes. However, it has been difficult to convincingly identify the hypothesized cell assemblies due to also recent conceptual doubts about it (Harris et al., 2003; Harris, 2005; Truccolo et al., 2010).

In the present study, a first attempt was made to directly assess about local connectivity between pyramidal neurons that became active during the photostimulation-guided behaviour. Care was taken to record from layer 2/3 pyramidals, and not from deeper layers, due to the light scattering through the brain tissue, not enabling in this way the activation of neurons in deeper cortical layers. Although recent breakthroughs have been developed that could allow for a improved spatial resolution of neuronal activation in ChR2-expressing neurons along the cortical column using two-photon excitation (Andrasfalvy et al., 2010), they still do not offer a convincing alternative for neuronal activation in freely behaving animals (due to current technical limitations), as compared with other methods that made use of small LED's (Huber et al., 2008), or laser

photostimulation (Choi et al., 2010) to drive behaviours. A future combination between advanced microscopic techniques, coupled with non-invasive methods for selectively activating a desired population of cortical ChR2-expressing neurons would be of great importance. Although in the present study a broad range of cortical neurons along the cortical column were stably infected with ChR2, and hence could participate in the photostimulation–based behaviour (but see previous comment), recent reports, in which activation of solely ChR2-positive layer 2/3 pyramids was made, convincingly proved about the sufficiency of these supragranular neurons in driving behaviour (Huber et al., 2008). At this point one could only speculate about the truthiness of such finding translated to the present auditory cortex activation experiments.

Also, according to Hebb's definition (Hebb, 1949), an assembly is characterized as well by the potentiation of synaptic weights between assembly members than with other neurons, which became weaker, thus reinforcing useful pathways in the brain (for review see Abbot and Nelson, 2000). Not only the hardwire of connections between neurons in an assembly is important, but their relative weight as well. Moreover, strong and immutable connectivity might not be a good way for the proper segregation of neurons into groups, since synaptic weight distributions are in constant change in an activity-dependent manner (Reyes and Salzmann, 1999; Holmgren et al., 2003; Sakata and Harris, 2009). So, the knowledge of spiking profile is insufficient to properly describe the state of the cortical network unless the moment-to-moment distribution of synaptic weights is also known. Naturally, if the transiently formed assembly members are anatomically interconnected, their co-activation can strengthen their membership and facilitate their future joint recurrence. However, this correlation-based plasticity (named Hebbian plasticity) between pre- and postsynaptic neurons in an assembly is prone to instability: synapses that are strengthened become more effective at depolarizing the postsynaptic neuron and will continue to be strengthened in an unconstrained positive feedback cycle, eventually driving neuronal activity to saturation (Abbot and Nelson, 2000; Miller, 1996). However, neurons can sense how active they are and adjust their properties to maintain stable function (Turrigiano, 1999), circumventing the initial stability problem inherent to Hebb's proposals. Through a homeostatic mechanism, neurons can adjust their synaptic weights up or down to keep their activity close to some set-point value. In neocortical neurons, such mechanism is termed "synaptic scaling", because it was observed to globally scale all of a neuron's

excitatory synapses up or down in strength in the correct direction to stabilize neuronal firing (Turrigiano et al., 1998). In so, upon the active acquisition of the photostimulation-driven behaviour, three possible scenarios are in play: first, one in which there's an increase in neuronal connectivity, at the expense of a low amplitude of synaptic weights; second, one in which local connectivity is kept low, but there is a localized increase in synaptic weights in particular excitatory connections; third, a joint combination of the first two scenarios. However, mainly due to the surprisingly low number of connections detected in slices from trained and non-trained mice, one should be careful in drawing strong conclusions at this point. Nevertheless, as stated before, the average amplitude of the EPSP responses in trained and non-trained mice were the same magnitude as its counterparts from naïve mice, which might be an indication that if changes in local circuitry do really happen, it might not be at the expense of increases in synaptic weights.

Here, for the first time a *in vitro* analysis of previously photostimulated neurons was made. It was found that, in the regime of 1 to 2 training sessions per day, neither aberrant plasticity that might lead to an overpotentiation of synaptic inputs, nor triggering of homeostatic processes that would lead to silencing of neurons.

8. References

Aaron, G. and Yuste, R. (2006), Reverse optical probing (ROPING) of neocortical circuits, *Synapse*, 60:437–440

Abbott, L.F., and Nelson, S.B. (2000), Synaptic plasticity: Taming the beast, *Nat. Neurosci*., 3:1178-1183

Adesnik, H. and Scanziani, M. (2010), Lateral competition for cortical space by layer-specific horizontal circuits, *Nature*, 464:1155-1160

Afraz, S. R., Kiani, R., Esteky, H.(2006), Microstimulation of inferotemporal cortex influences face categorization, *Nature*, 442:692-695

Agmon, A. and Connors, B. W. (1992), Correlation between intrinsic firing patterns and thalamocortical synaptic responses of neurons in mouse barrel cortex, *J. Neurosci.*,12:319-329

Alonso, J. M. and Swadlow H. A. (2005), Thalamocortical specificity and the synthesis of sensory cortical receptive fields, *J. Neurosci.*, 94:26-32

Anderson, J. C., Martin, K. A. C. (2006), Synaptic connection from cortical area V4 to V2 in macaque monkey, *J. Comp. Neurol.*, 495:709-721

Anderson, C. T., Sheets, P. L., Kiritani, T., Sheperd, G. M. G. (2010), Sublayer-specific microcircuits of corticospinal and corticostriatal neuros in motor cortex, *Nature Neuroscience*, 13:739-746

Andrasfalvy, B. K., Zemelman, B. V., Tang, J., Vaziri, A. (2010), Two-photon single-cell optogenetic control of neuronal activity by sculpted light, *Proc. Natl Acad. Sci. USA*, 107:11981-11986

Arenkiel, B. R., Peca, J., Davison, I. G., Feliciano, C., Deisseroth, K., Augustine, G. J., Ehlers, M. D., Feng, G. (2007), In vivo light-induced activation of neural circuitry in transgenic mice expressing channelrhodopsin-2, *Neuron*, 54:205-218

Atencio, C. A., Schreiner, C. E. (2010), Columnar connectivity and laminar processing in cat primary auditory cortex, *PLoS One*, 5:1-18

Bamann, C., Kirsch, T., Nagel, G., Bamberg, E. (2008), Spectral characteristics of the photocycle of channelrhodopsin-2 and its implication for channel function, *J. Mol. Biol.*, 375:686-694

Bandyopadhyay, S., Shamma, S.A., Kanold, P.O. (2010), Dichotomy of functional organization in the mouse auditory cortex *Nat. Neurosci.*, 13:361-368

Bannister, N. J., Nelson, J. C., Jack, J. J. (2002), Excitatory inputs to spiny cells in layers 4 and 6 of cat striate cortex, *Phil. Trans. R. Soc. London*, 357:1793 – 1808

Barbour, D. L. and Callaway, E. M. (2008), Excitatory local connections of superficial neurons in rat auditory cortex, *J. Neurosci.*, 28:11174 -11185

Barkat, T. R., Polley, D. B., Hensch, T K. (2011), A critical period for auditory thalamocortical connectivity, *Nat. Neurosci.*, 14:1189-1194

Bathellier, B., Ushakova, L., Rumpel, S. (2012), Spontaneous association of sounds by discrete neuronal activity patterns in the neocortex, *Neuron*, in press

Bean, B. P. (2007), The action potential in mammalian central neurons, *Nat. Rev. Neurosci.*, 8:451:465

Beaulieu, C. and Colonnier, M. (1985), A laminar analysis of the number of round-asymmetric and flat-symmetric synapses on spines, dendritic trunks, and cell bodies in area 17 of the cat, *J. Comp. Neurol.*, 231:180-189

Binzegger, T., Douglas, R.J., Martin, K.A.C. (2004), A quantitative map of the circuit of cat primary visual cortex, *J. Neurosci*., 24:8441–8453

Bock, D. D., Lee, W. C., Kerlin, A. M., Andermann, M. L., Hood, G., Wetzel, A. W., Yurgenson, S., Soucy, E. R., Kim, H. S., Reid, R. C. (2011), Network anatomy and in vivo physiology of visual cortical neurons, *Nature*, 471:177–182

Boyden, E.S., Zhang, F., Bamberg, E., Nagel, G., Deisseroth, K. (2005), Millisecond-timescale, genetically targeted optical control of neural activity, *Nat. Neurosci.*, 8:1263-1268

Braitenberg, V. and Schűz, A. (1998), Cortex: Statistics and Geometry of Neuronal Connectivity, Second Edition (Berlin: Springer)

Bremaud, A., West, D. C., Thomson, A. M. (2007), Binomial parameters differ across neocortical layers and with different classes of connections in adult rat and cat neocortex, *Proc. Natl Acad. Sci. USA* 104:14134-14139

Brunel, N., Hakim, V., Isope, P., Nadal, J. P., Barbour, B. (2004), Optimal information storage and the distribution of synaptic weights: perceptron versus Purkinje cell, *Neuron*, 43:745-757

Buonomano, D.V., and Maass, W. (2009), State-dependent computations: spatiotemporal processing in cortical networks, *Nat. Rev. Neurosci.*, 10:113–125

Burgin, K. E., Washam, M. N., Rickling, S., Westgate, S. A., Mobley, W. C., Kelly, P. T. (1990), In situ hybridization histochemistry of Ca2+/calmodulin-dependent protein kinase in developing rat brain, *J. Neurosci.*, 10:1788-1798

Burkhalter, A. (1989), Intrinsic connections of rat primary visual cortex: laminar organization of axonal projections, *J. Comp. Neurol.*, 279:171-186

Buzsaki, G. (1984), Feed-forward inhibition in the hippocampal formation, *Prog. Neurobiol.*, 22:131-153

Callaway, E. M. and Katz, L. C. (1993), Photostimulation using caged glutamate reveals functional circuitry in living brain slices, *Proc. Natl. Acad. Sci. U. S. A.*, 90:7661–7665

Chagnac-Amitai, Y., Luhmann, H. J., Prince, D. (1990) Burst generating and regular spiking layer 5 pyramidal neurons of the rat neocortex have different morphological features, *J. Comp. Neurol.*, 296:598-613

Chklovskii, D. B. and Koulakov, A. A. (2004), Maps in the brain: what can we learn from them?, *Annu. Rev. Neurosci.*, 27:369-392

Choi, G. B. Stettler, D. D., Kallman, B. R., Bhaskar, S. T., Fleischmann, A., Axel, R. (2011), Driving opposing behaviors with ensembles of piriform neurons, *Cell*, 146:1004-1015

Claridge-Chang, A., Roorda, R.D., Vrontou, E., Sjulson, L., Li, H., Hirsh, J., Miesenböck, G. (2009), Writing memories with light-addressable reinforcement circuitry. *Cell*, 139:405-415

Connors, B. W., Gutnick, M. J., Prince, D. A. (1982), Electrophysiological properties of neocortical neurons in vitro, *J. Neurophysiol.*, 48:1302-1320

Connors, B. W., Gutnick, M. J. (1990) Intrinsic firing patterns of diverse neocortical neurons, *Trends Neurosci*., 13:99-104

Cruikshank, S. J., Lewis, T. J., Connors, B. M. (2007), Synaptic basis for intense thalamocortical activation of feedforward inhibitory cells in neocortex, *Nat. Neurosci.*, 10:463-468

Cruikshank, S. J., Urabe, H., Nurmikko, A. V., Connors, B. W. (2010), Pathway-specific feedforward circuits between thalamus and neocortex revealed by selective optical stimulation of axons, *Neuron*, 65:230-245

DeFelipe, J., Fariñas, I (1992). The pyramidal neuron of the cerebral cortex: morphological and chemical characteristics of the synaptic inputs, *Progr. Neurobiol.*, 39:563-607

DeFelipe, J., Alonso-Nanclares, L., Arellano, J. I. (2002), Microstructure of the neocortex: comparative aspects, *J. Neurocytol.*, 31:299-316

del Castillo, J. and Katz, B. (1954), Quantal components of the end plate potential, *J. Physiol*, 124:560-573

Desai, N.S., Rutherford, L.C., Turrigiano, G.G. (1999), Plasticity in the intrinsic excitability of cortical pyramidal neurons, *Nat. Neurosci*., 2:515-520

Douglas, R. J., Martin, K. A., Whitteridge, D. (1989), A canonical microcircuit for neocortex, *Neural. Comput.*, 1:480–488

Douglas, R. J. and Martin, K. A. (1991), A functional microcircuit for cat visual cortex, *J. Physiol*., 440:735–769

Douglas, R. J., Koch, C., Mahowald, M., Martin, K.A., Suarez, H.H. (1995), Recurrent excitation in neocortical circuits, *Science*, 269:981–985

Douglas, R. J., Martin, K. A. (2004), Neuronal circuits of the neocortex, *Annu. Rev. Neurosci.*, 27:419-451

Douglas, R. J. and Martin, K. A. (2007), Recurrent neuronal circuits in the neocortex, *Current Biology*, 17:R496-R500

Douglas, R. J. and Martin, K. A. (2007b), Mapping the matrix: the ways of neocortex, *Neuron*, 56:226-238

Ecker, A. S., Berens, P., Keliris, G.A., Bethge, M., Logothetis, N. K., Tolias, A. S. (2010), Decorrelated neuronal firing in cortical microcircuits, *Science*, 327:584-587

Feldman, D.E. (2000), Timing-based LTP and LTD at vertical inputs to layer II/III pyramidal cells in rat barrel cortex, *Neuron*, 27:45-56

Feldmeyer, D., Lübke, J., Sakmann, B. (2006), Efficacy and connectivity of intracolumnar pairs of layer 2/3 pyramidal cells in the barrel cortex of juvenile rats, *J. Physiol.*, 575:583-602

Felleman, D.J., Van Essen, D. C. (1991), Distributed hierarchical processing in the primate cerebral cortex, *Cereb. Cortex*, 1:1-47

Fitzpatrick, D., Itoh, K., Diamond, I. T. (1983), The laminar organization of the lateral geniculate body and the striate cortex in the squirrel monkey (Saimiri sciureus), *J. Neurosci.*, 3:673-702

Frick, A., Feldmeyer, D., Helmstaedter, M., Sakmann, B. (2008), Monosynaptic connections between pairs of L5A pyramidal neurons in columns of juvenile rat somatosensory cortex, *Cereb. Cortex*, 18:397-406

Games, K.D. and Winer, J.A. (1988), Layer V in rat auditory cortex: projections to the inferior colliculus and contralateral cortex, *Hear. Res.*, 34:1-25

Gilbert, C.D. and Wiesel, T.N. (1979), Morphology and intracortical projections of functionally characterised neurons in the cat visual cortex, *Nature*, 280:120–125

Goold, C. P. and Nicoll, R. A. (2010), Single-cell optogenetic excitation drives homeostatic synaptic depression, *Neuron*, 68:512-528

Grossberg, S., Raizada, R. D. (2000), Contrast-sensitive perceptual grouping and object-based attention in the laminar circuits of primary visual cortex, *Vision Res.*, 40:1413-1432

Grubb, M.S., and Burrone, J. (2010), Activity-dependent relocation of the axon initial segment fine-tunes neuronal excitability, *Nature*, 465:1070-1074

Gunaydin, L. A., Yizhar, O., Berndt, A., Sohal, V. S., Deisseroth, K., Hegemann, P. (2010), Ultrafast optogenetic control, *Nat. Neurosci.*, 13:387-392

Gur, M. Snodderly, D. M. (2008), Physiological differences between neurons in layer 2 and layer 3 of primary visual cortex (V1) of alert macaque monkeys, *J. Physiol.*, 586: 2293-2306

Hackett, T. A., Barkat, T. R., O´Brien, B. M. J., Hensch, T. K. Polley, D. B. (2011), Linking topography to tonotopy in the mouse auditory thalamocortical circuit, *J. Neurosci.*, 1:2983-2995

Hahnloser, R. H., Sarpeshkar, R., Mahowald, M., Douglas, R., Seung, S. (2000), Digital selection and analogue amplification coexist in a cortex-inspired silicon circuit, *Nature*, 405:947-951

Hahnloser, R.H., Douglas, R.J., Hepp, K. (2002), Attentional recruitment of inter-areal recurrent networks for selective gain control, *Neural Comput*., 14:1669–1689

Hanse, E. and Gustafsson, B. (2001), Quantal variability at glutamatergic synapses in area CA1 of the rat neonatal hippocampus, *J. Physiol.*, 531:467-480

Harris, K.D., Csicsvari, J., Hirase, H., Dragoi, G., Buzsaki, G. (2003), Organization of cell assemblies in the hippocampus. *Nature*, 424:552-556

Harris, K. D. (2005), Neural signatures of cell assembly organization, *Nat. Rev. Neurosci.*, 6:399-407

Hebb, D. O. (1949), The Organization of Behavior - A Neuropsychological Theory, Wiley, New York

Helmstaedter, M., de Kock, C. P., Feldmeyer, D., Bruno, R. M., Sakmann, B. (2007), Reconstruction of an average cortical column in silico, *Brain Res. Rev.*, 55:193–203

Hestrin, S., Armstrong, W. E. (1996), Morphology and physiology of cortical neurons in layer I, *J. Neurosci.*, 16:5290–5300

Holmgren, C., Harkany, T., Svennenfors, B., Zilberter, Y. (2003), Pyramidal cell communication within local networks in layer 2/3 of rat neocortex, *J. Physiol.*, 551:139-153

Hopfield, J. J. (1982), Neural networks and physical systems with emergent collective computational abilities, *Proc. Natl. Acad. Sci. U.S.A.*, 79:2554-2558

Horton, J.C. and Adams, D.L. (2005), The cortical column: a structure without a function, *Philos. Trans. R. Soc. Lond. B Biol. Sci.*, 360:837–862

Houweling, A. R. and Brecht, M. (2008), Behavioural report of single neuron stimulation in somatosensory cortex, *Nature*, 451: 65-68

Hromádka, T., Deweese, M. R., Zador, A. M. (2008), Sparse representation of sounds in the unanesthetized auditory cortex, *PLoS Biol.*, 6:e16

Hubel, D. H. (1982), Cortical neurobiology: a slanted historical perspective, *Annu. Rev. Neurosci.*, 66:390-413

Hubel, D. H., Wiesel, T. N. (1974), Uniformity of monkey striate cortex: a parallel relationship between field size, scatter, and magnification factor, *J. Comp. Neurol.*, 158:295–305

Hubener, M., Schwarz, C., Bolz, J. (1990), Morphological types of projection neurons in layer 5 of cat visual cortex, *J. Comp. Neurol.*, 301:655-674

Huber, D., Petreanu, L., Ghitani, N., Ranade, S., Hromadka, T, Mainen, Z., Svoboda, K. (2008), Sparse optical microstimulation in barrel cortex drives learned behaviour in freely moving mice, *Nature*, 451:61-64

Huggenberger, S., Vater, M., Deisz, R. A. (2009), Interlaminar differences of intrinsic properties of pyramidal neurons in the auditory cortex of mice, *Cerebral Cortex*, 19:1008-1018

Huntley, G. W. and Jones, E. G. (1991), The emergence of architectonic field structure and areal boundaries in developing monkey sensorimotor cortex, *Neuroscience*, 44:287-310

Ikegaya, Y., Sasaki, T., Ishikawa, D., Honma, N., Tao, K., Takahashi, N, Minamisawa, G., Ujita, S., Matsuki, N. (2012), Interpyramidal spike transmission stabilizes the sparseness of recurrent network activity, *Cerebral Cortex*, doi:10.1093/cercor/bhs006

Imig, T.J. and Brugge, J.F. (1978), Sources and terminations of callosal axons related to binaural and frequency maps in primary auditory cortex of the cat, *J. Comp. Neurol.*, 182:637-660

Izhikevich, E. M., Gally, J. A., Edelman, G. M. (2004), Spike-timing dynamics of neuronal groups, *Cereb. Cortex*,14:933-944

Jones, E. G. (2001), The thalamic matrix and thalamocortical synchrony, *Trends Neurosci.*, 24:595-601

Kasper, E. M., Larkman, A. U., Lübke, J., Blackemore, C. (1994), Pyramidal neurons in layer 5 of the rat visual cortex. I. Correlation among cell morphology, intrinsic electrophysiological properties, and axon targets, *J. Comp. Neurol*., 339:495-518

Kaur, S., Lazar, R., Metherate, R. (2004), Intracortical pathways determine breadth of subthreshold frequency receptive fields in primary auditory cortex, *J. Neurophysiol.*, 91:2551-2567

Kim, D. K., Kwak, J., Kim, S. J., Kim, J. (2008), Long-lasting enhancement in the intrinsic excitability of deep dorsal horn neurons, *Pain*, 139:181-189

Kobayashi, T. (1963), Brain-to-body ratios and time of maturation of the mouse brain, *Am. J. Physiol.*, 204:343-346

Kole, M., Hallermann, S., Stuart, G. (2006), Single Ih channels in pyramidal neuron dendrites: properties, distribution, and impact on action potential output, *J. Neurosci.*,26:1677-1687

Kootstra, N.A., and Verma, I.M. (2003), Gene therapy with viral vectors. *Annu. Rev. Pharmacol. Toxicol.*, 43:413-439

Kravitz, A. V., Tye, L. D., Kreitzer, A. C. (2012), Distinct roles for direct and indirect pathway striatal neurons in reinforcement, *Nat. Neurosci.,* 15:816-818

Kügler, S., Kilic, E., Bähr, M. (2002), Human synapsin 1 gene promoter confers highly neuron-specific long-term transgene expression from an adenoviral vector in the adult rat brain depending on the transduced area, *Gene Therapy*, 10:337-247

Larkman, A. U., Major, G., Stratford, K. J., Jack, J. J. (1992), Dendritic morphology of pyramidal neurones of the visual cortex of the rat. IV: Electrical geometry, *J. Comp. Neurol*., 323:137-152

Le, R.N., Amar, M., Baux, G., Fossier, P. (2006), Homeostatic control of the excitation-inhibition balance in cortical layer 5 pyramidal neurons, *Eur. J. Neurosci.*, 24:3507-3518

Le Be, J. V., Markram, H. (2006), Spontaneous and evoked synaptic rewiring in the neonatal neocortex, *Proc. Natl. Acad. Sci. U.S.A,*.103:13214-13219

Lewis, T. L. Jr, Mao, T., Svoboda, K., Arnold, D. B. (2009), Myosin-dependent targeting of transmembrane proteins to neuronal dendrites, *Nat. Neurosci.*, 12:568-576

Lima, S.Q., Hromádka, T., Znamenskiy, P., Zador, A.M. (2009), PINP: a new method of tagging neuronal populations for identification during in vivo electrophysiological recording. *PLoS ONE*, 4:e6099

Lin, J. Y., Lin, M. Z., Steinbach, P., Tsien, R. Y. (2009), Characterization of engineered channelrhodopsin variants with improved properties and kinetics, *Biophys. J.*, 96:1803-1814

Liu, X., Ramirez, S., Pang, P. T., Puryear, C. B., Govindarajan, A., Deisseroth, K., Tonegawa, S. (2012), Optogenetic stimulation of a hippocampal engram activates fear memory recall, *Nature*, 484:381-385

Loebel, A., Silberberg, G., Helbig, D., Markram, H., Tsodyks, M., Richardson, M. J. E. (2009), Multiquantal release underlies the distribution of synaptic effi cacies in the neocortex, *Front. Comput. Neurosci.* 3:27.doi: 10.3389/neuro.10.027.2009

London, M., Roth, A., Beeren, L., Hausser, M., Latham, P. E. (2010), Sensitivity to perturbations in vivo implies high noise and suggests rate coding in cortex, *Nature*,466:123-127

Loewenstein, Y., Kuras, Y., Rumpel, S. (2011), Multiplicative dynamics underlie the emergence of the log-normal distribution of spine sizes in the neocortex in vivo, *J. Neurosci.*, 31:59481-59488

Lubke, J., Roth, A., Feldmeyer, D., Sakmann, B. (2003), Morphometric analysis of the columnar innervations domain of neurons connecting layer 4 and layer 2/3 of juvenile rat barrel cortex. *Cereb. Cortex*, 13:1051-1063

Lund, J. S. (1984), Spiny stellate cells. In: Peters, A. and Jones, E. G., eds. *Cerebral Cortex, Vol.1. Cellular components of the cerebral cortex*, pp. 255-308, New York, Plenum Press

Maass, W (2000), On the computation power of winner-take-all, Neural Comput., 12:2519-2525

Magee, J. C. (1998), Dendritic hyperpolarization-activated currents modify the integrative properties of hippocampal CA1 pyramidal neurons, *J. Neurosci.*, 18:7613-7624

Mao, T., Kusefoglu, D., Hooks, B. M., Huber, D., Petreanu, P., Svoboda, K. (2011), Long-range neuronal circuits underlying the interaction between sensory and motor cortex, *Neuron*, 71:111-123

Markram, H., Lubke, J., Frotscher, M., Sakmann, B. (1997), A network of tufted layer five pyramidal neurons, *Cereb. Cortex*,7:523-533

Markram, H., (2006), The blue brain project, *Nat. Rev. Neurosci.*, 7:153–160

Markram, H. (2010), Microcircuits of the neocortex. In: Shepherd, G. M. and Grillner, S., eds., *Handbook of brain microcircuits*, pp. 22-30, Oxford University Press, Inc., New York

Markram, H., Toledo-Rodriguez, M. Wang, Y., Gupta, A., Silberberg, G., Wu, C. (2004), Interneurons of the neocortical inhibitory system, *Nat. Rev. Neurosci.*, 5:793-807

Matsuno-Yagi, A., and Mukohata, Y. (1977), Two possible roles of bacteriorhodopsin; a comparative study of strains of Halobacterium halobium differing in pigmentation, *Biochem. Biophys. Res. Commun.*, 78:237–243

Melzer, S., Michael, M., Caputi, A., Eliava, M., Fuchs, E. C., Whittington, M. A., Monyer, H. (2012), Long-range-projecting GABAergic neurons modulate inhibition in hippocampus and entorhinal cortex, *Science*, 335:1506-1510

Merzenich, M. M., Knight, P. L., Roth, G. L. (1975), Representation of cochlea within primary auditory cortex in the cat, *J. Neurophysiol.*, 38:231-249

Miller, K.D. (1996), Synaptic economics: Competition and cooperation in synaptic plasticity, *Neuron*, 17:371-374

Monier, C., Chavane, F., Baudot, P., Graham, L.J., Fregnac, Y. (2003), Orientation and direction selectivity of synaptic inputs in visual cortical neurons: a diversity of combinations produces spike tuning, *Neuron*, 37:663-680

Mountcastle, V. B. (1957), Modality and topography properties of single neurons of cat's somatic sensory cortex, *J. Neurophysiol.*, 20:408-434

Mountcastle, V. B., An organizing principle for cerebral function. In: Edelman GM, Mountcastle VB, editors. The mindful brain. Cambridge (MA): MIT Press, 1978:7-50

Mountcastle, V. B. (1997), The columnar organization of the neocortex, *Brain*, 120:701-722

Murray Sherman, S., Guillery, R. W. (1996), Functional organization of thalamocortical relays, *Journal of Neurophysiology*, 76:1367-1395

Nagel, G., Szellas, T., Huhn, W., Kateriya, S., Adeishvili, N., Berthold, P., Ollig, D., Hegemann, P., Bamberg, E. (2003), Channelrhodopsin-2, a directly light-gated cation-selective membrane channel, *Proc. Natl. Acad. Sci. USA*, 100:13940-13945

O'Connell, M. N., Falchier, A., McGinnis, T., Schroeder, C. E., Lakatos, P. (2011), Dual mechanism of neuronal ensemble inhibition in primary auditory cortex, *Neuron*, 69:805-817

O'Connor, D. H., Peron, S. P., Huber, D., Svoboda, K. (2010), Neural activity in barrel cortex underlying vibrissa-based object localization in mice, *Neuron*, 67:1048-1061

Oertner, T. G., Sabatini, B. L., Nimchinsky, E. A., Svoboda, K. (2002), Facilitation at single synapses probed with optical quantal analysis, *Nat. Neurosci.*, 5:657-664

Oesterhelt, D., and Stoeckenius, W. (1973),Functions of a new photoreceptor membrane, *Proc. Natl. Acad. Sci. USA*, 70:2853-2857

Ohki, K., Chung, S., Ch'ng, Y.H., Kara, P., Reid, R.C. (2005), Functional imaging with cellular resolution reveals precise micro-architecture in visual cortex, *Nature*, 433:597–603

Ohki, K., Chung, S., Kara, P., Hubener, M., Bonhoeffer, T., Reid, R.C. (2006), Highly ordered arrangement of single neurons in orientation pinwheels, *Nature*, 442:925–928

O'Leary, T., van Rossum, M. C. W., Wyllie, D. J. A. (2010), Homeostasis of intrinsic excitability in hippocampal neurones: dynamics and mechanism of the response to chronic depolarization, *J. Physiol.*, 588:157-170

Oswald, A. M. and Reyes, A. D. (2008), Maturation of intrinsic and synaptic properties of layer 2/3 pyramidal neurons in mouse auditory cortex, *J. Neurophysiol*., 99:2998-3008

Otto, K. J., Rousche, P. J., Kipke, D. R. (2005), Cortical microstimulation in auditory cortex of rat elicits best-frequency dependent behaviors, *J. Neural Eng*., 2:42-51

Oviedo, H. V., Bureau, I., Svoboda, K., Zador, A. M. (2010), The functional asymmetry of auditory cortex is reflected in the organization of local cortical circuits, *Nat. Neurosci*., 13:1413-1423

Packer, A. M. and Yuste, R. (2011), Dense, unspecific connectivity of neocortical parvalbumin-positive interneurons: a canonical microcircuit for inhibition?, *J. Neurosci.*, 31:13260-13271

Paxinos, G., Franklin, K. B. J. (2001), The mouse brain in stereotactic coordinates, San Diego (CA), Academic Press.

Peterlin, Z. A., Kozloski, J., Mao, B. Q., Tsiola, A., Yuste, R. (2000), Optical probing of neuronal circuits with calcium indicators, *Proc. Natl. Acad. Sci. U. S. A.*, 97:3619–3624

Petreanu, L., Huber, D., Sobczyk, A., Svoboda, K., (2007), Channelrhodopsin-2-assisted circuit mapping of long-range callosal projections, *Nat. Neurosci*.,10:663-668

Petersen, C. C. H. (2007), The functional organization of the barrel cortex, *Neuron*, 56:339-355

Porter, L. L., White, E. L. (1986), Synaptic connections of callosal projection neurons in the vibrissal region of mouse primary motor cortex: an electron microscopic/horseradish peroxidase study, *J. Comp. Neurol.*, 248:573-587

Poulet, J. F. A. and Petersen, C. C. H. (2008), Internal brain state regulates membrane potential synchrony in barrel cortex of behaving mice, *Nature*, 454:881-885

Renart, A., de la Rocha, J., Bartho, P., Hollender, L., Parga, N., Reyes, A., Harris, K. D. (2010), The synchronous state in cortical circuits, *Science*, 327:587-590

Reyes, A. and Sakmann, B. (1999). Developmental switch in the short-term modification of unitary EPSPs evoked in layer 2/3 and layer 5 pyramidal neurons of rat neocortex, *J Neurosci.*, 19:3827-3835

Ribrault, C., Sekimoto, K., Triller, A. (2011), From the stochasticity of molecular processes to the variability of synaptic transmission, *Nat. Rev. Neurosci.*, 12:375-387

Riesenhuber, M., Poggio, T. (1999), Hierarchical models of object recognition in cortex, *Nat. Neurosci.*, 2:1019-25

Romo, R., Hernandez, A., Zainos, A., Salinas, E. (1998), Somatosensory discrimination based on cortical microstimulation, *Nature*, 392:387-390

Rothschild, G., Nelken, I., Mizrahi, A. (2010), Functional organization and population dynamics in the mouse primary auditory cortex, *Nat. Neurosci.*,13:353-360

Rousche, P. J., Otto, K. J., Reilly, M. P., Kipke, D. R. (2003), Single electrode micro-stimulation of rat auditory cortex: an evaluation of behavioral performance, *Hearing Res.*, 179:62-71

Sakata, S and Harris, K .D. (2009), Laminar structure of spontaneous and sensory-evoked population activity in auditory cortex, *Neuron*, 64:404-418

Salzman, C. D., Britten, K. H., Newsome, W. T. (1990), Cortical microstimulation influences perceptual judgements of motion direction, *Nature*, 346:174-177

Sato, T. R., Gray, N. W., Mainen, Z. F., Svoboda, K. (2007), The functional microacchitecture of the mouse barrel cortex, *PLoS Biology*, 5:1440-1452

Scanziani, M., and Häusser, M. (2009), Electrophysiology in the age of light, *Nature*, 461:930-939

Schreiner, C. E. and Winer, J. A. (2007), Auditory cortex mapmaking: principles, projections, and plasticity, *Neuron*. 56:356-365

Schroll, C., Riemensperger, T., Bucher, D., Ehmer, J., Völler, T., Erbguth, K., Gerber, B., Hendel, T., Nagel, G., Buchner, E., et al. (2006), Light-induced activation of distinct modulatory neurons triggers appetitive or aversive learning in Drosophila larvae, *Curr. Biol.*, 16:1741-1747

Schultz, W. (1998), Predictive reward signal of dopamine neurons, *J. Neurophysiol.*, 80:1-27

Shen, J., Xu, Z., Yao, Y. (1999), Evidence of columnar organization in the auditory cortex of the mouse, *Hearing Research*, 137:174-177

Shu, Y., Hasenstaub, A., McCormick, D.A. (2003), Turning on and off recurrent balanced cortical activity, *Nature*, 423:288-293

Silberberg, G., Grillner, S., LeBeau, F. E. N., Maex, R., Markram, H. (2005), Synaptic pathways in neural microcircuits, *Trends in Neuroscience*, 28:-541551

Silver, R. A., Lubke, J., Sakmann, B., Feldmeyer, D. (2003), High- probability uniquantal transmission at excitatory synapses in barrel cortex, *Science*, 302:1981-1984

Sjöström, P.J., Turrigiano, G.G., Nelson, S.B. (2001), Rate, timing, and cooperativity jointly determine cortical synaptic plasticity, *Neuron*, 32:1149-1164

Song, S., Sjostrom, P. J, Reigl, M., Nelson, S., Chklovskii, D. B. (2005), Highly nonrandom features of synaptic connectivity in local cortical circuits, PLoS Biology, 3:507-519

Song, L., McGee, J. A., Walsh, E. J. (2006), Frequency- and level-dependent changes in auditory brainstem responses (ABRs) in developing mice, *J. Acoust. Soc. Am.*, 119:2242-2257

Spruston, N. (2008), Pyramidal neurons: dendritic structure and synaptic integration, *Nat. Rev. Neurosci.*, 9:206-221

Stiebler, I., Neulist, R., Fichtel, I., Ehret, G. (1997), The auditory cortex of the house mouse: left-right differences, tonotopic organization and quantitative analysis of frequency representation, *J. Comp. Physiol.*, 181:559-571

Tang, W., Ehrlich, I., Wolff, S. B. E., Michalski, A-M., Woelfl, S., Hasa, M. T., Luethi, A., Sprengel, R. (2009), Faithful expression of multiple proteins via 2A-peptide self-processing: a versatile and reliable method for manipulating brain circuits, *J. Neurosci.*, 29:8621-8629

Thomson, A. M. and Lamy, C. (2007), Functional maps of neocortical local circuitry, *Front. Neurosci.*, 1:19–42

Thomson, A. M. and Bannister, A. P. (1998), Postsynaptic pyramidal target selection by descending layer III pyramidal axons: dual intracellular recordings and biocytin filling in slices of rat neocortex, *Neuroscience*, 84:669-683

Thomson, A. M., West, D. C., Wang, Y., Bannister, A. P. (2002), Synaptic connections and small circuits involving excitatory and inhibitory neurons in layers 2-5 of adult rat and cat neocortex: triple intracellular recordings and biocytin labeling in vitro, *Cereb. Cortex*, 12: 936-953

Thomson, A. M. and Bannister, A. P. (2003), Interlaminar connections in the neocortex, *Cerebral Cortex*, 13:5-14

Truccolo, W., Hochberg, L.R., Donoghue, J.P. (2010), Collective dynamics in human and monkey sensorimotor cortex: Predicting single neuron spikes, *Nat. Neurosci*, 13:105-111

Tsai, H. C., Zhang, F., Adamantidis, A., Stuber, G. D., Bonci, A., de Lecea, L., Deisseroth, K. (2009), Phasic firing in dopaminergic neurons is sufficient for behavioral conditioning, *Science*, 324:1080-1084

Turrigiano, G. G. (1999), Homeostatic plasticity in neuronal networks: The more things change, the more they stay the same, *Trends Neurosci*., 22:221-227

Turrigiano, G .G., Leslie, K. R., Desai, N.S., Rutherford, L. C., Nelson, S. B. (1998), Activity-dependent scaling of quantal amplitude in neocortical neurons, *Nature*, 391:892-896

Turrigiano, G. G and Nelso, S. B. (2004), Homeostatic plasticity in the developing nervous system, *Nat. Rev. Neurosci*.,5:97-107

Usrey, W. M., Alonso, J. M., Reid, R.C. (2000), Synaptic interactions between thalamic inputs to simple cells in cat visual cortex, *J. Neurosci.*, 20:5461-5467

von Neumann, J. (2000), The Computer and the Brain, Second Edition (New Haven, CT: Yale University Press)

Walcott, E. C., Langdon, R. B. (2002), Synaptically driven spikes and long-term potentiation in neocortical layer 2/3, *Neuroscience*, 112:815-826

Wandell, B. A. and Smirnakis, S, M. (2009), Plasticity and stability of visual field maps in adult primary visual cortex, *Nat. Rev. Neurosci*., 10:873-884

Wang, Z. and MrCormick, D. A. (1993), Control of firing mode of corticotectal and corticopontine layer V burst-generating neurons by norepinephrine, acetylcholine and 1S,3R-ACPD, *L. Neurosci.*,13:2199-2216

Wang, J., Liu, Y., Qin, L., Chimoto, S., Nakamoto, K., Sato, Y. (2012), Chronic microstimulation of cat auditory cortex effective to evoke detection behaviors, *Neuroscience*, 206:81-88

Wehr, M. and Zador, A. M. (2003), Balanced inhibition underlies tuning and sharpens spike timing in auditory cortex, *Nature*, 426:442-446

Wennekers, T., Sommer, F., Aertsen, A. (2003), Neuronal assemblies, *Theory Biosci*., 122:1-104

White, E.L. (2007), Reflections on the specificity of synaptic connections, *Brain Res. Brain Res. Rev*,.55:422–429

Wickersham, I. R., Lyon, D. C., Barnard, R. J., Mori, T., Finke, S., Conzelmann, K. K., Young, J. A., Callaway, E. M. (2007), Monosynaptic restriction of transsynaptic tracing from single, genetically targeted neurons, *Neuron*, 53:639–647

Yang, Y., DeWesse, M. R., Otazu, G. H., Zador, A. M. (2008), Milisecond-scale differences in neural activity in auditory cortex can drive decisions, *Nat. Neurosci.*, 11:1262-1263

Yizhar, O., Fenno, L. E., Davidson, T. J., Mogri, M., Deisseroth, K. (2011), Optogenetics in neural systems, *Neuron*, 71:9-34

Yoshimura, Y., Callaway, E. M. (2005), Fine-scale specificity of cortical networks depends on inhibitory cell type and connectivity, *Nature Neurosci*., 8:1552-1559

Yoshimura, Y., Dantzker, J.L., Callaway, E.M. (2005), Excitatory cortical neurons form fine-scale functional networks, *Nature*, 433:868-873

Zador, A. M., Agmon-Snir, H., Segev, I. (1995), The morphoelectrotonic transform: a graphical approach to dendritic function, *J. Neurosci.,* 15:1669-1682

Zhang, F., Wang, L-P., Brauner, M., Liewald, J. F., Kay, K., Watzke, N., Wood, P. G., Bamberg, E., Nagel, G., Gottschalk, A., Deisseroth, K. (2007), Multimodal fast optical interrogation of neural circuitry, *Nature*, 446:633-639

Zhang, F., Prigge, M., Beyriere, F., Tsunoda, S. P., Mattis, J., Yizhar, O., Hegemann, P., Deisseroth, K. (2008), Red-shifted optogenetic excitation: a tool for fast neural control derived from *Volvox carteri*, *Nat. Neurosci.,* 11:631-633

Zhang, Z., Jiao, Y.-Y-, Sun, Q.-Q. (2011), Developmental maturation of excitation and inhibition balance in principal neurons across four layers of somatosensory cortex, *Neuroscience*, 174:10-25

Zilles, K. (1990), Anatomy of the neocortex: cytoarchitecture and myeloarchitecture, pp 77-113, Cambridge, MA, MIT

Zucker, R. S. and Regehr, W. G. (2002), Short-term synaptic plasticity, *Annu. Rev. Physiol*., 64:355-405

9. Acknowledgements

To prevent the “age of forgetting” (Tony Judt), my sincere and long-lasting thank to:

Simon, for taking me in his lab 4 years ago and teaching me how to do intelligent and enjoyable science, for his constant support, discussions and daily enthusiasm. This work would never have seen the light of day without his knowledge and care. Lessons to the future;

Juliane, with whom I share part of the present work effort, for her daily friendship, enjoyable times doing experiments and rewardable exchange of opinions, stories and infinite laughs. Memorable friend;

Brice, Dominik, Evi, Jiss, Kaja, Lyubov, Manuel, Tanja, Tina, my lab colleagues, for their constant friendship, help in every moment, and time and will for funny moments in and outside the lab. Working as a group makes all the sense;

Bettina and Valerie, for their solid rock friendship. A safe harbor to come back always;

my parents and sister, though far away, always extremely close. At the end of the day, there is nothing better one could ask for;

GABBA, the Graduate Program in Areas of Basic and Applied Biology, University of Porto, in the shape of its coordinators and colleagues, for an amazing opportunity, for betting that I could do a proper job. Only can hope that I didn´t let anyone down;

FCT, Fundação para a Ciência e a Tecnologia, for financial support.

10. Curriculum Vitae

Personal Data

Name: Bruno Miguel da Palma Pedrosa Fontinha
Date of Birth: January 13th, 1982
Place of Birth: Faro, Portugal
Contact: fontinha.bruno@gmail.com

Academic Degrees

2008 - Present: PhD Candidate at the Research Institute of Molecular Pathology (I.M.P.), Vienna, Austria, under the supervision of Dr. Simon Rumpel

2002 - 2006: Bachelor of Science (B.Sc.) in Biochemistry, Faculty of Sciences, University of Lisbon, Portugal (final grade 16/20) with a original final thesis "Adenosine modulation upon brain-derived neurotrophic factor effect on hippocampal long-term potentiation" (final grade 19/20)

Awards and Fellowships

2010 – Scholarship Travel Grant assigned by the Portuguese Society for Neuroscience (SPN) to attend the 7th Forum of European Neuroscience Societies (FENS) in Amsterdam, The Netherlands

2008 – Present: Doctoral Grant SFRH/BD/33250/2007 supported by Fundação para a Ciência e a Tecnologia (FCT), as being a PhD Student from the Graduate Program in Areas of Basic and Applied Biology (GABBA), Porto, Portugal

October 2007 – December 2007: European Science Foundation COST-STSM-B30-1367 as a Research Trainee in División de Neurociencias, Universidad Pablo de Olavide, Sevilla, Spain, to study modulatory events upon long-term potentiation plasticity in alert behaving mice, under the supervision of Prof. Dr. José M. Delgado-García

January 2007 – December 2007: Research Grant IMM/BI/3-2007 supported by Fundação para a Ciência e a Tecnologia (FCT), to study the effect of neurotrophic factors upon hippocampal long-term potentiation and its interplay with adenosine, under the supervision of Profª. Drª. Ana M. Sebastião

Publications

5. Batalha, V. L., Pego, J.M., Fontinha, B. M., Costenla, A. R., Valadas, J. S., Baqi, Y., Radjainia, H., Müller, C. E., Sebastião, A. M., Lopes, L. V. (2012), Adenosine A(2A) receptor blockade reverts hippocampal stress-induced deficits and restores corticosterone circadian oscillation, *Molecular Phsychiatry*, doi:10.1038/mp.2012.8

4. Diógenes, M. J., Costenla, A. R., Lopes, L. V., Jeronimo-Santos, A., Sousa, V. C., Fontinha, B. M., Ribeiro, J. A., Sebastião, A. M. (2011), Enhancement of LTP in aged rats is dependent on endogenous BDNF, *Neuropsychopharmacology*, 36:1823-36

3. Fontinha, B. M., Delgado-Garcia, J. M., Madronal, N., Ribeiro, J. A., Sebastião, A. M., Gruart, A. (2009), Adenosine A(2A) receptor modulation of hippocampal CA3-CA1 synapse plasticity during associative learning in behaving mice, *Neuropsychopharmacology*, 34:1865-74

2. Fontinha, B.M., Diógenes, M. J., Ribeiro, J. A., Sebastião, A. M. (2008), Enhancement of long-term potentiation by brain-derived neurotrophic factor requires adenosine A2A receptor activation by endogenous adenosine, *Neuropharmacology*, 54: 924-33

1. Cunha-Reis, D., Fontinha, B. M., Ribeiro, J. A., Sebastião, A. M. (2007), Tonic adenosine A1 and A2A receptor activation is required for the excitatory action of VIP on synaptic transmission in the CA1 area of the hippocampus, *Neuropharmacology*, 52: 313-20